Engineering Journal

American Institute of Steel Construction

Fourth Quarter 2013 Volume 50, No. 4

CELEBRATING 50 YEARS OF STEEL KNOWLEDGE

ENGINEERING JOURNAL

AMERICAN INSTITUTE OF STEEL CONSTRUCTION

Dedicated to the development and improvement of steel construction, through the interchange of ideas, experiences and data.

The articles contained herein are not intended to represent official attitudes, recommendations or policies of the Institute. The Institute is not responsible for any statements made or opinions expressed by contributors to this Journal.

The opinions of the authors herein do not represent an official position of the Institute, and in every case the officially adopted publications of the Institute will control and supersede any suggestions or modifications contained in any articles herein.

The information presented herein is based on recognized engineering principles and is for general information only. While it is believed to be accurate, this information should not be applied to any specific application without competent professional examination and verification by a licensed professional engineer. Anyone making use of this information assumes all liability arising from such use.

Manuscripts are welcomed, but publication cannot be guaranteed. All manuscripts should be submitted in duplicate. Authors do not receive a remuneration. A "Guide for Authors" is printed on the inside back cover.

ENGINEERING JOURNAL (ISSN 0013-8029) is published quarterly. Subscriptions: Members: one subscription, $40 per year, included in dues; Additional Member Subscriptions: $40 per year. Non-Members U.S.: $160 per year. Foreign (Canada and Mexico): Members $80 per year. Non-Members $160 per year. Published by the American Institute of Steel Construction at One East Wacker Drive, Suite 700, Chicago, IL 60601.

Periodicals postage paid at Chicago, IL and additional mailing offices. **Postmaster:** Send address changes to ENGINEERING JOURNAL in care of the American Institute of Steel Construction, One East Wacker Drive, Suite 700, Chicago, IL 60601.

Torsional and Constrained-Axis Flexural-Torsional Buckling Tables for Steel W-Shapes in Compression

DI LIU, BRAD DAVIS, LEIGH ARBER and RAFAEL SABELLI

ABSTRACT

Torsional buckling (TB), an applicable limit state for W-shape members subject to axial compression, often controls when the torsional effective unbraced length exceeds the minor-axis flexural buckling effective unbraced length. Constrained-axis flexural-torsional buckling (CAFTB) is a potential limit state for W-shape members that are constrained to buckle with the center of twist at a location other than the centroidal axis, as is the case for a typical beam with one flange braced by a diaphragm and the other unbraced. Manual calculation of the TB or CAFTB available compressive strength is a somewhat lengthy process, especially when the section is slender for axial compression, and no design aid currently exists in the AISC *Manual*. This paper provides tables that facilitate the determination of TB and CAFTB available compressive strengths. Several example calculations are also provided.

Keywords: members, columns, stability, buckling, torsion.

INTRODUCTION

Hot-rolled W-shape members are subjected to compressive axial forces when used as columns, braces, struts or collectors. The available compressive strength—LRFD design strength or ASD allowable strength—per the AISC *Specification* (AISC, 2010) Chapter E is the minimum based on the limit states of flexural buckling (FB) and torsional buckling (TB; see Figure 1a). W-shape FB available strength calculations are facilitated by design aids in Part 4 of the AISC *Steel Construction Manual* (AISC, 2011), especially Tables 4-1 and 4-22. TB is not included in these design aids because when the weak-axis FB effective unbraced length, $(KL)_y$, equals the TB effective unbraced length, K_zL, TB only controls for very few cases, and in those cases only by a margin of less than 0.5%.

However, there are some common situations for which the TB strength is likely to control by a significant margin, the most common being a column or collector with K_zL exceeding $(KL)_y$. For example, a column might have a mid-height weak-axis brace that restrains lateral translation but not twist; in that case, K_zL is twice as large as $(KL)_y$, and torsional buckling is likely to control. When faced with one of these situations, the engineer must manually calculate the available compressive strength using the AISC *Specification* (2010) Sections E3, E4 and often E7.

There are also common situations in which the member has a potential buckling mode with combined lateral translation and twist, similar to flexural-torsional buckling except that the boundary conditions force the center of twist to be at a specific location. This mode is referred to as constrained-axis flexural-torsional buckling (CAFTB). The most common example is a floor or roof beam connected to a deck diaphragm, in which the top flange is continuously braced in the lateral direction and the bottom flange is unbraced between the supports as shown in Figure 1b, thus constraining the section to twist about the axis defined by the intersection of web centerline and outside face of the top flange. The AISC *Specification* (2010) does not provide an equation for determining the CAFTB available compressive strength, nor does the AISC *Manual* (2011) include a design aid with CAFTB available strengths. Thus, when designing a member with a potential CAFTB mode, designers usually resort to a conservative approach such as evaluating the aforementioned beam for weak-axis FB (a mode that does not apply in this example) with $(KL)_y$ equal to the member length in lieu of computing the CAFTB strength.

Many ASTM A992 W-shapes that are commonly used as beams have webs that are slender for axial compression per the AISC *Specification* (AISC, 2010) Table B4.1a (e.g., W14×22 through W14×43, W18×35 through W18×60 and W21×44 through W21×83), indicating that they cannot be axially loaded to the yield stress without local buckling. The relatively lengthy calculations in Section E7 must be used to determine the available compressive strength for these slender sections.

Di Liu, Ph.D. Candidate, Civil Engineering Department, University of Kentucky, Lexington, KY. E-mail: liu.di@uky.edu

Brad Davis, Assistant Professor, Civil Engineering Department, University of Kentucky, Lexington, KY (corresponding). E-mail: bdavis@engr.uky.edu

Leigh Arber, Staff Engineer, American Institute of Steel Construction, Chicago, IL. E-mail: arber@aisc.org

Rafael Sabelli, Principal and Director of Seismic Design, Walter P Moore, San Francisco, CA. E-mail: rsabelli@walterpmoore.com

Therefore, the main objective of this paper is to provide a design aid that will facilitate the determination of W-shape TB and CAFTB available strengths over a common range of effective unbraced lengths for the most common yield stress in use today, $F_y = 50$ ksi. The CAFTB available strength depends on the distance from the centroid and shear center to the constraining axis. However, a common constraining axis location is at the intersection of the web centerline and the outside face of one flange, so CAFTB available strengths are included for that case. Due to space considerations, only the LRFD design strength, ϕP_n, is shown. However, the ASD allowable strength is quickly determined by dividing the tabulated strength by the resistance factor, $\phi_c = 0.9$, and then dividing that value by the safety factor, $\Omega_c = 1.67$. A secondary objective is to provide guidance for computing the CAFTB strength for members with discrete bracing.

TORSIONAL BUCKLING AVAILABLE STRENGTH

The TB design strength is computed using the AISC *Specification* (2010), as follows. First, the elastic TB stress is computed using the AISC *Specification* Equation E4-4, shown here. The derivation is included in Timoshenko and Gere (1961), Allen and Bulson (1980), and Salmon et al. (2009). The member ends are restrained against transverse displacement and twist, but not warping.

$$F_e = \left[\frac{\pi^2 E C_w}{\left(K_z L\right)^2} + GJ\right]\frac{1}{I_x + I_y} \tag{1}$$

where

C_w = warping constant
K_zL = effective length between points that are braced against twist of the cross section
J = torsional constant
I_x = major principal axis moment-of-inertia
I_y = minor principal axis moment-of-inertia

The critical stress, F_{cr}, and nominal compressive strength, P_n, are then computed using the equations in the AISC *Specification* (2010) Section E3 or E7, depending on the local buckling classification. Finally, the tabulated design strength, ϕP_n, is computed by applying the resistance factor $\phi_c = 0.9$.

CONSTRAINED-AXIS FLEXURAL-TORSIONAL BUCKLING AVAILABLE STRENGTHS FOR CONTINUOUSLY BRACED MEMBERS

The AISC *Specification* (2010) does not include an equation for the elastic buckling stress for CAFTB. However, Timoshenko and Gere (1961) provided an equation—their Equation 5-56—for the elastic buckling strength of a doubly symmetric member constrained to buckle about a continuous fixed axis that is offset from each principal axis. The member ends are restrained against transverse displacement and twist, but not warping. Timoshenko and Gere's Equation 5-56 becomes the following equation when the constraining axis is in the plane of the web.

$$P_e = \left[\frac{\pi^2 E\left(C_w + I_y a^2\right)}{\left(K_z L\right)^2} + GJ\right]\frac{1}{r_x^2 + r_y^2 + a^2} \tag{2}$$

where

a = distance from the constraining axis to the centroid
K_zL = effective unbraced length for CAFTB (e.g., the member length if one flange is continuously laterally braced and the other flange unbraced)
r_x = major principal axis radius of gyration
r_y =minor principal axis radius of gyration

Equation 2 is valid only if the object(s) providing the bracing force and stiffness do not deform. Helwig and Yura (1999) recommended reducing the elastic strength by 0.90 "to account for the finite stiffness provided by typical lateral

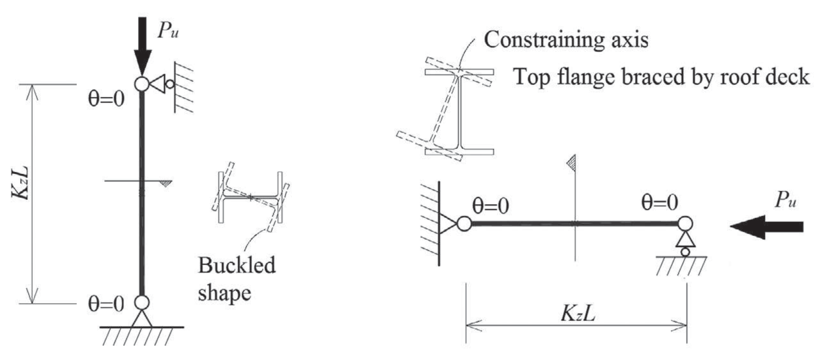

Fig. 1. Buckling mode illustrations: (a) torsional buckling; (b) constrained-axis flexural-torsional buckling.

bracing systems," a recommendation adopted for this paper. The elastic CAFTB stress, F_e, is the elastic buckling strength, $0.9P_e$, divided by the gross area, A_g; F_{cr} is computed using the AISC *Specification* (2010) Section E3 or E7, depending on the local buckling classification (nonslender or slender for axial compression). In summary, each tabulated CAFTB tabulated strength was computed in the following sequence:

1. P_e using Equation 2 with $a = d/2$
2. $F_e = 0.9P_e/A$
3. F_{cr} using Section E3 or E7
4. $P_n = F_{cr}A$
5. ϕP_n where $\phi = 0.9$

Table 1, included at the end of this paper, was generated for the case of $a = 0.5d$, which the authors consider to be a common case. It is also possible, however, to have $a > 0.5d$. Helwig and Yura (1999) indicated that the elastic CAFTB strength decreases with increasing a/d ratio when the constrained axis is in the plane of the web. Therefore, if $a > 0.5d$, the CAFTB available strength is less than the tabulated strength, and the available strength must be computed rather than pulled from the tables.

CONSTRAINED-AXIS FLEXURAL-TORSIONAL BUCKLING OF DISCRETELY BRACED MEMBERS

CAFTB is also a potential limit state for discretely braced members—such as moment frame columns that are braced against transverse displacement at the outside flange by each girt while the inside flanges are only braced at selected girts, thus creating a potential CAFTB mode between the inside flange brace locations. Equation 2 does not directly apply to such situations, so the elastic buckling strength must be evaluated using some other method, such as eigenvalue buckling analysis within a finite element analysis (FEA) program. The following describes the development of a simplified procedure—based on Equation 2—that applies within specific limitations.

An ANSYS FEA model was created of each W-shape (W10 through W44) at each unbraced length ranging from 10 ft to 40 ft. Each W-shape member was modeled by two-node, seven-degree-of-freedom BEAM188 elements, which include torsional warping. Member ends were restrained against transverse displacement and twist, but not against warping. Discrete braces, each modeled by a rigid bar connecting the centroid of the W-shape and the constraint axis at $a = d/2$, were placed at one-third points along the member length. A linear spring element (COMBIN14) was used to model the finite support stiffness as shown in Figure 2.

Linear eigenvalue analysis was used to compute the elastic buckling load, which was divided by the value from Equation 2. This buckling load ratio varied from member to member and by span length. The lowest ratio for each member size is a reduction factor that can be applied to Equation 2 instead of the 0.90 factor discussed in the paragraph following Equation 2, thus providing a conservative and simple method for computing the CAFTB strength of discretely braced members subject to specific limitations.

For one-third point (or closer) spacing of discrete braces with $k \geq 10$ kip/in., and $a = d/2$, a 0.75 reduction factor (instead of 0.9) can be used for the following sections: W10 under 60 lb/ft; W12 under 100 lb/ft; W14, W16, W18 under 120 lb/ft; W21, W24 under 150 lb/ft; W27 under 200 lb/ft; and W30 through W44 under 250 lb/ft. For one-third point (or closer) spacing of discrete braces with $k \geq 30$ kip/in., and $a = d/2$, a 0.75 reduction factor (instead of 0.9) can be used for the following sections: W10 and W12 under 100 lb/ft; W14, W16, W18 under 150 lb/ft; W21 through W27 under 250 lb/ft; W30 through W44 under 350 lb/ft. In summary, the CAFTB strength is computed in the following sequence:

1. P_e using Eq. (2) with $a = d/2$
2. $F_e = 0.75P_e/A$
3. F_{cr} using Section E3 or E7
4. $P_n = F_{cr}A$
5. ϕP_n where $\phi = 0.9$

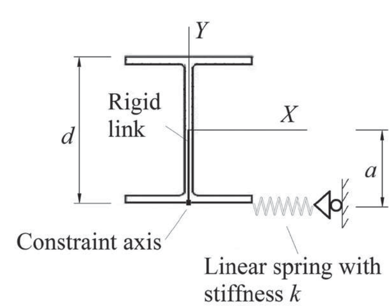

Fig. 2. Constraining axis condition for FEA modeling.

EXAMPLE 1

Torsional Buckling Available Strength of W-Shape

Given:

Determine the torsional buckling available strength of a W14×48 in axial compression.

$K_zL = 32.0$ ft $F_y = 50$ ksi $E = 29000$ ksi $G = 11200$ ksi $A_g = 14.1$ in.^{2} $I_x = 484$ in.^{4}

$I_y = 51.4$ in.^{4} $J = 1.45$ in. $C_w = 2240$ in.^{6}

Solution:

Local Buckling Classification

From AISC *Manual* Table 1-1, the W14×48 is nonslender for compression. AISC *Specification* Sections E3 and E4 apply.

Torsional Buckling about z-z Axis

$$F_e = \left[\frac{\pi^2 EC_w}{(K_zL)^2} + GJ\right]\frac{1}{I_x + I_y} = \left[\frac{\pi^2(29000)(2240)}{\left[32(12)\right]^2} + 11200(1.45)\right]\frac{1}{484 + 51.4} = 38.4 \text{ ksi}$$

$$\frac{F_y}{F_e} = \frac{50 \text{ ksi}}{38.4 \text{ ksi}} = 1.30 < 2.25$$

$$F_{cr} = \left[0.658^{\frac{F_y}{F_e}}\right]F_y = \left[0.658^{1.30}\right]50 = 29.0 \text{ ksi}$$

$$P_n = F_{cr}A_g = 29.0 \text{ ksi}(14.1 \text{ in.}^2) = 409 \text{ kips}$$

LRFD Design Strength

$\phi_c P_n = 0.9(409 \text{ kips}) = 368$ kips (matches table)

ASD Allowable Strength

$P_n/\Omega_c = 409 \text{ kips}/1.67 = 245$ kips

EXAMPLE 2

Torsional Buckling Available Strength of W-Shape

Given:

Determine torsional buckling available strength (LRFD) of a W16×26 in axial compression.

$K_zL = 8$ ft $F_y = 50$ ksi $E = 29000$ ksi $G = 11200$ ksi $A_g = 7.68$ in.^{2} $d = 15.7$ in. $t_w = 0.250$ in.

$b_f = 5.50$ in. $t_f = 0.345$ in. $k = 0.747$ in. $I_x = 301$ in.^{4} $I_y = 9.59$ in.^{4} $J = 0.262$ in.^{4} $C_w = 565$ in.^{6}

Solution:

Local Buckling Classification

From AISC *Specification* Table B 4.1a, Case 1, the limiting width-to-thickness ratio for the flange is

$$\lambda_r = 0.56\sqrt{\frac{29000}{50}} = 13.5$$

For the W16×26,

$$\frac{b_f}{2t_f} = \frac{5.50}{2(0.345)} = 7.97$$

$$\frac{b_f}{2t_f} = 7.97 < 13.5, \text{ the flange is nonslender}$$

From AISC *Specification* Table B 4.1a, Case 5, the limiting width-to-thickness ratio for the web is

$$\lambda_r = 1.49\sqrt{\frac{29000}{50}} = 35.9$$

For the W16×26,

$$\frac{h}{t_w} = \frac{d-2(k)}{t_w} = \frac{15.7-2(0.747)}{0.250} = 56.8$$

$$\frac{h}{t_w} = 56.8 > 35.9, \text{ the web is slender for axial compression. AISC Specification Section E7 applies.}$$

Reduction Factor (Q_a) for Slender Web

$$F_e = \left[\frac{\pi^2 EC_w}{\left(K_z L\right)^2} + GJ\right]\frac{1}{I_x + I_y} = \left[\frac{\pi^2\left(29000\right)\left(565\right)}{\left[8\left(12\right)\right]^2} + 11200\left(0.262\right)\right]\frac{1}{301+9.59} = 65.9 \text{ ksi}$$

$$\frac{F_y}{F_e} = \frac{50 \text{ ksi}}{65.9 \text{ ksi}} = 0.759 < 2.25$$

$$f = F_{cr} = \left[0.658^{\frac{F_y}{F_e}}\right]F_y = \left[0.658^{0.759}\right]50 = 36.4 \text{ ksi}$$

$$b_e = 1.92t\sqrt{\frac{E}{f}}\left[1 - \frac{0.34}{\left(b/t\right)}\sqrt{\frac{E}{f}}\right] = 1.92\left(0.250\right)\sqrt{\frac{29000}{36.4}}\left[1 - \frac{0.34}{56.8}\sqrt{\frac{29000}{36.4}}\right] = 11.3 \text{ in.}$$

$$A_e = 7.68 - (14.2 - 11.3)(0.250) = 6.96 \text{ in.}^2$$

$$Q = Q_a = {}^{A_e}\!/\!_{A_g} = {}^{6.96}\!/\!_{7.68} = 0.906$$

Torsional Buckling about z-z Axis

$$\frac{QF_y}{F_e} = \frac{0.906(50)}{65.9} = 0.687 < 2.25$$

$$F_{cr} = Q\left[0.658^{\frac{QF_y}{F_e}}\right]F_y = 0.906\left(0.658^{0.687}\right)50 = 34.0 \text{ ksi}$$

$$P_n = F_{cr}A_g = 34.0 \text{ ksi}(7.68 \text{ in.}^2) = 261 \text{ kips}$$

LRFD Available Strength

$$\phi_c P_n = 0.9(261 \text{ kips}) = 235 \text{ kips (matches table)}$$

EXAMPLE 3

W-Shape Available Strength Calculation

Given:

The following W14×90 column supports the axial load shown in Figure 3. The column is simply supported and torsionally pinned at its top and bottom. It is restrained against weak-axis translation at mid-height. $(KL)_y$ = 15 ft, $(KL)_x = K_zL$ = 30 ft. Determine the column's available strength (LRFD) in axial compression considering all applicable limit states, and determine whether it is adequate to support the given loads.

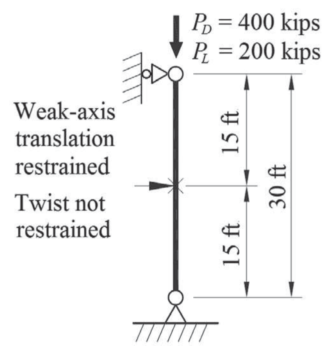

Fig. 3. Example 3.

Solution:

From AISC *Manual* Table 1-1, for W14×90, A_g = 26.5 in.^{2}, r_x = 6.14 in., r_y = 3.70 in.

Local Buckling Classification

From Table 1-1, the W14×90 is nonslender for compression; therefore AISC *Specification* Sections E3 and E4 apply.

Flexural Buckling about Weak (y-y) *Axis*

The effective unbraced length in the *y-y* axis, $(KL)_y$, is 15 ft.

From AISC *Manual* Table 4-1, $\phi_c P_n$ = 1000 kips

Flexural Buckling about Strong (x-x) *Axis*

The effective unbraced length in the *x-x* axis, $(KL)_x$, is 30 ft.

$$(KL)_x / r_x = 30(12)/6.14 = 58.6$$

From AISC *Manual* Table 4-22,

$$\phi_c F_{cr} = 35.0 \text{ ksi}$$

$$\phi_c P_n = \phi_c F_{cr} A_g = (35.0)(26.5) = 928 \text{ kips}$$

Torsional Buckling

The effective length for torsional buckling, $K_z L$, is 30 ft.

From the table in this paper, $\phi_c P_n = 838$ kips.

Torsional buckling controls: $\phi_c P_n = 838$ kips > $P_u = (1.2)400 + 1.6\,(200) = 800$ kips; therefore the column is adequate.

EXAMPLE 4

Constrained Axis Flexural Torsional Buckling Available Strength of W-Shape

Given:

Determine the constrained axis flexural torsional buckling available strength of a W18×35 in axial compression. The constrained axis is located at the intersection of the web centerline and the outside face of flange.

$K_z L = 8.00$ ft	$F_y = 50$ ksi	$E = 29000$ ksi	$G = 11200$ ksi	$A_g = 10.3$ in.^{2}	$d = 17.7$ in.
$t_w = 0.300$ in.	$b_f = 6.00$ in.	$t_f = 0.425$ in.	$k = 0.827$ in.	$I_x = 510$ in.^{4}	$r_x = 7.04$ in.
$I_y = 15.3$ in.^{4}	$r_y = 1.22$ in.	$J = 0.506$ in.^{4}	$C_w = 1140$ in.^{6}		

Solution:

Local Buckling Classification

From AISC *Specification* Table B 4.1a, Case 1, the limiting width-to-thickness ratio for the flange is

$$\lambda_r = 0.56\sqrt{\frac{29000}{50}} = 13.5$$

For the W18×35,

$$\frac{b_f}{2t_f} = \frac{6.00}{2(0.425)} = 7.06$$

Because $\dfrac{b_f}{2t_f} = 7.06 < 13.5$, the flange is nonslender.

From Table B 4.1a, Case 5, the limiting width-to-thickness ratio for the web is

$$\lambda_r = 1.49\sqrt{\frac{29000}{50}} = 35.9$$

For the W18×35,

$$\frac{h}{t_w} = \frac{d-2(k)}{t_w} = \frac{17.7-2(0.827)}{0.300} = 53.5$$

Because $\dfrac{h}{t_w} = 53.5 > 35.9$, the web is slender, and AISC *Specification* Section E7 applies.

$$F_e = 0.9\left[\frac{\pi^2 E\left(C_w + I_y a^2\right)}{\left(K_z L\right)^2} + GJ\right]\frac{1}{\left(r_x{}^2 + r_y{}^2 + a^2\right)A_g}$$

$$= 0.9\left[\frac{\pi^2\left(29000\right)\left(1140 + 15.3\left(\frac{17.7}{2}\right)^2\right)}{\left[8\left(12\right)\right]^2} + 11200\left(0.506\right)\right]\frac{1}{[7.04^2 + 1.22^2 + \left(0.5(17.7)\right)^2](10.3)} = 52.9 \text{ ksi}$$

$$F_y/F_e = 50/52.9 = 0.945 < 2.25$$

$$f = F_{cr} = \left[0.658^{\frac{F_y}{F_e}}\right]F_y = \left(0.658^{0.945}\right)50 = 33.7 \text{ ksi}$$

$$b_e = 1.92t\sqrt{\frac{E}{f}}\left[1 - \frac{0.34}{\left(b/t\right)}\sqrt{\frac{E}{f}}\right] = 1.92\left(0.300\right)\sqrt{\frac{29000}{33.7}}\left[1 - \frac{0.34}{53.5}\sqrt{\frac{29000}{33.7}}\right] = 13.7 \text{ in.}$$

$$A_e = 10.3 - (16.0 - 13.7)(0.300) = 9.61 \text{ in.}^2$$

$$Q = Q_a = A_e/A_g = 9.61/10.3 = 0.933$$

$$QF_y/F_e = 0.933\ (50)\ /\ 52.9 = 0.882 < 2.25$$

$$F_{cr} = Q\left[0.658^{\frac{QF_y}{F_e}}\right]F_y = 0.933\left(0.658^{0.882}\right)50 = 32.2 \text{ ksi}$$

$$P_n = F_{cr}A_g = 32.2\left(10.3\right) = 332 \text{ kips}$$

LRFD Available Strength

$\phi_c P_n = 0.9(331 \text{ kips}) = 299 \text{ kips}$ (matches table)

EXAMPLE 5

Available Strength of W-Shape in Axial Compression

Given:

Determine the available strength (LRFD) of a W14×132 in axial compression (see Figure 4).

$(KL)_x = 40.0$ ft $K_z L = 40.0$ ft $F_y = 50$ ksi $E = 29000$ ksi
$A_g = 38.8$ in.^{2} $r_x = 6.28$ in.

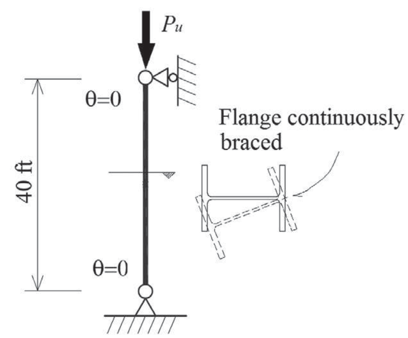

Fig. 4. Example 5.

Solution:

Local Buckling Classification

From Table 1-1, the W14×132 is nonslender for compression; therefore AISC *Specification* Sections E3 and E4 apply.

Flexural Buckling about Strong (x-x) Axis

The effective unbraced length about the *x-x* axis, $(KL)_x$, is 40 ft.

$$(KL)_x/r_x = 40(12)/6.28 = 76.4$$

From AISC *Manual* Table 4-22,

$$\phi_c F_{cr} = 29.4 \text{ ksi}$$

$$\phi_c P_n = \phi_c F_{cr} A_g = 29.4(38.8) = 1140 \text{ kips}$$

Constrained Axis Flexural Torsional Buckling

The effective length for CAFTB, $K_z L$, is 40 ft.

From the table in this paper, $\phi_c P_n = 1090$ kips.

LRFD Design Strength

$\phi_c P_n = 1090$ kips

REFERENCES

AISC (2010), *Specification for Structural Steel Buildings*, ANSI/AISC 360-10, American Institute of Steel Construction, Chicago, IL.

AISC (2011), *Steel Construction Manual*, 14th ed., American Institute of Steel Construction, Chicago, IL.

Allen, H.G. and Bulson, P.S. (1980), *Background to Buckling*, McGraw-Hill Book Company (UK) Limited, Maidenhead, Berkshire, England.

Helwig, T.A. and Yura, J.A. (1999), "Torsional Bracing of Columns," *Journal of Structural Engineering*, ASCE, Vol. 125, No. 5, pp. 547–555.

Salmon, C.G., Johnson, J.E. and Malhas F.A. (2009), *Steel Structures, Design and Behavior*, Pearson Education, Upper Saddle River, NJ.

Timoshenko, S.P. and Gere, J.M. (1961), *Theory of Elastic Stability*, 2nd ed., McGraw-Hill, New York, NY.

F_y = 50 ksi

Table 1.
Torsional Buckling Design Strength in Axial Compression
$\phi_c P_n$, kip

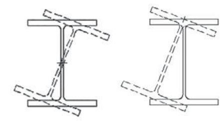

TB CAFTB

Shape		W36×													
lb / ft		**800**		**652**		**529**		**487**		**441**		**395**		**361**	
Design		**TB**	**CAFTB**	**TB**	**CAFTB**	**TB**	**CAFTB**	**TB**	**CAFTB**	**TB**	**CAFTB**	**TB**	**CAFTB**	**TB**	**CAFTB**
Unbraced Length $K_z L$ (ft)	**0**	10600	10600	8640	8640	7020	7020	6430	6430	5850	5850	5220	5220	4770	4770
	6	10500	10400	8500	8460	6900	6860	6320	6290	5740	5710	5120	5090	4680	4650
	7	10400	10300	8460	8390	6860	6810	6280	6230	5710	5660	5090	5050	4650	4610
	8	10400	10300	8410	8320	6820	6750	6240	6180	5670	5610	5050	5000	4610	4560
	9	10300	10200	8360	8250	6770	6680	6200	6120	5630	5550	5010	4950	4580	4510
	10	10300	10100	8310	8170	6720	6610	6150	6050	5580	5490	4970	4890	4540	4460
	11	10200	10000	8260	8090	6680	6540	6110	5980	5540	5420	4930	4820	4490	4400
	12	10200	9910	8210	8010	6630	6460	6060	5910	5490	5350	4880	4760	4450	4340
	13	10100	9820	8170	7920	6580	6380	6010	5830	5450	5280	4840	4690	4410	4270
	14	10100	9730	8120	7830	6530	6300	5960	5750	5400	5210	4790	4620	4360	4210
	15	10000	9640	8070	7750	6490	6220	5920	5670	5350	5130	4750	4550	4320	4140
	16	10000	9550	8030	7660	6440	6130	5870	5590	5310	5050	4700	4470	4270	4070
	17	9960	9460	7990	7580	6400	6050	5830	5510	5260	4970	4660	4400	4230	4000
	18	9930	9380	7950	7490	6360	5970	5780	5430	5220	4900	4610	4330	4180	3920
	19	9890	9300	7920	7410	6310	5890	5740	5360	5170	4820	4570	4250	4140	3850
	20	9860	9220	7880	7330	6280	5810	5700	5280	5130	4740	4530	4180	4100	3780
	22	9810	9070	7820	7180	6200	5660	5630	5130	5060	4590	4450	4030	4010	3640
	24	9770	8940	7760	7040	6140	5510	5560	4980	4980	4450	4370	3890	3940	3500
	26	9730	8820	7720	6910	6080	5370	5500	4850	4920	4310	4300	3760	3870	3370
	28	9690	8700	7670	6790	6030	5250	5450	4720	4860	4180	4240	3630	3800	3240
	30	9660	8610	7640	6680	5990	5130	5400	4600	4810	4060	4180	3510	3740	3120
	32	9640	8520	7610	6580	5950	5020	5350	4490	4760	3950	4130	3390	3680	3010
	34	9620	8440	7580	6490	5910	4920	5310	4390	4720	3850	4080	3290	3630	2900
	36	9600	8360	7550	6410	5880	4830	5280	4300	4680	3750	4040	3190	3590	2800
	38	9580	8300	7530	6330	5850	4750	5250	4210	4640	3660	4000	3100	3540	2710
	40	9570	8240	7510	6270	5820	4670	5220	4140	4610	3580	3970	3020	3510	2630

F_y = 50 ksi

Table 1. (continued)
Torsional Buckling Design Strength in Axial Compression
$\phi_c P_n$, kip

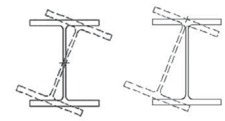

TB CAFTB

Shape		W36×													
lb / ft		330		302		282		262		247		231		256	
Design		TB	CAFTB	TB	CAFTB	TB	CAFTB	TB	CAFTB	TB	CAFTB	TB	CAFTB	TB	CAFTB
Unbraced Length $K_z L$ (ft)	0	4360	4360	4000	4000	3720	3720	3410	3410	3170	3170	2940	2940	3390	3390
	6	4270	4250	3930	3900	3650	3630	3350	3340	3110	3100	2890	2870	3270	3220
	7	4250	4210	3900	3870	3630	3600	3330	3310	3090	3070	2870	2850	3230	3170
	8	4210	4170	3870	3830	3600	3560	3310	3280	3070	3040	2850	2830	3180	3100
	9	4180	4120	3840	3780	3570	3520	3280	3240	3050	3010	2830	2800	3140	3040
	10	4140	4070	3800	3740	3540	3480	3260	3210	3020	2980	2800	2760	3090	2970
	11	4100	4020	3760	3690	3500	3430	3230	3170	2990	2940	2780	2730	3040	2890
	12	4060	3960	3720	3630	3460	3380	3190	3120	2960	2900	2750	2690	2990	2820
	13	4020	3900	3680	3570	3420	3320	3160	3080	2930	2850	2720	2650	2940	2740
	14	3970	3830	3640	3510	3380	3260	3130	3030	2900	2810	2690	2610	2890	2660
	15	3930	3770	3600	3450	3340	3210	3090	2970	2860	2760	2660	2560	2850	2580
	16	3890	3700	3550	3390	3300	3140	3050	2910	2830	2710	2630	2520	2800	2500
	17	3840	3640	3510	3320	3250	3080	3020	2850	2790	2660	2590	2470	2750	2420
	18	3800	3570	3470	3260	3210	3020	2980	2790	2760	2610	2560	2420	2710	2350
	19	3750	3500	3420	3190	3170	2960	2930	2730	2720	2560	2520	2370	2670	2270
	20	3710	3430	3380	3130	3130	2890	2890	2670	2690	2500	2490	2320	2630	2200
	22	3630	3290	3300	2990	3040	2760	2810	2550	2610	2380	2420	2210	2550	2060
	24	3550	3160	3220	2860	2960	2640	2730	2420	2540	2260	2350	2100	2490	1940
	26	3480	3030	3140	2740	2890	2510	2650	2300	2460	2140	2280	1990	2430	1820
	28	3410	2900	3070	2610	2820	2400	2580	2180	2390	2030	2210	1880	2370	1710
	30	3340	2790	3000	2500	2750	2280	2510	2070	2320	1920	2150	1770	2330	1620
	32	3290	2670	2940	2390	2690	2170	2440	1960	2250	1810	2080	1670	2280	1530
	34	3230	2570	2880	2280	2630	2070	2380	1860	2190	1710	2020	1570	2250	1460
	36	3180	2470	2830	2180	2570	1970	2330	1770	2130	1620	1960	1480	2210	1390
	38	3140	2380	2780	2090	2520	1880	2270	1680	2080	1530	1900	1390	2180	1320
	40	3100	2290	2740	2000	2470	1800	2220	1590	2030	1450	1850	1310	2150	1270

F_y = 50 ksi

Table 1. (continued)
Torsional Buckling Design Strength in Axial Compression
$\phi_c P_n$, kip

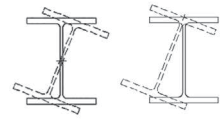

TB CAFTB

Shape		W36×													
lb / ft		**232**		**210**		**194**		**182**		**170**		**160**		**150**	
Design		**TB**	**CAFTB**	**TB**	**CAFTB**	**TB**	**CAFTB**	**TB**	**CAFTB**	**TB**	**CAFTB**	**TB**	**CAFTB**	**TB**	**CAFTB**
Unbraced Length $K_z L$ (ft)	**0**	3020	3020	2710	2710	2430	2430	2250	2250	2050	2050	1900	1900	1760	1760
	6	2920	2890	2620	2590	2350	2330	2180	2150	1990	1970	1840	1820	1710	1690
	7	2890	2840	2590	2550	2330	2290	2150	2120	1970	1940	1820	1790	1690	1660
	8	2860	2800	2560	2500	2300	2250	2130	2080	1950	1900	1800	1760	1670	1640
	9	2820	2730	2530	2450	2270	2210	2100	2040	1920	1870	1780	1730	1650	1600
	10	2780	2670	2490	2400	2240	2160	2070	2000	1890	1830	1750	1690	1620	1570
	11	2730	2600	2450	2340	2200	2110	2040	1950	1860	1780	1720	1650	1600	1530
	12	2690	2530	2410	2280	2170	2050	2000	1900	1830	1740	1690	1610	1570	1490
	13	2640	2450	2370	2210	2130	1990	1970	1850	1800	1690	1660	1560	1540	1450
	14	2590	2380	2330	2140	2090	1940	1930	1790	1760	1640	1630	1510	1510	1400
	15	2540	2300	2290	2060	2050	1870	1890	1740	1730	1580	1600	1460	1480	1360
	16	2500	2230	2240	1990	2010	1810	1860	1680	1690	1530	1560	1410	1450	1310
	17	2450	2150	2190	1920	1980	1740	1820	1620	1660	1480	1530	1360	1420	1260
	18	2410	2080	2150	1850	1940	1680	1780	1560	1620	1420	1500	1310	1380	1210
	19	2370	2010	2110	1780	1900	1610	1750	1500	1590	1370	1460	1260	1350	1160
	20	2330	1940	2060	1710	1860	1540	1710	1440	1560	1310	1430	1200	1320	1110
	22	2250	1810	1980	1580	1790	1420	1640	1310	1490	1200	1360	1100	1250	1010
	24	2180	1680	1910	1460	1720	1300	1580	1200	1420	1090	1300	993	1190	909
	26	2120	1570	1840	1340	1650	1190	1510	1090	1360	986	1240	895	1130	813
	28	2060	1470	1780	1240	1590	1090	1450	997	1310	893	1180	803	1080	724
	30	2010	1370	1730	1150	1530	1000	1390	908	1250	807	1130	723	1020	650
	32	1960	1290	1680	1060	1480	919	1340	831	1200	736	1080	658	974	590
	34	1920	1210	1630	987	1430	851	1290	767	1150	677	1030	604	927	540
	36	1890	1140	1590	924	1390	793	1250	713	1110	628	990	558	883	498
	38	1860	1080	1560	870	1350	745	1210	667	1070	586	950	520	843	462
	40	1830	1030	1520	824	1320	703	1180	629	1030	551	914	487	806	432

F_y = 50 ksi

Table 1. (continued)
Torsional Buckling Design Strength in Axial Compression
$\phi_c P_n$, kip

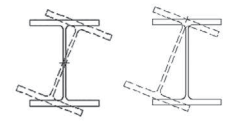
TB CAFTB

Shape	W36×		W33×											
lb / ft	135		387		354		318		291		263		241	
Design	TB	CAFTB	TB	CAFTB	TB	CAFTB	TB	CAFTB	TB	CAFTB	TB	CAFTB	TB	CAFTB
Unbraced Length $K_z L$ (ft)														
0	1550	1550	5130	5130	4680	4680	4220	4220	3850	3850	3480	3480	3190	3190
6	1510	1490	5030	5000	4580	4560	4130	4100	3770	3750	3410	3390	3130	3110
7	1490	1460	4990	4950	4550	4520	4100	4060	3740	3710	3380	3350	3110	3080
8	1470	1440	4960	4900	4520	4470	4070	4020	3710	3670	3350	3320	3080	3040
9	1450	1410	4920	4850	4480	4420	4030	3970	3680	3620	3320	3270	3050	3000
10	1430	1380	4880	4790	4440	4360	3990	3920	3640	3580	3290	3230	3020	2960
11	1400	1340	4840	4730	4400	4300	3960	3870	3610	3520	3250	3180	2980	2920
12	1380	1300	4790	4660	4360	4240	3920	3810	3570	3470	3210	3130	2950	2870
13	1350	1270	4750	4590	4320	4180	3870	3750	3530	3410	3180	3080	2910	2820
14	1330	1220	4710	4530	4280	4110	3830	3680	3490	3350	3140	3020	2870	2760
15	1300	1180	4670	4460	4230	4040	3790	3620	3450	3290	3100	2960	2840	2710
16	1270	1140	4620	4380	4190	3980	3750	3560	3410	3230	3060	2910	2800	2650
17	1240	1090	4580	4310	4150	3910	3710	3490	3370	3170	3020	2850	2760	2600
18	1210	1040	4540	4240	4110	3840	3670	3420	3330	3100	2980	2790	2720	2540
19	1180	998	4510	4170	4070	3770	3630	3360	3290	3040	2940	2730	2680	2480
20	1150	951	4470	4100	4040	3710	3590	3290	3250	2980	2900	2670	2640	2420
22	1080	856	4400	3970	3970	3570	3520	3170	3170	2850	2830	2550	2570	2310
24	1020	763	4340	3840	3900	3450	3450	3040	3100	2730	2760	2430	2490	2190
26	966	672	4280	3720	3840	3330	3390	2920	3040	2620	2690	2320	2430	2080
28	910	594	4230	3610	3790	3220	3330	2810	2980	2510	2630	2210	2360	1980
30	857	531	4190	3500	3740	3110	3280	2700	2920	2400	2570	2110	2300	1880
32	808	480	4150	3410	3700	3010	3230	2610	2870	2300	2520	2010	2240	1780
34	760	437	4110	3320	3660	2920	3190	2510	2830	2210	2470	1920	2190	1690
36	717	402	4080	3230	3620	2840	3150	2430	2790	2130	2420	1840	2140	1600
38	676	372	4050	3160	3590	2760	3110	2350	2750	2050	2380	1760	2100	1530
40	640	346	4020	3090	3560	2690	3080	2280	2710	1970	2340	1690	2060	1450

F_y = 50 ksi

Table 1. (continued)
Torsional Buckling Design Strength in Axial Compression
$\phi_c P_n$, kip

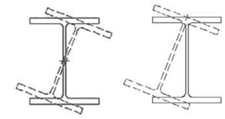

TB CAFTB

Shape	W33×													
lb / ft	221		201		169		152		141		130		118	
Design	TB	CAFTB	TB	CAFTB	TB	CAFTB	TB	CAFTB	TB	CAFTB	TB	CAFTB	TB	CAFTB
Unbraced Length $K_z L$ (ft)														
0	2880	2880	2550	2550	2090	2090	1860	1860	1690	1690	1530	1530	1350	1350
6	2830	2810	2510	2490	2020	1990	1800	1770	1630	1610	1480	1460	1310	1290
7	2810	2790	2490	2470	1990	1960	1780	1750	1610	1590	1460	1440	1290	1270
8	2790	2760	2470	2450	1970	1920	1750	1710	1590	1560	1440	1410	1280	1250
9	2760	2730	2450	2420	1940	1880	1730	1680	1570	1520	1420	1380	1260	1220
10	2740	2690	2430	2390	1910	1840	1700	1640	1540	1490	1400	1350	1240	1190
11	2710	2650	2400	2350	1880	1790	1670	1600	1520	1450	1370	1310	1210	1160
12	2680	2610	2370	2320	1850	1750	1640	1550	1490	1410	1350	1280	1190	1120
13	2650	2570	2350	2280	1810	1700	1610	1510	1460	1360	1320	1240	1170	1090
14	2620	2530	2320	2240	1780	1640	1580	1460	1430	1320	1290	1190	1140	1050
15	2580	2480	2290	2200	1750	1590	1550	1410	1400	1270	1260	1150	1110	1010
16	2550	2420	2260	2160	1710	1540	1510	1360	1370	1230	1240	1110	1090	971
17	2520	2370	2220	2110	1680	1480	1480	1310	1340	1180	1210	1060	1060	930
18	2480	2310	2190	2070	1650	1430	1450	1260	1310	1130	1180	1020	1030	888
19	2440	2260	2160	2020	1610	1370	1420	1210	1280	1080	1150	974	1010	846
20	2400	2200	2130	1970	1580	1310	1390	1160	1250	1040	1120	929	978	803
22	2330	2090	2060	1870	1520	1200	1330	1050	1190	940	1060	839	923	719
24	2250	1980	2000	1770	1460	1100	1270	954	1130	846	1010	750	869	637
26	2180	1870	1940	1660	1410	1010	1210	865	1080	760	952	667	818	559
28	2120	1770	1870	1560	1360	928	1160	782	1030	681	902	593	769	495
30	2060	1670	1810	1470	1310	851	1120	709	982	614	855	533	722	443
32	2000	1580	1750	1380	1270	784	1070	648	937	560	811	484	679	401
34	1940	1490	1690	1290	1230	728	1030	598	896	515	770	444	638	366
36	1890	1400	1640	1210	1200	681	994	556	859	478	732	410	600	337
38	1850	1330	1600	1140	1170	641	961	521	825	446	698	381	566	312
40	1800	1250	1550	1070	1140	607	932	491	795	419	667	356	537	291

F_y = 50 ksi

Table 1. (continued)
Torsional Buckling Design Strength in Axial Compression
$\phi_c P_n$, kip

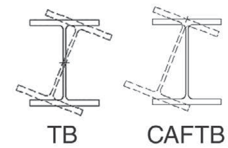

Shape		W30×													
lb/ft		391		357		326		292		261		235		211	
Design		TB	CAFTB	TB	CAFTB	TB	CAFTB	TB	CAFTB	TB	CAFTB	TB	CAFTB	TB	CAFTB
Unbraced Length $K_z L$ (ft)	0	5170	5170	4720	4720	4320	4320	3870	3870	3460	3460	3120	3120	2800	2800
	6	5070	5040	4620	4590	4220	4190	3780	3760	3380	3360	3040	3020	2740	2720
	7	5030	4990	4590	4550	4190	4150	3750	3720	3360	3330	3020	2990	2710	2690
	8	5000	4940	4560	4500	4160	4110	3720	3680	3330	3290	2990	2960	2690	2650
	9	4960	4880	4520	4450	4120	4060	3690	3630	3300	3240	2960	2920	2660	2620
	10	4920	4820	4480	4390	4080	4000	3650	3580	3260	3200	2930	2870	2630	2580
	11	4880	4760	4440	4330	4050	3950	3620	3530	3230	3150	2900	2830	2600	2540
	12	4840	4700	4400	4270	4010	3890	3580	3470	3190	3100	2860	2780	2570	2490
	13	4800	4630	4370	4210	3970	3830	3540	3420	3150	3040	2830	2730	2530	2440
	14	4770	4560	4330	4150	3930	3770	3500	3360	3120	2990	2790	2680	2500	2390
	15	4730	4500	4290	4080	3900	3700	3470	3300	3080	2930	2760	2620	2460	2340
	16	4690	4430	4260	4020	3860	3640	3430	3240	3040	2870	2720	2570	2430	2290
	17	4660	4370	4220	3960	3820	3580	3400	3180	3010	2810	2690	2510	2390	2240
	18	4630	4300	4190	3890	3790	3520	3360	3120	2970	2760	2650	2460	2360	2190
	19	4600	4240	4160	3830	3760	3460	3330	3060	2940	2700	2620	2410	2320	2140
	20	4570	4180	4130	3770	3730	3400	3300	3000	2910	2640	2580	2350	2290	2090
	22	4520	4070	4070	3660	3670	3280	3240	2890	2840	2530	2520	2240	2220	1980
	24	4470	3960	4020	3550	3620	3170	3180	2780	2790	2420	2460	2140	2160	1880
	26	4430	3860	3980	3450	3570	3070	3130	2680	2730	2320	2400	2040	2100	1780
	28	4400	3770	3940	3350	3530	2980	3080	2580	2680	2230	2350	1950	2050	1690
	30	4370	3680	3910	3270	3490	2890	3040	2500	2640	2140	2310	1860	2000	1610
	32	4340	3610	3880	3190	3460	2810	3010	2410	2600	2060	2260	1780	1950	1520
	34	4320	3540	3850	3120	3430	2740	2970	2340	2560	1980	2220	1700	1910	1450
	36	4300	3480	3830	3060	3410	2670	2940	2270	2530	1910	2190	1630	1870	1380
	38	4280	3420	3810	3000	3380	2610	2920	2210	2500	1840	2160	1570	1840	1310
	40	4260	3370	3790	2940	3360	2560	2890	2150	2470	1790	2130	1510	1800	1250

F_y = 50 ksi		Table 1. (continued) Torsional Buckling Design Strength in Axial Compression $\phi_c P_n$, kip												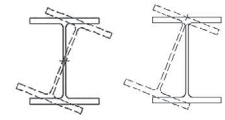	
Shape		**W30×**													
lb / ft		**191**		**173**		**148**		**132**		**124**		**116**		**108**	
Design		**TB**	**CAFTB**	**TB**	**CAFTB**	**TB**	**CAFTB**	**TB**	**CAFTB**	**TB**	**CAFTB**	**TB**	**CAFTB**	**TB**	**CAFTB**
Unbraced Length $K_z L$ (ft)	**0**	2490	2490	2220	2220	1880	1880	1640	1640	1520	1520	1400	1400	1280	1280
	6	2440	2420	2170	2160	1800	1770	1570	1550	1460	1430	1350	1330	1230	1210
	7	2420	2400	2150	2140	1780	1740	1550	1520	1440	1410	1330	1300	1210	1190
	8	2400	2370	2130	2110	1750	1700	1530	1480	1410	1370	1310	1270	1190	1160
	9	2380	2340	2110	2090	1720	1660	1500	1450	1390	1340	1280	1240	1170	1130
	10	2350	2310	2090	2060	1690	1610	1470	1410	1360	1300	1260	1200	1150	1090
	11	2320	2280	2070	2020	1660	1560	1440	1360	1340	1260	1230	1160	1120	1060
	12	2300	2240	2040	1990	1630	1510	1410	1320	1310	1220	1210	1120	1100	1020
	13	2270	2190	2020	1960	1590	1460	1380	1270	1280	1180	1180	1080	1070	982
	14	2240	2150	1990	1920	1560	1410	1350	1220	1250	1130	1150	1040	1050	941
	15	2200	2100	1960	1880	1530	1350	1320	1180	1220	1090	1120	995	1020	900
	16	2170	2050	1940	1840	1500	1290	1290	1120	1190	1040	1090	950	991	858
	17	2140	2000	1910	1800	1470	1240	1260	1070	1160	993	1070	906	964	815
	18	2100	1960	1880	1760	1440	1180	1230	1020	1130	944	1040	861	937	773
	19	2070	1910	1850	1710	1410	1130	1200	971	1100	896	1010	814	910	730
	20	2040	1860	1820	1660	1380	1080	1180	923	1080	849	983	769	884	686
	22	1970	1760	1760	1570	1320	990	1120	833	1020	762	931	684	832	605
	24	1910	1660	1700	1480	1270	905	1070	751	976	682	882	607	784	530
	26	1850	1570	1640	1390	1230	829	1020	677	928	609	836	538	739	468
	28	1790	1480	1580	1300	1190	761	978	611	885	549	792	483	695	418
	30	1740	1400	1530	1220	1150	701	941	559	846	499	753	438	655	378
	32	1690	1320	1480	1150	1120	652	907	515	811	459	718	402	620	345
	34	1650	1240	1440	1070	1090	611	877	480	781	426	686	371	588	318
	36	1610	1180	1390	1010	1070	576	850	450	753	398	658	346	560	295
	38	1570	1110	1360	945	1050	547	826	424	728	374	633	325	533	276
	40	1540	1050	1320	887	1030	522	805	402	706	354	611	306	511	260

F_y = 50 ksi		**Table 1. (continued) Torsional Buckling Design Strength in Axial Compression $\phi_c P_n$, kip**													
Shape		**W30×**				**W27×**									
lb / ft		**99**		**90**		**539**		**368**		**336**		**307**		**281**	
Design		**TB**	**CAFTB**	**TB**	**CAFTB**	**TB**	**CAFTB**	**TB**	**CAFTB**	**TB**	**CAFTB**	**TB**	**CAFTB**	**TB**	**CAFTB**
Unbraced Length $K_z L$ (ft)	**0**	1150	1150	1010	1010	7150	7150	4900	4900	4460	4460	4060	4060	3740	3740
	6	1100	1080	968	952	7020	6970	4790	4760	4360	4330	3960	3930	3650	3620
	7	1080	1060	954	933	6980	6910	4760	4710	4330	4280	3930	3890	3620	3580
	8	1070	1040	939	911	6940	6850	4730	4660	4290	4230	3900	3840	3590	3540
	9	1050	1010	922	887	6910	6780	4690	4600	4260	4180	3860	3790	3550	3490
	10	1030	978	903	861	6870	6710	4650	4550	4220	4130	3830	3740	3520	3440
	11	1000	945	884	833	6840	6650	4620	4490	4190	4070	3790	3690	3480	3390
	12	982	911	863	803	6810	6580	4580	4430	4150	4010	3760	3630	3450	3330
	13	958	876	842	772	6780	6520	4550	4360	4120	3950	3730	3570	3420	3280
	14	933	838	820	739	6750	6450	4520	4300	4090	3890	3690	3520	3380	3220
	15	907	800	797	705	6730	6390	4490	4240	4060	3830	3660	3460	3350	3160
	16	882	761	774	671	6710	6340	4460	4190	4030	3780	3630	3400	3320	3110
	17	856	722	751	636	6690	6280	4440	4130	4000	3720	3610	3350	3290	3050
	18	830	682	727	601	6670	6230	4410	4070	3980	3670	3580	3290	3270	3000
	19	805	643	704	565	6650	6180	4390	4020	3950	3610	3550	3240	3240	2950
	20	780	603	680	530	6640	6130	4370	3970	3930	3560	3530	3190	3210	2900
	22	730	526	634	461	6610	6050	4330	3870	3890	3460	3490	3090	3170	2800
	24	683	457	590	397	6590	5980	4300	3790	3850	3380	3450	3000	3130	2710
	26	639	401	548	348	6570	5910	4270	3710	3820	3300	3420	2920	3090	2620
	28	597	357	509	309	6560	5860	4250	3640	3800	3220	3390	2850	3060	2550
	30	558	322	472	277	6550	5810	4230	3580	3770	3160	3360	2780	3030	2480
	32	523	293	437	251	6540	5760	4210	3520	3750	3100	3340	2720	3010	2410
	34	491	269	407	230	6530	5730	4190	3470	3740	3050	3320	2660	2990	2360
	36	463	249	382	212	6520	5690	4180	3420	3720	3000	3300	2620	2970	2310
	38	440	232	361	196	6510	5660	4170	3380	3710	2960	3290	2570	2950	2260
	40	420	217	343	183	6510	5640	4160	3350	3700	2920	3270	2530	2940	2220

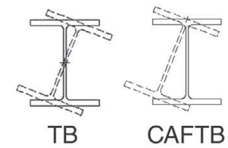

F_y = 50 ksi	Table 1. (continued) Torsional Buckling Design Strength in Axial Compression $\phi_c P_n$, kip													
Shape	**W27×**													
lb / ft	**258**		**235**		**217**		**194**		**178**		**161**		**146**	
Design	**TB**	**CAFTB**	**TB**	**CAFTB**	**TB**	**CAFTB**	**TB**	**CAFTB**	**TB**	**CAFTB**	**TB**	**CAFTB**	**TB**	**CAFTB**
Unbraced Length $K_z L$ (ft)														
0	3420	3420	3120	3120	2880	2880	2570	2570	2360	2360	2130	2130	1900	1900
6	3340	3310	3040	3020	2800	2780	2500	2480	2300	2280	2080	2070	1850	1840
7	3310	3280	3020	2980	2770	2750	2480	2450	2280	2250	2060	2040	1830	1820
8	3280	3230	2990	2950	2750	2710	2450	2420	2250	2220	2040	2010	1820	1790
9	3250	3190	2960	2900	2720	2670	2420	2380	2220	2180	2010	1980	1800	1770
10	3210	3140	2920	2860	2690	2630	2390	2340	2200	2150	1990	1940	1780	1740
11	3180	3090	2890	2810	2660	2580	2360	2300	2170	2110	1960	1910	1750	1710
12	3150	3040	2860	2760	2620	2530	2330	2260	2140	2060	1930	1870	1730	1680
13	3110	2990	2830	2710	2590	2490	2300	2210	2110	2020	1900	1830	1700	1640
14	3080	2930	2790	2660	2560	2440	2270	2160	2080	1980	1870	1780	1680	1610
15	3050	2880	2760	2610	2530	2390	2240	2120	2040	1930	1840	1740	1650	1570
16	3020	2820	2730	2550	2490	2340	2210	2070	2010	1880	1810	1700	1630	1530
17	2990	2770	2700	2500	2460	2280	2180	2020	1980	1840	1780	1650	1600	1480
18	2960	2720	2670	2450	2430	2230	2150	1970	1950	1790	1750	1610	1570	1440
19	2930	2660	2640	2400	2400	2190	2120	1920	1920	1740	1720	1560	1540	1400
20	2900	2610	2610	2350	2380	2140	2090	1880	1890	1700	1690	1520	1510	1360
22	2860	2520	2560	2250	2320	2040	2030	1790	1840	1600	1640	1430	1460	1270
24	2810	2430	2520	2160	2280	1950	1980	1700	1780	1520	1580	1350	1400	1190
26	2770	2340	2470	2080	2230	1870	1940	1620	1740	1440	1530	1270	1350	1120
28	2740	2260	2440	2000	2200	1790	1900	1540	1690	1360	1490	1190	1310	1040
30	2710	2190	2400	1930	2160	1720	1860	1470	1650	1290	1450	1120	1260	975
32	2680	2130	2370	1860	2130	1650	1830	1400	1610	1220	1410	1060	1220	911
34	2660	2070	2350	1800	2100	1590	1790	1340	1580	1160	1370	997	1190	852
36	2640	2010	2330	1740	2080	1540	1770	1280	1550	1100	1340	941	1150	798
38	2620	1970	2300	1690	2050	1490	1740	1230	1520	1050	1310	889	1120	747
40	2600	1920	2290	1650	2030	1440	1720	1190	1500	1000	1280	842	1090	701

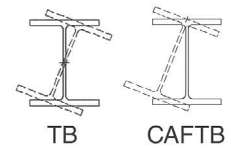

F_y = 50 ksi

Table 1. (continued)
Torsional Buckling Design Strength in Axial Compression
$\phi_c P_n$, kip

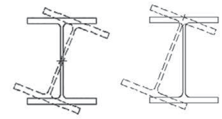

TB CAFTB

Shape	W27×										W24×			
lb / ft	129		114		102		94		84		370		335	
Design	TB	CAFTB	TB	CAFTB	TB	CAFTB	TB	CAFTB	TB	CAFTB	TB	CAFTB	TB	CAFTB
Unbraced Length $K_z L$ (ft): 0	1650	1650	1440	1440	1240	1240	1120	1120	982	982	4900	4900	4420	4420
6	1580	1550	1370	1350	1190	1170	1080	1060	939	924	4790	4740	4310	4270
7	1550	1520	1350	1320	1170	1150	1060	1040	924	904	4750	4690	4280	4230
8	1530	1480	1330	1290	1150	1120	1040	1010	908	881	4720	4640	4250	4180
9	1500	1440	1300	1250	1130	1090	1020	981	890	856	4690	4590	4220	4120
10	1470	1400	1280	1220	1110	1050	1000	951	871	829	4660	4530	4190	4070
11	1440	1350	1250	1180	1080	1020	977	919	851	800	4630	4470	4160	4010
12	1410	1300	1220	1140	1060	981	954	885	830	770	4600	4420	4130	3960
13	1380	1250	1200	1090	1030	943	931	849	808	738	4580	4360	4100	3900
14	1350	1200	1170	1050	1010	904	907	813	786	705	4560	4310	4080	3850
15	1320	1150	1140	1000	982	865	882	776	763	672	4540	4260	4060	3800
16	1290	1100	1110	953	957	825	858	739	740	638	4520	4210	4040	3750
17	1260	1050	1090	908	932	785	834	701	718	603	4500	4160	4020	3710
18	1240	1010	1060	863	907	744	810	664	695	569	4480	4120	4000	3660
19	1210	964	1040	820	883	704	787	627	673	535	4470	4080	3980	3620
20	1180	922	1010	779	860	665	764	590	651	502	4460	4040	3970	3580
22	1140	843	960	703	816	593	721	520	609	437	4430	3970	3940	3510
24	1100	773	917	634	775	528	680	457	569	379	4410	3910	3920	3440
26	1060	711	878	572	736	469	643	405	532	334	4400	3850	3910	3390
28	1030	655	844	519	701	423	607	364	497	299	4390	3810	3890	3340
30	1000	606	813	476	669	386	575	331	465	270	4370	3770	3880	3290
32	979	566	786	441	641	356	546	303	437	246	4360	3730	3870	3260
34	958	533	762	412	617	331	521	281	411	227	4360	3700	3860	3220
36	939	505	741	388	595	310	498	262	389	210	4350	3670	3850	3190
38	922	481	722	367	575	292	478	246	370	197	4340	3650	3840	3170
40	908	461	706	350	558	277	460	232	354	185	4340	3630	3840	3140

F_y = 50 ksi

Table 1. (continued)
Torsional Buckling Design Strength in Axial Compression
$\phi_c P_n$, kip

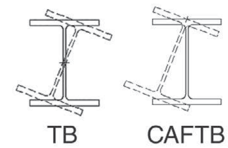

Shape	W24×													
lb / ft	306		279		250		229		207		192		176	
Design	TB	CAFTB	TB	CAFTB	TB	CAFTB	TB	CAFTB	TB	CAFTB	TB	CAFTB	TB	CAFTB
Unbraced Length $K_z L$ (ft)														
0	4040	4040	3690	3690	3310	3310	3020	3020	2730	2730	2540	2540	2330	2330
6	3930	3900	3590	3550	3210	3190	2940	2910	2650	2630	2460	2440	2250	2230
7	3900	3850	3560	3510	3190	3150	2910	2870	2620	2590	2440	2410	2230	2200
8	3870	3800	3520	3470	3160	3100	2880	2830	2600	2550	2410	2370	2200	2170
9	3840	3750	3490	3420	3120	3060	2850	2790	2570	2510	2380	2340	2180	2130
10	3810	3700	3460	3370	3090	3010	2820	2740	2540	2470	2360	2290	2150	2090
11	3780	3650	3430	3310	3060	2960	2790	2690	2510	2420	2330	2250	2120	2050
12	3750	3590	3400	3260	3030	2910	2760	2640	2480	2380	2300	2200	2090	2010
13	3720	3540	3380	3210	3010	2860	2730	2590	2450	2330	2270	2160	2060	1960
14	3690	3490	3350	3160	2980	2810	2700	2550	2420	2280	2240	2110	2030	1920
15	3670	3440	3320	3110	2950	2760	2680	2500	2390	2230	2210	2070	2010	1870
16	3650	3390	3300	3060	2930	2710	2650	2450	2370	2190	2180	2020	1980	1830
17	3630	3340	3280	3010	2910	2660	2630	2400	2340	2140	2160	1980	1950	1780
18	3610	3290	3260	2970	2880	2620	2600	2360	2320	2090	2130	1930	1930	1740
19	3590	3250	3240	2920	2860	2580	2580	2310	2300	2050	2110	1890	1900	1700
20	3580	3210	3230	2880	2850	2530	2560	2270	2280	2010	2090	1850	1880	1660
22	3550	3140	3190	2810	2810	2450	2530	2190	2240	1930	2050	1770	1840	1580
24	3530	3070	3170	2740	2780	2380	2500	2120	2200	1850	2010	1690	1800	1500
26	3510	3010	3150	2670	2760	2320	2470	2050	2170	1790	1980	1620	1770	1430
28	3490	2960	3130	2620	2740	2260	2450	1990	2150	1730	1950	1560	1740	1370
30	3480	2910	3110	2570	2720	2210	2420	1940	2120	1670	1930	1500	1710	1310
32	3460	2870	3100	2530	2700	2160	2410	1890	2100	1620	1910	1450	1690	1260
34	3450	2830	3090	2490	2690	2120	2390	1850	2090	1580	1890	1410	1670	1220
36	3440	2800	3080	2460	2680	2090	2380	1810	2070	1540	1870	1360	1650	1170
38	3430	2770	3070	2420	2670	2050	2370	1770	2060	1500	1850	1330	1630	1130
40	3430	2750	3060	2400	2660	2030	2350	1740	2040	1470	1840	1290	1610	1100

F_y = 50 ksi

Table 1. (continued)
Torsional Buckling Design Strength in Axial Compression
$\phi_c P_n$, kip

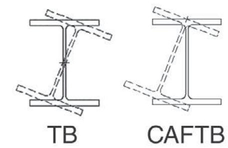

Shape		**W24×**													
lb / ft		**162**		**146**		**131**		**117**		**104**		**103**		**94**	
Design		**TB**	**CAFTB**	**TB**	**CAFTB**	**TB**	**CAFTB**	**TB**	**CAFTB**	**TB**	**CAFTB**	**TB**	**CAFTB**	**TB**	**CAFTB**
Unbraced Length $K_z L$ (ft)	**0**	2150	2150	1930	1930	1740	1740	1510	1510	1320	1320	1330	1330	1190	1190
	6	2080	2070	1870	1860	1680	1660	1470	1460	1280	1270	1260	1230	1130	1110
	7	2060	2040	1850	1830	1660	1640	1450	1440	1270	1250	1230	1200	1110	1080
	8	2040	2000	1830	1800	1640	1610	1440	1420	1250	1230	1210	1160	1090	1040
	9	2010	1970	1800	1770	1620	1580	1420	1390	1230	1210	1180	1120	1060	1010
	10	1980	1930	1780	1730	1590	1550	1400	1370	1220	1190	1160	1080	1040	974
	11	1960	1890	1750	1690	1570	1510	1380	1340	1200	1160	1130	1030	1010	936
	12	1930	1850	1720	1660	1540	1480	1350	1310	1180	1140	1100	989	988	896
	13	1900	1810	1700	1620	1510	1440	1330	1280	1160	1110	1070	944	964	853
	14	1870	1770	1670	1580	1490	1400	1310	1240	1140	1080	1050	899	939	811
	15	1840	1720	1640	1530	1460	1360	1290	1200	1120	1050	1020	856	916	769
	16	1820	1680	1610	1490	1430	1320	1260	1170	1100	1020	996	815	891	729
	17	1790	1640	1590	1450	1410	1280	1240	1130	1070	990	973	775	867	691
	18	1760	1600	1560	1410	1380	1250	1210	1090	1050	959	951	738	844	654
	19	1740	1550	1540	1370	1350	1210	1180	1060	1030	926	930	702	823	619
	20	1710	1510	1510	1330	1330	1170	1160	1020	1010	891	911	669	802	586
	22	1670	1430	1470	1250	1280	1090	1110	950	965	824	876	607	765	526
	24	1630	1360	1420	1180	1240	1020	1070	883	923	760	845	554	733	473
	26	1590	1290	1380	1110	1200	956	1030	819	881	699	819	506	704	428
	28	1560	1230	1350	1050	1160	894	988	760	842	642	796	467	680	392
	30	1530	1170	1320	993	1130	837	953	705	806	590	776	435	658	363
	32	1500	1120	1290	940	1100	785	920	654	773	542	759	409	639	339
	34	1480	1070	1260	892	1070	737	891	608	743	496	744	388	623	320
	36	1460	1020	1240	848	1040	694	865	565	716	459	731	370	608	303
	38	1440	985	1220	808	1020	653	840	528	690	427	719	355	595	290
	40	1420	949	1200	772	999	617	818	497	667	399	709	342	584	278

F_y = 50 ksi	Table 1. (continued) Torsional Buckling Design Strength in Axial Compression $\phi_c P_n$, kip													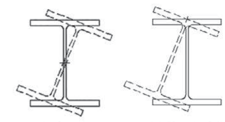
Shape	**W24×**										**W21×**			
lb / ft	**84**		**76**		**68**		**62**		**55**		**201**		**182**	
Design	**TB**	**CAFTB**	**TB**	**CAFTB**	**TB**	**CAFTB**	**TB**	**CAFTB**	**TB**	**CAFTB**	**TB**	**CAFTB**	**TB**	**CAFTB**
Unbraced Length $K_z L$ (ft)														
0	1030	1030	917	917	804	804	724	724	621	621	2670	2670	2410	2410
6	978	959	868	851	761	746	664	636	569	545	2590	2560	2330	2310
7	960	933	852	828	747	725	644	607	552	520	2560	2530	2310	2280
8	940	906	834	803	731	703	623	575	534	492	2530	2490	2290	2250
9	919	875	815	776	714	678	601	540	514	461	2510	2450	2260	2210
10	897	843	794	747	696	652	578	504	494	429	2480	2410	2230	2170
11	875	809	773	716	676	624	555	468	473	396	2460	2370	2210	2130
12	852	774	752	684	657	595	532	430	451	363	2430	2320	2180	2090
13	828	739	730	651	636	564	510	392	430	329	2410	2280	2160	2050
14	805	703	708	618	616	534	488	356	410	296	2380	2240	2140	2000
15	783	666	687	584	595	503	466	322	389	264	2360	2200	2110	1960
16	761	628	665	551	575	472	446	290	370	237	2340	2160	2090	1920
17	739	592	644	517	555	441	426	264	351	215	2320	2120	2070	1890
18	719	557	624	484	535	410	407	242	333	196	2310	2080	2050	1850
19	699	524	604	452	516	381	389	223	316	180	2290	2040	2040	1810
20	679	492	586	422	498	352	373	207	300	167	2270	2010	2020	1780
22	642	435	550	367	462	302	343	182	270	145	2250	1940	1990	1710
24	609	385	517	322	430	264	318	162	246	129	2220	1890	1960	1650
26	579	346	486	288	400	234	297	147	228	116	2200	1830	1940	1600
28	553	315	460	260	373	211	280	135	214	106	2190	1790	1920	1550
30	530	289	436	238	349	192	266	125	202	97.4	2170	1750	1910	1510
32	511	269	416	220	328	176	255	117	192	90.7	2160	1710	1890	1470
34	493	252	398	205	310	163	246	111	184	85.1	2150	1680	1880	1440
36	478	238	381	193	296	153	238	105	178	80.5	2140	1650	1870	1410
38	464	226	367	182	283	143	231	101	172	76.5	2130	1620	1860	1380
40	452	215	355	173	273	136	226	96.6	167	73.1	2120	1600	1850	1350

F_y = 50 ksi

Table 1. (continued)
Torsional Buckling Design Strength in Axial Compression
$\phi_c P_n$, kip

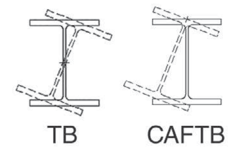

Shape	W21×													
lb / ft	166		147		132		122		111		101		93	
Design	TB	CAFTB	TB	CAFTB	TB	CAFTB	TB	CAFTB	TB	CAFTB	TB	CAFTB	TB	CAFTB
Unbraced Length $K_z L$ (ft) 0	2200	2200	1940	1940	1750	1750	1620	1620	1470	1470	1320	1320	1230	1230
6	2120	2110	1880	1860	1690	1670	1560	1540	1410	1400	1280	1270	1140	1110
7	2100	2080	1860	1830	1670	1640	1540	1520	1400	1380	1270	1250	1120	1070
8	2080	2040	1830	1800	1640	1620	1520	1490	1380	1360	1250	1230	1090	1030
9	2050	2010	1810	1770	1620	1590	1500	1470	1360	1330	1230	1210	1060	990
10	2030	1970	1790	1740	1600	1550	1470	1430	1340	1300	1220	1190	1040	947
11	2000	1930	1760	1700	1570	1520	1450	1400	1310	1270	1200	1160	1010	905
12	1980	1890	1740	1660	1550	1480	1430	1370	1290	1240	1170	1130	985	864
13	1950	1850	1710	1620	1530	1450	1400	1330	1270	1200	1150	1100	961	823
14	1930	1810	1690	1580	1500	1410	1380	1300	1240	1170	1130	1070	939	784
15	1900	1770	1660	1550	1480	1370	1360	1260	1220	1140	1110	1030	918	747
16	1880	1730	1640	1510	1450	1340	1330	1230	1200	1100	1080	1000	899	712
17	1860	1700	1620	1470	1430	1300	1310	1190	1170	1070	1060	969	880	679
18	1840	1660	1600	1430	1410	1260	1290	1160	1150	1040	1040	937	864	648
19	1820	1620	1580	1400	1390	1230	1270	1120	1130	1000	1020	906	848	619
20	1810	1590	1560	1360	1370	1200	1250	1090	1110	972	997	875	834	592
22	1770	1520	1520	1290	1330	1130	1210	1030	1070	909	958	815	809	544
24	1750	1460	1490	1230	1300	1070	1170	965	1040	851	921	758	788	502
26	1720	1410	1460	1170	1270	1010	1140	909	1000	796	888	704	770	466
28	1700	1360	1440	1120	1240	960	1110	858	974	746	857	655	754	435
30	1680	1320	1410	1080	1220	913	1090	811	948	700	829	610	741	411
32	1670	1280	1390	1030	1200	871	1070	768	924	658	804	569	729	391
34	1650	1240	1380	995	1180	832	1040	729	902	620	781	531	720	374
36	1640	1210	1360	960	1160	797	1030	694	883	585	761	496	711	360
38	1630	1180	1350	929	1140	766	1010	662	865	553	742	466	704	348
40	1620	1150	1340	901	1130	737	996	633	849	525	726	440	697	338

F_y = 50 ksi

Table 1. (continued)
Torsional Buckling Design Strength in Axial Compression
$\phi_c P_n$, kip

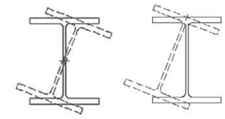

TB CAFTB

Shape	W21×													
lb / ft	83		73		68		62		55		48		57	
Design	TB	CAFTB	TB	CAFTB	TB	CAFTB	TB	CAFTB	TB	CAFTB	TB	CAFTB	TB	CAFTB
Unbraced Length $K_z L$ (ft)														
0	1090	1090	929	929	850	850	761	761	657	657	555	555	690	690
6	1020	988	870	849	796	777	712	695	615	600	519	506	625	596
7	993	954	852	822	779	753	697	673	602	581	507	489	605	566
8	968	917	832	793	760	726	679	649	586	560	494	470	584	534
9	942	878	811	762	741	698	661	623	570	536	480	450	563	501
10	916	839	789	729	720	667	642	595	553	512	464	428	541	466
11	890	799	767	693	700	636	623	566	536	486	449	405	521	431
12	865	759	746	656	679	604	604	536	518	459	432	381	500	395
13	841	721	725	620	659	570	584	506	500	432	416	356	481	361
14	818	684	702	585	639	536	565	477	482	405	399	332	462	330
15	797	648	680	551	619	503	546	445	464	378	383	307	445	302
16	777	614	660	518	601	472	528	415	447	350	366	283	428	275
17	758	582	641	488	581	443	510	387	430	323	350	258	412	252
18	741	551	622	459	563	415	494	360	413	298	335	235	397	233
19	724	523	606	432	546	388	477	335	397	274	319	215	384	217
20	709	497	590	407	530	364	461	311	382	253	305	197	372	204
22	682	449	561	361	501	320	432	270	353	219	277	169	350	182
24	659	407	537	323	476	285	406	240	327	192	252	148	333	165
26	639	374	516	294	454	258	384	216	305	172	230	132	318	152
28	623	347	498	271	436	237	364	197	285	156	212	118	305	142
30	608	325	482	252	420	220	348	182	268	143	198	108	295	133
32	595	307	468	237	406	206	333	169	253	132	186	99.1	286	126
34	585	293	457	224	393	194	320	159	242	123	176	91.9	278	121
36	575	280	446	214	383	184	309	150	232	116	168	85.9	271	116
38	567	270	437	205	373	176	299	143	223	109	161	80.8	266	112
40	559	261	429	197	365	169	290	136	216	104	155	76.5	261	109

F_y = 50 ksi

Table 1. (continued)
Torsional Buckling Design Strength in Axial Compression
$\phi_c P_n$, kip

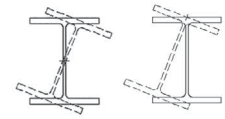

Shape	W21×				W18×									
lb / ft	50		44		311		283		258		234		211	
Design	TB	CAFTB	TB	CAFTB	TB	CAFTB	TB	CAFTB	TB	CAFTB	TB	CAFTB	TB	CAFTB
Unbraced Length $K_z L$ (ft)														
0	592	592	505	505	4120	4120	3750	3750	3420	3420	3090	3090	2800	2800
6	535	509	456	434	4010	3970	3650	3600	3320	3280	2990	2960	2710	2680
7	517	482	440	410	3990	3920	3620	3560	3300	3240	2970	2920	2690	2640
8	498	453	423	384	3970	3880	3600	3520	3270	3200	2950	2880	2670	2610
9	478	422	406	357	3950	3840	3580	3480	3250	3160	2920	2840	2640	2570
10	458	390	387	329	3930	3800	3560	3440	3230	3120	2900	2800	2620	2530
11	438	358	369	300	3920	3760	3550	3400	3220	3080	2890	2760	2600	2490
12	418	325	351	271	3910	3720	3530	3360	3200	3040	2870	2720	2590	2450
13	399	294	333	242	3890	3690	3520	3330	3190	3010	2860	2690	2570	2420
14	381	264	315	215	3880	3660	3510	3290	3180	2970	2840	2660	2560	2380
15	363	237	299	192	3880	3630	3500	3260	3170	2940	2830	2620	2540	2350
16	347	215	283	173	3870	3610	3490	3240	3160	2910	2820	2600	2530	2320
17	331	196	267	157	3860	3580	3480	3210	3150	2890	2810	2570	2520	2290
18	316	180	253	144	3860	3560	3480	3190	3140	2860	2800	2540	2510	2260
19	302	167	240	133	3850	3540	3470	3170	3130	2840	2800	2520	2500	2240
20	289	156	227	123	3850	3520	3460	3150	3130	2820	2790	2500	2500	2220
22	268	138	205	108	3840	3490	3460	3120	3120	2780	2780	2460	2480	2170
24	249	124	189	96.3	3830	3470	3450	3090	3110	2750	2770	2430	2470	2140
26	234	113	176	87.3	3830	3450	3440	3060	3100	2730	2760	2400	2460	2110
28	222	105	166	80.1	3820	3430	3440	3040	3100	2710	2760	2380	2460	2080
30	212	97.8	158	74.4	3820	3410	3430	3030	3090	2690	2750	2360	2450	2060
32	204	92.2	151	69.6	3820	3400	3430	3010	3090	2670	2750	2340	2450	2040
34	198	87.5	146	65.7	3820	3390	3430	3000	3090	2660	2740	2330	2440	2020
36	192	83.6	141	62.4	3810	3380	3430	2990	3080	2650	2740	2310	2440	2010
38	188	80.3	137	59.6	3810	3370	3420	2980	3080	2640	2740	2300	2430	2000
40	184	77.5	134	57.3	3810	3360	3420	2970	3080	2630	2740	2290	2430	1990

F_y = 50 ksi	Table 1. (continued) Torsional Buckling Design Strength in Axial Compression $\phi_c P_n$, kip

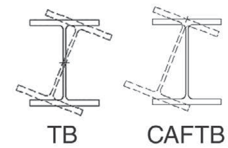

Shape		W18×													
lb / ft		192		175		158		143		130		119		106	
Design		TB	CAFTB	TB	CAFTB	TB	CAFTB	TB	CAFTB	TB	CAFTB	TB	CAFTB	TB	CAFTB
Unbraced Length $K_z L$ (ft)	0	2530	2530	2310	2310	2080	2080	1890	1890	1720	1720	1580	1580	1400	1400
	6	2440	2420	2230	2210	2010	1980	1820	1800	1660	1640	1520	1500	1340	1330
	7	2420	2380	2210	2170	1980	1950	1800	1770	1630	1610	1500	1470	1320	1300
	8	2400	2340	2190	2140	1960	1920	1770	1740	1610	1580	1480	1440	1300	1280
	9	2370	2310	2160	2100	1940	1880	1750	1700	1590	1550	1450	1410	1280	1250
	10	2350	2270	2140	2060	1920	1850	1730	1670	1570	1510	1430	1380	1260	1220
	11	2330	2230	2120	2020	1900	1810	1710	1630	1550	1480	1410	1350	1240	1190
	12	2320	2190	2100	1990	1880	1780	1690	1600	1530	1450	1390	1320	1220	1160
	13	2300	2160	2080	1950	1860	1740	1670	1560	1510	1410	1370	1280	1200	1120
	14	2280	2120	2070	1920	1840	1710	1650	1530	1490	1380	1350	1250	1180	1090
	15	2270	2090	2050	1880	1830	1670	1640	1500	1470	1350	1330	1220	1160	1060
	16	2260	2060	2040	1850	1810	1640	1620	1460	1460	1310	1310	1190	1140	1030
	17	2250	2030	2030	1820	1800	1610	1600	1430	1440	1280	1300	1150	1120	1000
	18	2240	2000	2020	1790	1780	1580	1590	1410	1430	1250	1280	1130	1110	971
	19	2230	1980	2000	1770	1770	1560	1580	1380	1410	1230	1270	1100	1090	942
	20	2220	1960	2000	1740	1760	1530	1570	1350	1400	1200	1250	1070	1080	915
	22	2200	1910	1980	1700	1740	1480	1550	1300	1380	1150	1230	1020	1050	864
	24	2190	1880	1970	1660	1730	1440	1530	1260	1360	1110	1200	971	1030	818
	26	2180	1840	1950	1620	1720	1410	1520	1220	1340	1070	1190	930	1010	776
	28	2170	1820	1940	1590	1710	1370	1500	1190	1330	1030	1170	893	988	739
	30	2170	1790	1940	1570	1700	1350	1490	1160	1320	1000	1160	860	972	705
	32	2160	1770	1930	1550	1690	1320	1480	1140	1310	974	1140	830	958	675
	34	2160	1750	1920	1530	1680	1300	1480	1110	1300	950	1130	804	946	649
	36	2150	1740	1920	1510	1680	1280	1470	1090	1290	928	1120	781	935	625
	38	2150	1720	1910	1490	1670	1270	1460	1080	1280	909	1110	760	925	604
	40	2150	1710	1910	1480	1670	1250	1460	1060	1280	892	1110	742	917	585

F_y = 50 ksi

Table 1. (continued)
Torsional Buckling Design Strength in Axial Compression
$\phi_c P_n$, kip

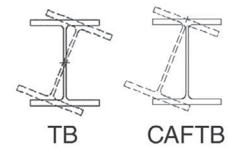

Shape	W18×													
lb / ft	97		86		76		71		65		60		55	
Design	TB	CAFTB	TB	CAFTB	TB	CAFTB	TB	CAFTB	TB	CAFTB	TB	CAFTB	TB	CAFTB
Unbraced Length $K_z L$ (ft) 0	1280	1280	1140	1140	991	991	940	940	859	859	775	775	701	701
6	1230	1210	1090	1080	952	943	863	834	786	760	717	696	648	630
7	1210	1190	1070	1060	939	926	841	802	765	730	699	670	631	607
8	1190	1170	1050	1030	924	908	818	768	743	698	681	639	614	582
9	1170	1140	1040	1010	909	887	796	733	722	665	660	608	596	555
10	1150	1110	1020	983	892	863	774	698	700	631	639	576	578	526
11	1130	1080	997	956	874	838	754	664	680	598	619	544	560	495
12	1110	1050	977	928	855	812	734	630	660	566	599	514	542	466
13	1090	1020	957	900	836	786	716	598	641	536	580	484	523	437
14	1070	993	938	871	816	759	699	568	624	506	563	455	505	409
15	1050	963	918	843	798	732	683	539	608	479	546	429	489	383
16	1030	933	900	814	779	706	669	513	593	453	531	403	473	358
17	1010	904	881	786	761	679	656	488	580	428	517	380	458	335
18	998	875	864	759	744	653	644	465	567	406	504	358	445	314
19	981	848	847	732	727	628	633	444	555	385	492	338	433	294
20	966	821	831	706	711	603	623	424	545	366	481	319	421	275
22	938	771	802	657	680	556	605	389	526	331	462	285	401	244
24	913	725	775	612	653	513	590	359	511	303	445	259	383	220
26	891	683	752	571	628	473	578	335	497	280	431	239	368	202
28	872	646	730	534	605	437	568	315	486	262	420	223	356	187
30	854	612	712	500	585	404	559	299	477	248	409	210	345	175
32	839	582	695	470	567	374	551	286	469	236	401	199	336	165
34	826	555	680	443	552	349	545	275	462	227	393	190	328	157
36	814	531	667	418	537	328	539	266	456	219	387	183	321	150
38	804	510	656	398	524	309	534	259	450	212	381	177	315	145
40	794	490	645	380	513	294	530	252	446	206	376	171	310	140

F_y = 50 ksi

Table 1. (continued)
Torsional Buckling Design Strength in Axial Compression
$\phi_c P_n$, kip

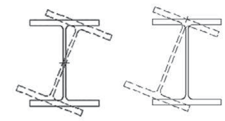
TB CAFTB

Shape		W18×								W16×					
lb / ft		50		46		40		35		100		89		77	
Design		TB	CAFTB	TB	CAFTB	TB	CAFTB	TB	CAFTB	TB	CAFTB	TB	CAFTB	TB	CAFTB
Unbraced Length $K_z L$ (ft)	0	620	620	567	567	477	477	405	405	1320	1320	1180	1180	1020	1020
	6	573	557	506	481	425	404	360	342	1260	1250	1120	1110	967	955
	7	558	536	489	454	410	381	346	321	1240	1220	1110	1090	951	935
	8	542	514	471	426	393	357	332	299	1230	1200	1090	1060	934	912
	9	526	490	452	397	377	331	316	276	1210	1170	1070	1040	916	889
	10	509	465	435	366	361	306	301	252	1190	1140	1050	1010	898	864
	11	492	439	418	336	345	280	286	229	1170	1110	1030	981	880	838
	12	475	413	401	308	329	255	271	205	1150	1080	1010	953	863	812
	13	459	386	386	281	315	230	256	182	1130	1050	996	925	845	786
	14	443	360	371	257	301	208	242	162	1120	1020	979	897	828	760
	15	428	335	357	235	288	187	229	145	1100	995	963	870	812	734
	16	414	311	344	216	276	170	217	131	1090	969	948	843	796	709
	17	399	289	332	199	264	156	205	120	1070	943	934	818	781	684
	18	385	269	322	185	254	145	195	110	1060	918	920	793	767	660
	19	373	249	313	174	244	135	185	102	1050	895	908	770	754	638
	20	361	232	304	164	235	126	175	95.1	1040	873	896	748	742	616
	22	340	204	289	148	220	113	160	84.0	1020	832	876	706	719	575
	24	322	183	277	135	207	102	149	75.5	1010	796	858	669	699	539
	26	306	166	267	126	196	94.5	140	69.0	991	765	842	637	681	506
	28	293	153	259	118	188	88.1	132	63.8	980	737	829	608	666	477
	30	282	143	252	112	181	82.9	127	59.5	970	712	817	582	653	451
	32	272	134	246	107	175	78.7	122	56.1	961	691	807	559	641	428
	34	264	127	241	103	170	75.3	118	53.3	953	672	799	539	631	408
	36	256	121	236	99.8	166	72.3	115	50.9	947	655	791	521	622	389
	38	250	116	233	96.9	163	69.9	112	48.8	941	640	784	506	614	373
	40	244	112	229	94.4	160	67.7	110	47.1	936	627	778	492	607	359

F_y = 50 ksi

Table 1. (continued)
Torsional Buckling Design Strength in Axial Compression
$\phi_c P_n$, kip

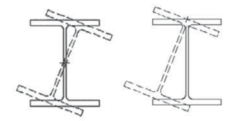

TB CAFTB

Shape	W16×													
lb / ft	67		57		50		45		40		36		31	
Design	TB	CAFTB	TB	CAFTB	TB	CAFTB	TB	CAFTB	TB	CAFTB	TB	CAFTB	TB	CAFTB
Unbraced Length $K_z L$ (ft)														
0	882	882	756	756	653	653	577	577	496	496	438	438	367	367
6	837	827	686	660	597	576	527	510	453	440	400	387	321	302
7	823	809	666	631	579	550	512	489	440	422	388	371	307	282
8	807	789	647	602	560	522	497	466	426	402	375	353	293	261
9	791	768	628	572	541	495	481	441	412	381	362	333	279	240
10	774	745	609	542	523	467	465	415	397	360	348	313	265	218
11	757	722	592	513	506	440	449	389	383	338	334	293	251	196
12	740	698	576	485	489	413	433	363	369	317	321	272	239	176
13	723	674	561	459	474	388	417	339	355	294	307	251	227	156
14	706	650	547	434	460	365	402	316	342	273	294	231	215	139
15	690	626	535	411	447	343	389	295	329	253	282	212	205	126
16	674	602	523	390	434	322	376	275	318	234	270	194	195	115
17	659	579	513	370	423	303	365	256	306	216	259	177	186	106
18	644	556	503	352	413	285	354	239	295	200	247	162	178	98.1
19	631	535	495	336	404	269	344	223	285	185	237	149	171	91.6
20	618	514	487	321	395	254	335	209	276	173	228	139	164	86.1
22	594	474	473	294	381	228	319	187	260	153	211	122	152	77.1
24	573	439	462	272	368	209	306	169	246	137	196	109	143	70.4
26	554	407	453	254	358	194	295	156	234	125	184	98.5	136	65.1
28	537	378	445	240	349	182	285	145	224	116	174	90.5	131	60.9
30	523	353	438	229	342	172	277	137	216	108	165	84.0	126	57.5
32	510	330	433	220	335	164	270	130	209	102	158	78.7	123	54.8
34	498	310	428	212	330	158	264	124	202	97.1	153	74.3	120	52.5
36	488	294	424	206	325	152	259	119	197	92.8	148	70.6	117	50.6
38	479	280	420	201	321	147	255	115	192	89.2	144	67.5	115	48.9
40	471	268	417	196	317	143	251	112	188	86.0	140	64.8	113	47.5

F_y = 50 ksi	Table 1. (continued) Torsional Buckling Design Strength in Axial Compression $\phi_c P_n$, kip													
Shape	W16×		W14×											
lb / ft	26		730		665		605		550		500		455	
Design	TB	CAFTB	TB	CAFTB	TB	CAFTB	TB	CAFTB	TB	CAFTB	TB	CAFTB	TB	CAFTB
Unbraced Length $K_z L$ (ft)														
0	297	297	9670	9670	8820	8820	8010	8010	7290	7290	6610	6610	6030	6030
6	259	243	9570	9530	8720	8680	7910	7870	7190	7160	6520	6490	5940	5910
7	247	226	9550	9490	8700	8640	7890	7840	7170	7130	6500	6460	5920	5880
8	235	208	9540	9450	8680	8600	7870	7800	7160	7090	6480	6430	5900	5850
9	222	189	9520	9420	8670	8570	7860	7770	7140	7060	6470	6390	5880	5820
10	209	169	9510	9390	8660	8540	7850	7740	7130	7030	6450	6360	5870	5780
11	197	151	9500	9360	8650	8510	7840	7710	7120	7000	6440	6330	5860	5750
12	184	132	9500	9330	8640	8480	7830	7680	7110	6970	6430	6300	5850	5730
13	173	116	9490	9310	8630	8460	7820	7660	7100	6940	6420	6280	5840	5700
14	162	102	9480	9280	8630	8430	7820	7630	7090	6920	6420	6250	5830	5680
15	152	91.8	9480	9260	8620	8410	7810	7610	7090	6900	6410	6230	5820	5650
16	142	83.2	9470	9250	8620	8400	7810	7600	7080	6880	6410	6210	5820	5630
17	133	76.0	9470	9230	8610	8380	7800	7580	7080	6860	6400	6200	5810	5610
18	125	70.0	9470	9220	8610	8370	7800	7560	7070	6850	6400	6180	5810	5600
19	118	64.9	9470	9200	8610	8350	7800	7550	7070	6830	6390	6160	5800	5580
20	112	60.6	9460	9190	8610	8340	7790	7540	7070	6820	6390	6150	5800	5570
22	103	53.6	9460	9170	8600	8320	7790	7520	7060	6800	6380	6130	5790	5540
24	95.3	48.3	9460	9160	8600	8310	7780	7500	7060	6780	6380	6110	5790	5520
26	89.7	44.2	9450	9150	8600	8290	7780	7490	7060	6770	6380	6090	5780	5500
28	85.2	40.9	9450	9140	8590	8280	7780	7470	7050	6750	6370	6080	5780	5490
30	81.6	38.3	9450	9130	8590	8270	7780	7460	7050	6740	6370	6070	5780	5480
32	78.7	36.1	9450	9120	8590	8260	7780	7460	7050	6730	6370	6060	5780	5470
34	76.2	34.3	9450	9110	8590	8260	7770	7450	7050	6730	6370	6050	5770	5460
36	74.2	32.8	9450	9110	8590	8250	7770	7440	7050	6720	6370	6040	5770	5450
38	72.4	31.6	9450	9100	8590	8250	7770	7440	7050	6710	6360	6040	5770	5440
40	71.0	30.5	9450	9100	8590	8240	7770	7430	7050	6710	6360	6030	5770	5440

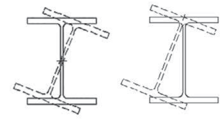
TB CAFTB

F_y = 50 ksi

Table 1. (continued)
Torsional Buckling Design Strength in Axial Compression
$\phi_c P_n$, kip

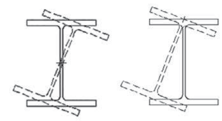

TB CAFTB

Shape		W14×													
lb / ft		426		398		370		342		311		283		257	
Design		TB	CAFTB	TB	CAFTB	TB	CAFTB	TB	CAFTB	TB	CAFTB	TB	CAFTB	TB	CAFTB
Unbraced Length $K_z L$ (ft)	0	5620	5620	5260	5260	4900	4900	4540	4540	4110	4110	3750	3750	3400	3400
	6	5540	5510	5180	5160	4820	4800	4460	4450	4030	4020	3670	3660	3330	3320
	7	5520	5480	5160	5130	4800	4770	4440	4420	4010	3990	3650	3640	3310	3300
	8	5500	5450	5140	5100	4780	4740	4420	4390	4000	3960	3630	3610	3290	3270
	9	5480	5420	5120	5060	4760	4710	4410	4360	3980	3930	3620	3580	3270	3240
	10	5470	5390	5110	5030	4750	4680	4390	4330	3960	3900	3600	3550	3260	3210
	11	5450	5360	5090	5000	4730	4650	4380	4300	3950	3870	3580	3520	3240	3180
	12	5440	5330	5080	4970	4720	4620	4360	4270	3930	3850	3570	3490	3220	3160
	13	5430	5300	5070	4950	4710	4590	4350	4240	3920	3820	3550	3460	3210	3130
	14	5420	5280	5060	4920	4700	4570	4340	4210	3910	3790	3540	3440	3200	3100
	15	5420	5260	5050	4900	4690	4540	4330	4190	3900	3770	3530	3410	3180	3080
	16	5410	5230	5050	4880	4680	4520	4320	4170	3890	3740	3520	3390	3170	3050
	17	5400	5220	5040	4860	4680	4500	4310	4150	3880	3720	3510	3370	3160	3030
	18	5400	5200	5040	4840	4670	4480	4310	4130	3870	3700	3500	3340	3150	3010
	19	5400	5180	5030	4820	4670	4460	4300	4110	3870	3680	3500	3320	3150	2980
	20	5390	5170	5030	4810	4660	4450	4300	4090	3860	3670	3490	3310	3140	2970
	22	5380	5140	5020	4780	4650	4420	4290	4060	3850	3630	3480	3270	3130	2930
	24	5380	5120	5010	4760	4650	4400	4280	4040	3840	3610	3470	3240	3120	2900
	26	5380	5100	5010	4740	4640	4380	4280	4010	3840	3580	3460	3220	3110	2870
	28	5370	5090	5010	4720	4640	4360	4270	3990	3830	3560	3460	3200	3100	2850
	30	5370	5070	5000	4710	4630	4340	4270	3980	3830	3550	3450	3180	3090	2830
	32	5370	5060	5000	4700	4630	4330	4260	3960	3820	3530	3450	3160	3090	2810
	34	5360	5050	5000	4690	4630	4320	4260	3950	3820	3520	3440	3150	3080	2790
	36	5360	5040	5000	4680	4630	4310	4260	3940	3820	3510	3440	3130	3080	2780
	38	5360	5040	4990	4670	4630	4300	4260	3930	3810	3500	3440	3120	3080	2770
	40	5360	5030	4990	4660	4620	4290	4250	3920	3810	3490	3430	3110	3070	2760

F_y = 50 ksi		Table 1. (continued) Torsional Buckling Design Strength in Axial Compression $\phi_c P_n$, kip												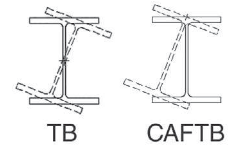	
Shape		**W14×**													
lb / ft		**233**		**211**		**193**		**176**		**159**		**145**		**132**	
Design		**TB**	**CAFTB**	**TB**	**CAFTB**	**TB**	**CAFTB**	**TB**	**CAFTB**	**TB**	**CAFTB**	**TB**	**CAFTB**	**TB**	**CAFTB**
Unbraced Length $K_z L$ (ft)	**0**	3080	3080	2790	2790	2560	2560	2330	2330	2100	2100	1920	1920	1750	1750
	6	3010	3010	2730	2720	2500	2490	2270	2270	2050	2050	1870	1870	1700	1690
	7	3000	2980	2710	2700	2480	2470	2260	2250	2030	2030	1860	1850	1680	1680
	8	2980	2960	2690	2670	2460	2450	2240	2230	2020	2010	1840	1830	1670	1660
	9	2960	2930	2670	2650	2440	2420	2220	2200	2000	1980	1820	1810	1650	1640
	10	2940	2900	2650	2620	2420	2400	2200	2180	1980	1960	1810	1790	1630	1610
	11	2920	2870	2630	2590	2400	2370	2180	2150	1960	1940	1790	1770	1610	1590
	12	2910	2850	2620	2570	2390	2340	2170	2130	1940	1910	1770	1740	1600	1570
	13	2890	2820	2600	2540	2370	2320	2150	2100	1930	1890	1750	1720	1580	1540
	14	2880	2790	2590	2510	2360	2290	2130	2080	1910	1860	1740	1690	1560	1520
	15	2860	2770	2570	2490	2340	2260	2120	2050	1890	1840	1720	1670	1550	1500
	16	2850	2740	2560	2460	2330	2240	2110	2020	1880	1810	1700	1640	1530	1470
	17	2840	2720	2550	2440	2320	2210	2090	2000	1870	1790	1690	1620	1520	1450
	18	2830	2690	2540	2410	2300	2190	2080	1980	1850	1760	1680	1600	1510	1420
	19	2820	2670	2530	2390	2290	2170	2070	1950	1840	1740	1660	1570	1490	1400
	20	2820	2650	2520	2370	2280	2150	2060	1930	1830	1720	1650	1550	1480	1380
	22	2800	2620	2500	2330	2270	2110	2040	1890	1810	1670	1630	1510	1460	1340
	24	2790	2580	2490	2300	2250	2070	2020	1850	1790	1630	1610	1470	1440	1300
	26	2780	2550	2480	2260	2240	2040	2010	1820	1770	1600	1590	1430	1420	1260
	28	2770	2530	2470	2240	2230	2010	1990	1790	1760	1570	1570	1400	1410	1230
	30	2760	2510	2460	2210	2220	1980	1980	1760	1750	1540	1560	1370	1400	1200
	32	2760	2490	2450	2190	2210	1960	1970	1730	1740	1510	1550	1340	1380	1170
	34	2750	2470	2450	2170	2200	1940	1970	1710	1730	1490	1540	1310	1370	1150
	36	2750	2450	2440	2150	2200	1920	1960	1690	1720	1460	1530	1290	1370	1130
	38	2740	2440	2440	2140	2190	1900	1950	1670	1710	1450	1520	1270	1360	1110
	40	2740	2430	2430	2130	2190	1890	1950	1660	1700	1430	1510	1250	1350	1090

F_y = 50 ksi

Table 1. (continued)
Torsional Buckling Design Strength in Axial Compression
$\phi_c P_n$, kip

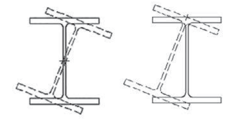

Shape		W14×													
lb / ft		120		109		99		90		82		74		68	
Design		TB	CAFTB	TB	CAFTB	TB	CAFTB	TB	CAFTB	TB	CAFTB	TB	CAFTB	TB	CAFTB
Unbraced Length $K_z L$ (ft)	0	1590	1590	1440	1440	1310	1310	1190	1190	1080	1080	981	981	900	900
	6	1540	1540	1400	1400	1270	1270	1160	1150	1030	1010	931	921	853	844
	7	1530	1520	1380	1380	1260	1250	1140	1140	1010	994	917	902	839	826
	8	1510	1510	1370	1360	1240	1240	1130	1130	996	972	901	881	824	806
	9	1500	1490	1350	1350	1230	1220	1120	1110	980	949	886	860	809	785
	10	1480	1470	1340	1330	1210	1200	1100	1090	964	926	870	837	794	763
	11	1460	1440	1320	1300	1200	1180	1090	1080	949	902	855	814	779	741
	12	1450	1420	1300	1280	1180	1160	1070	1060	935	878	841	792	764	719
	13	1430	1400	1290	1260	1170	1140	1060	1040	922	855	827	769	750	697
	14	1410	1370	1270	1240	1150	1120	1040	1020	909	832	814	747	737	676
	15	1400	1350	1260	1220	1130	1100	1020	996	897	810	802	726	724	655
	16	1380	1330	1240	1190	1120	1080	1010	975	886	789	790	705	712	634
	17	1370	1300	1230	1170	1100	1060	993	955	876	770	779	685	701	615
	18	1350	1280	1210	1150	1090	1040	978	934	867	751	770	666	691	596
	19	1340	1260	1200	1130	1070	1010	963	913	858	733	760	648	681	578
	20	1330	1240	1180	1110	1060	993	949	892	850	716	752	631	672	561
	22	1300	1200	1160	1060	1030	952	923	852	837	685	737	600	656	530
	24	1280	1160	1140	1030	1010	913	899	814	825	658	724	572	642	502
	26	1260	1120	1120	990	990	877	877	778	815	635	713	548	630	477
	28	1250	1090	1100	956	971	843	856	744	807	614	704	526	620	456
	30	1230	1060	1080	925	954	811	838	712	799	596	696	508	611	436
	32	1220	1030	1070	897	939	782	822	683	793	580	689	491	604	420
	34	1210	1000	1060	871	925	756	807	656	788	567	683	477	597	405
	36	1200	981	1050	847	913	731	794	631	783	555	678	464	591	392
	38	1190	960	1040	826	902	709	782	609	779	544	673	452	586	380
	40	1180	941	1030	806	892	689	771	588	776	534	669	442	582	370

F_y = 50 ksi		Table 1. (continued) Torsional Buckling Design Strength in Axial Compression $\phi_c P_n$, kip													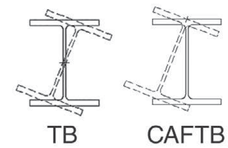
Shape		**W14×**												
lb / ft		**61**		**53**		**48**		**43**		**38**		**34**		**30**
Design		**TB**	**CAFTB**	**TB**	**CAFTB**	**TB**	**CAFTB**	**TB**	**CAFTB**	**TB**	**CAFTB**	**TB**	**CAFTB**	**TB**	**CAFTB**
Unbraced Length $K_z L$ (ft)	**0**	805	805	702	702	634	634	561	561	491	491	429	429	374	374
	6	762	754	650	635	586	573	521	511	446	431	389	377	338	327
	7	749	738	635	615	571	554	508	493	432	413	377	360	327	312
	8	735	720	620	593	557	534	494	474	419	391	364	342	315	295
	9	720	700	605	571	542	513	480	454	404	369	351	323	303	278
	10	706	680	590	548	528	491	466	434	389	347	338	304	291	260
	11	691	659	576	526	514	470	452	414	375	325	326	283	279	242
	12	676	638	563	504	500	449	439	394	361	304	313	263	267	223
	13	662	618	551	483	488	429	426	374	349	284	301	244	255	205
	14	649	597	539	463	476	409	414	356	337	265	289	226	244	188
	15	636	576	529	444	465	390	403	338	326	248	278	210	233	172
	16	624	557	519	426	455	373	392	320	316	231	268	194	222	158
	17	612	538	510	409	445	356	383	304	307	216	259	180	213	144
	18	601	519	502	393	437	340	373	289	299	203	250	166	204	132
	19	591	501	494	378	429	326	365	275	291	190	242	155	196	123
	20	581	485	487	365	421	312	357	262	284	179	235	145	188	114
	22	564	453	475	341	408	288	344	238	272	160	222	129	175	101
	24	549	425	465	320	398	267	332	217	262	146	211	117	164	90.5
	26	536	401	457	302	388	250	322	200	254	136	202	107	154	82.5
	28	525	379	450	287	381	234	313	186	247	127	195	99.9	146	76.2
	30	515	359	444	274	374	221	306	175	241	120	188	93.9	140	71.1
	32	506	342	439	262	368	211	300	165	236	114	183	88.9	134	66.9
	34	499	327	434	253	363	202	294	158	231	110	178	84.8	130	63.5
	36	492	313	431	245	359	195	290	151	227	106	174	81.4	126	60.6
	38	487	301	427	238	355	189	286	146	224	102	170	78.5	123	58.1
	40	481	291	424	232	352	183	282	142	221	99.6	167	76.0	120	56.0

F_y = 50 ksi

Table 1. (continued)
Torsional Buckling Design Strength in Axial Compression
$\phi_c P_n$, kip

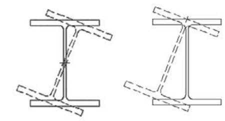

Shape		W14×				W12×									
lb / ft		26		22		336		305		279		252		230	
Design		TB	CAFTB	TB	CAFTB	TB	CAFTB	TB	CAFTB	TB	CAFTB	TB	CAFTB	TB	CAFTB
Unbraced Length $K_z L$ (ft)	0	318	318	259	259	4450	4450	4030	4030	3690	3690	3330	3330	3050	3050
	6	270	251	219	203	4370	4330	3950	3910	3610	3580	3260	3230	2970	2950
	7	257	232	207	186	4350	4300	3930	3890	3590	3550	3240	3200	2960	2920
	8	244	212	195	168	4340	4280	3920	3860	3580	3520	3230	3180	2940	2900
	9	232	192	184	150	4330	4250	3910	3830	3570	3500	3220	3150	2930	2870
	10	220	171	173	133	4330	4230	3900	3810	3560	3470	3210	3130	2920	2850
	11	209	153	162	116	4320	4210	3890	3790	3550	3450	3200	3110	2910	2820
	12	198	136	152	101	4310	4190	3890	3770	3550	3430	3190	3090	2900	2800
	13	189	121	142	89.3	4310	4170	3880	3750	3540	3410	3190	3070	2900	2780
	14	180	109	134	79.9	4300	4160	3880	3740	3530	3400	3180	3050	2890	2770
	15	172	99.8	125	72.3	4300	4140	3880	3720	3530	3380	3180	3030	2880	2750
	16	165	92.0	118	66.1	4300	4130	3870	3710	3530	3370	3170	3020	2880	2730
	17	158	85.5	112	60.9	4300	4120	3870	3700	3520	3360	3170	3010	2880	2720
	18	153	80.0	106	56.6	4290	4110	3870	3690	3520	3350	3170	3000	2870	2710
	19	148	75.4	101	53.0	4290	4100	3870	3680	3520	3340	3160	2990	2870	2700
	20	143	71.5	96.7	49.9	4290	4100	3860	3670	3520	3330	3160	2980	2870	2690
	22	136	65.1	90.0	44.9	4290	4080	3860	3660	3510	3310	3160	2960	2860	2670
	24	129	60.3	84.9	41.1	4290	4070	3860	3650	3510	3300	3150	2950	2860	2660
	26	124	56.6	80.9	38.1	4280	4060	3860	3640	3510	3290	3150	2940	2860	2650
	28	120	53.6	77.7	35.7	4280	4060	3850	3630	3510	3280	3150	2930	2850	2640
	30	117	51.2	75.2	33.8	4280	4050	3850	3630	3510	3280	3150	2920	2850	2630
	32	115	49.2	73.1	32.3	4280	4050	3850	3620	3500	3270	3150	2920	2850	2620
	34	112	47.6	71.4	31.0	4280	4040	3850	3620	3500	3270	3150	2910	2850	2610
	36	111	46.2	69.9	29.9	4280	4040	3850	3610	3500	3260	3140	2910	2850	2610
	38	109	45.1	68.7	29.0	4280	4040	3850	3610	3500	3260	3140	2900	2850	2600
	40	108	44.1	67.6	28.2	4280	4030	3850	3610	3500	3260	3140	2900	2850	2600

F_y = 50 ksi	Table 1. (continued) Torsional Buckling Design Strength in Axial Compression $\phi_c P_n$, kip

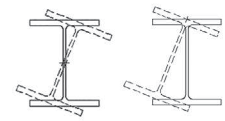

Shape		W12×													
lb / ft		**210**		**190**		**170**		**152**		**136**		**120**		**106**	
Design		**TB**	**CAFTB**	**TB**	**CAFTB**	**TB**	**CAFTB**	**TB**	**CAFTB**	**TB**	**CAFTB**	**TB**	**CAFTB**	**TB**	**CAFTB**
Unbraced Length $K_z L$ (ft)	**0**	2780	2780	2520	2520	2250	2250	2010	2010	1800	1800	1580	1580	1400	1400
	6	2710	2690	2450	2430	2180	2170	1950	1940	1740	1730	1530	1520	1350	1350
	7	2690	2660	2430	2410	2170	2140	1930	1910	1720	1700	1510	1500	1340	1330
	8	2680	2640	2420	2380	2150	2120	1920	1890	1710	1680	1500	1480	1320	1310
	9	2670	2610	2410	2360	2140	2100	1900	1870	1690	1660	1480	1460	1310	1290
	10	2650	2590	2390	2330	2130	2070	1890	1840	1680	1640	1470	1430	1290	1260
	11	2650	2560	2380	2310	2110	2050	1880	1820	1660	1610	1450	1410	1280	1240
	12	2640	2540	2370	2290	2100	2030	1870	1800	1650	1590	1440	1390	1270	1220
	13	2630	2520	2370	2270	2090	2010	1860	1780	1640	1570	1430	1370	1250	1200
	14	2620	2500	2360	2250	2090	1990	1850	1760	1630	1550	1420	1350	1240	1180
	15	2620	2490	2350	2230	2080	1970	1840	1740	1620	1530	1410	1330	1230	1160
	16	2610	2470	2350	2210	2070	1950	1830	1720	1610	1510	1400	1310	1220	1140
	17	2610	2460	2340	2200	2070	1930	1830	1700	1610	1490	1390	1290	1210	1120
	18	2600	2450	2340	2190	2060	1920	1820	1690	1600	1480	1380	1270	1200	1100
	19	2600	2430	2330	2170	2060	1910	1820	1670	1590	1460	1380	1260	1200	1090
	20	2600	2420	2330	2160	2050	1890	1810	1660	1590	1450	1370	1240	1190	1070
	22	2590	2400	2320	2140	2050	1870	1800	1640	1580	1420	1360	1210	1180	1040
	24	2590	2390	2320	2120	2040	1850	1800	1610	1570	1400	1350	1190	1170	1020
	26	2590	2380	2320	2110	2040	1840	1790	1600	1570	1380	1340	1170	1160	994
	28	2580	2370	2310	2100	2030	1830	1790	1580	1560	1360	1340	1150	1150	974
	30	2580	2360	2310	2090	2030	1810	1780	1570	1560	1350	1330	1140	1140	957
	32	2580	2350	2310	2080	2030	1800	1780	1560	1550	1340	1330	1120	1140	941
	34	2580	2340	2310	2070	2030	1800	1780	1550	1550	1330	1320	1110	1130	928
	36	2580	2340	2310	2070	2020	1790	1780	1540	1550	1320	1320	1100	1130	916
	38	2570	2330	2300	2060	2020	1780	1770	1530	1540	1310	1320	1090	1130	905
	40	2570	2330	2300	2050	2020	1780	1770	1530	1540	1300	1320	1080	1120	896

F_y = 50 ksi

Table 1. (continued)
Torsional Buckling Design Strength in Axial Compression
$\phi_c P_n$, kip

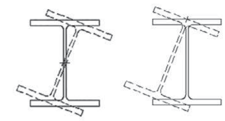

TB CAFTB

Shape		W12×													
lb / ft		96		87		79		72		65		58		53	
Design		TB	CAFTB	TB	CAFTB	TB	CAFTB	TB	CAFTB	TB	CAFTB	TB	CAFTB	TB	CAFTB
Unbraced Length $K_z L$ (ft)	0	1270	1270	1150	1150	1040	1040	949	949	859	859	765	765	702	702
	6	1220	1210	1110	1100	1000	998	910	907	823	820	724	718	663	657
	7	1210	1200	1090	1090	989	982	898	893	812	807	712	702	651	643
	8	1190	1180	1080	1070	975	966	885	877	799	792	699	686	639	627
	9	1180	1160	1060	1050	961	948	871	861	786	777	686	668	626	610
	10	1160	1140	1050	1030	947	929	858	843	773	760	672	650	613	593
	11	1150	1120	1040	1010	933	910	844	825	759	743	660	632	600	575
	12	1130	1100	1020	988	919	891	830	806	746	725	647	614	588	557
	13	1120	1080	1010	968	906	871	816	787	732	707	635	595	576	539
	14	1110	1050	996	948	893	851	803	768	719	689	624	577	564	522
	15	1100	1030	984	928	880	832	791	750	706	670	613	560	553	504
	16	1090	1020	973	909	869	813	779	731	694	652	603	543	542	487
	17	1080	997	962	890	858	794	767	713	683	635	594	527	532	471
	18	1070	979	952	872	847	776	756	695	671	617	585	511	523	455
	19	1060	962	943	855	837	759	746	678	661	601	577	496	515	441
	20	1050	946	935	838	828	742	737	662	651	584	569	482	507	426
	22	1040	916	920	807	812	711	719	630	632	553	556	456	492	400
	24	1030	889	906	780	798	683	704	602	616	525	545	433	480	376
	26	1020	866	895	755	785	658	691	576	601	499	535	413	469	356
	28	1010	845	886	733	775	635	679	553	589	475	526	395	459	337
	30	1000	826	877	713	765	614	669	532	577	454	519	379	451	321
	32	995	810	870	696	757	596	660	513	567	435	513	365	444	307
	34	990	795	864	680	750	580	652	496	559	418	507	353	438	294
	36	985	782	858	666	744	565	645	481	551	402	503	343	433	283
	38	981	771	854	654	739	552	639	467	544	388	498	333	428	273
	40	977	761	849	643	734	540	633	455	538	376	495	325	424	264

F_y = 50 ksi

Table 1. (continued)
Torsional Buckling Design Strength in Axial Compression
$\phi_c P_n$, kip

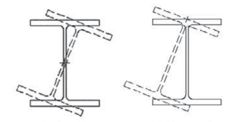

Shape		W12×													
lb / ft		**50**		**45**		**40**		**35**		**30**		**26**		**22**	
Design		**TB**	**CAFTB**	**TB**	**CAFTB**	**TB**	**CAFTB**	**TB**	**CAFTB**	**TB**	**CAFTB**	**TB**	**CAFTB**	**TB**	**CAFTB**
Unbraced Length $K_z L$ (ft)	**0**	657	657	589	589	526	526	462	462	382	382	323	323	278	278
	6	609	596	545	534	485	476	414	399	344	333	291	282	221	190
	7	596	578	532	517	473	460	400	379	333	318	281	269	208	168
	8	582	559	519	499	461	443	386	360	322	301	271	255	195	148
	9	569	539	506	480	448	425	373	340	310	284	260	240	184	130
	10	557	519	494	461	436	407	360	320	299	266	250	225	174	114
	11	545	500	482	443	424	390	349	301	288	248	239	210	166	101
	12	534	481	470	425	412	372	338	283	276	231	229	195	159	90.5
	13	524	463	460	407	401	355	327	266	266	215	220	180	153	82.6
	14	514	445	450	390	391	339	318	251	256	200	211	166	148	76.4
	15	506	429	441	374	382	323	310	236	247	186	202	153	143	71.3
	16	498	414	433	359	373	309	302	222	239	173	194	140	139	67.2
	17	491	400	425	345	365	295	295	210	231	161	186	129	136	63.8
	18	484	387	418	332	358	282	289	199	224	150	179	119	133	60.9
	19	478	374	412	319	351	269	283	189	218	140	172	110	131	58.5
	20	473	363	406	308	344	258	278	179	212	132	167	103	128	56.4
	22	464	343	396	288	333	238	269	163	203	118	156	91.5	125	53.1
	24	456	326	387	270	324	220	262	150	194	108	147	82.6	122	50.5
	26	450	311	380	255	316	205	256	141	187	100	140	75.7	119	48.6
	28	444	298	374	242	309	192	251	133	182	93.7	134	70.3	117	47.0
	30	440	288	369	231	303	182	246	127	177	88.6	128	65.9	116	45.7
	32	436	278	364	221	298	173	243	122	173	84.4	124	62.2	115	44.7
	34	432	270	361	213	294	166	240	118	169	81.0	120	59.3	113	43.8
	36	430	264	357	206	290	160	237	114	166	78.0	117	56.7	112	43.1
	38	427	257	355	201	287	155	235	111	163	75.6	114	54.6	112	42.5
	40	425	252	352	196	284	150	233	109	161	73.5	112	52.8	111	42.0

F_y = 50 ksi	Table 1. (continued) Torsional Buckling Design Strength in Axial Compression $\phi_c P_n$, kip													
Shape	W12×						W10×							
lb / ft	19		16		14		112		100		88		77	
Design	TB	CAFTB	TB	CAFTB	TB	CAFTB	TB	CAFTB	TB	CAFTB	TB	CAFTB	TB	CAFTB
Unbraced Length $K_z L$ (ft)														
0	230	230	188	188	160	160	1480	1480	1320	1320	1170	1170	1020	1020
6	180	157	145	124	123	104	1420	1410	1260	1250	1120	1110	972	963
7	169	137	134	106	113	88.4	1410	1390	1250	1230	1100	1090	960	946
8	157	118	123	88.3	103	72.9	1400	1370	1240	1210	1090	1070	948	928
9	147	101	113	73.2	93.1	59.6	1390	1350	1230	1190	1080	1050	936	910
10	137	86.3	103	61.9	84.2	50.1	1380	1330	1220	1180	1070	1030	926	893
11	128	75.4	94.6	53.6	75.9	43.1	1370	1310	1210	1160	1060	1020	916	875
12	121	67.1	87.1	47.3	68.5	37.8	1370	1300	1210	1140	1050	999	907	858
13	114	60.6	80.6	42.4	62.6	33.7	1360	1280	1200	1130	1050	983	899	842
14	109	55.5	75.0	38.5	57.9	30.4	1360	1270	1190	1110	1040	969	892	827
15	104	51.4	70.6	35.3	54.1	27.7	1350	1260	1190	1100	1040	955	886	813
16	99.6	48.0	67.0	32.7	51.0	25.5	1350	1250	1180	1090	1030	943	880	800
17	95.9	45.2	63.9	30.6	48.4	23.7	1350	1240	1180	1080	1030	931	875	788
18	92.7	42.8	61.4	28.8	46.3	22.2	1340	1230	1180	1070	1020	921	870	777
19	90.0	40.8	59.3	27.3	44.4	21.0	1340	1220	1170	1060	1020	911	866	766
20	87.7	39.2	57.4	26.0	42.9	19.9	1340	1210	1170	1050	1020	902	862	757
22	83.9	36.4	54.5	23.9	40.4	18.1	1340	1200	1170	1040	1010	887	856	739
24	81.1	34.3	52.3	22.3	38.5	16.8	1330	1190	1160	1030	1010	874	851	725
26	78.9	32.7	50.5	21.1	37.0	15.7	1330	1180	1160	1020	1000	863	847	712
28	77.2	31.5	49.2	20.1	35.8	14.9	1330	1180	1160	1010	1000	853	843	702
30	75.8	30.4	48.0	19.4	34.9	14.3	1330	1170	1160	1000	998	845	840	693
32	74.6	29.6	47.1	18.7	34.1	13.7	1330	1160	1160	998	996	839	838	685
34	73.7	28.9	46.4	18.2	33.5	13.3	1320	1160	1150	993	994	833	836	678
36	72.9	28.3	45.7	17.7	32.9	12.9	1320	1160	1150	989	993	828	834	672
38	72.2	27.8	45.2	17.3	32.5	12.6	1320	1150	1150	985	992	823	832	667
40	71.6	27.4	44.8	17.0	32.1	12.3	1320	1150	1150	982	991	819	831	663

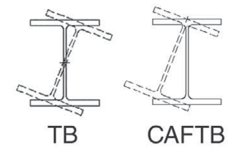

F_y = 50 ksi

Table 1. (continued)
Torsional Buckling Design Strength in Axial Compression
$\phi_c P_n$, kip

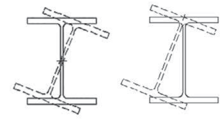

TB CAFTB

Shape	W10×													
lb / ft	68		60		54		49		45		39		33	
Design	TB	CAFTB	TB	CAFTB	TB	CAFTB	TB	CAFTB	TB	CAFTB	TB	CAFTB	TB	CAFTB
Unbraced Length $K_z L$ (ft) 0	895	895	796	796	711	711	648	648	598	598	517	517	437	437
6	850	843	754	748	671	667	611	607	555	545	477	469	401	394
7	838	827	742	733	660	653	600	594	544	529	466	454	390	381
8	826	811	730	718	649	638	589	580	533	513	456	439	380	367
9	814	793	718	701	637	623	577	565	522	497	445	424	370	352
10	803	776	707	684	626	607	566	550	513	481	435	408	359	338
11	793	759	696	668	615	591	555	535	504	465	426	393	350	323
12	783	743	686	652	605	576	545	519	496	451	417	378	341	309
13	775	727	677	636	595	560	535	504	488	436	409	364	332	296
14	767	712	668	620	586	545	526	489	482	423	402	351	324	283
15	760	698	661	606	578	531	517	475	476	411	395	339	317	270
16	753	684	653	592	570	517	509	461	471	400	389	327	310	259
17	748	672	647	579	563	504	501	448	466	389	384	316	304	248
18	742	660	641	567	556	491	494	436	462	380	379	306	298	238
19	738	649	635	555	550	480	488	424	458	371	374	297	293	228
20	733	639	630	544	545	469	482	413	454	362	370	288	288	219
22	726	620	622	525	535	449	472	392	448	348	363	273	280	204
24	720	605	615	508	527	431	463	374	444	336	357	260	273	191
26	715	591	609	493	520	416	455	358	440	326	353	249	268	179
28	710	580	604	480	514	402	449	345	436	317	349	240	263	169
30	707	570	599	469	510	390	443	332	434	309	345	232	258	161
32	704	561	596	459	505	380	439	322	431	303	342	225	255	154
34	701	553	592	451	502	371	434	312	429	298	340	219	252	148
36	699	547	590	444	499	363	431	304	428	293	338	214	249	143
38	697	541	587	437	496	357	428	297	426	289	336	209	247	139
40	696	536	585	432	493	350	425	291	425	285	334	206	245	136

F_y = 50 ksi

Table 1. (continued)
Torsional Buckling Design Strength in Axial Compression
$\phi_c P_n$, kip

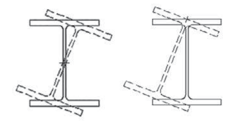

Shape	W10×													
lb / ft	30		26		22		19		17		15		12	
Design	TB	CAFTB	TB	CAFTB	TB	CAFTB	TB	CAFTB	TB	CAFTB	TB	CAFTB	TB	CAFTB
Unbraced Length $K_z L$ (ft)														
0	398	398	342	342	289	289	253	253	222	222	194	194	146	146
6	349	332	298	283	251	239	197	170	170	146	146	124	111	94.5
7	337	314	286	267	240	224	186	152	159	129	135	107	102	80.3
8	327	297	276	250	229	208	176	136	149	113	126	92.4	93.4	67.4
9	317	280	265	234	219	193	168	122	141	99.3	117	79.4	84.9	56.0
10	308	264	256	219	209	179	161	110	133	87.4	109	68.2	77.4	47.4
11	300	249	247	205	200	165	155	99.3	127	77.3	103	59.9	71.0	41.0
12	292	235	240	191	192	152	150	90.2	122	69.6	97.3	53.5	65.4	36.2
13	286	223	233	179	185	140	146	83.1	117	63.6	92.5	48.6	60.5	32.5
14	280	211	226	168	178	129	142	77.5	113	58.9	88.4	44.6	56.3	29.5
15	275	201	221	158	172	119	139	72.9	110	55.0	84.8	41.5	53.0	27.1
16	271	192	216	149	166	110	137	69.2	107	51.9	81.8	38.9	50.3	25.1
17	267	184	212	141	161	103	134	66.1	104	49.3	79.2	36.7	48.1	23.5
18	264	177	208	134	157	95.9	132	63.5	102	47.1	76.8	34.9	46.2	22.1
19	261	170	204	127	153	90.3	131	61.3	100	45.3	74.7	33.4	44.6	21.0
20	258	164	201	121	149	85.6	129	59.5	98.5	43.7	72.9	32.1	43.2	20.0
22	253	154	196	112	143	77.9	126	56.5	95.7	41.2	70.1	30.0	41.0	18.4
24	250	146	192	105	138	72.0	124	54.2	93.5	39.2	67.9	28.4	39.3	17.2
26	247	139	188	99.2	134	67.5	123	52.4	91.7	37.7	66.2	27.2	38.0	16.2
28	244	134	185	94.9	131	63.9	122	51.0	90.3	36.6	64.9	26.2	37.0	15.5
30	242	130	183	91.4	128	61.0	120	49.9	89.1	35.6	63.8	25.4	36.2	14.9
32	241	126	181	88.5	126	58.6	120	49.0	88.1	34.8	62.9	24.8	35.5	14.4
34	239	124	179	86.1	124	56.6	119	48.2	87.3	34.2	62.2	24.2	34.9	14.0
36	238	121	177	84.1	122	55.0	118	47.5	86.5	33.6	61.6	23.8	34.5	13.7
38	237	119	176	82.4	120	53.6	118	47.0	85.9	33.2	61.0	23.4	34.1	13.4
40	236	118	175	81.0	119	52.4	117	46.5	85.4	32.8	60.6	23.1	33.7	13.1

F_y = 50 ksi

Table 1. (continued)
Torsional Buckling Design Strength in Axial Compression
$\phi_c P_n$, kip

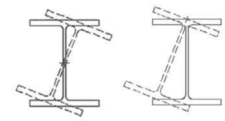

Shape		W8×													
lb / ft		67		58		48		40		35		31		28	
Design		TB	CAFTB	TB	CAFTB	TB	CAFTB	TB	CAFTB	TB	CAFTB	TB	CAFTB	TB	CAFTB
Unbraced Length $K_z L$ (ft)	0	886	886	769	769	634	634	526	526	463	463	411	411	371	371
	6	839	822	723	710	592	582	487	480	427	421	377	372	333	323
	7	830	807	714	695	582	568	478	466	417	408	367	360	325	310
	8	823	792	706	680	574	554	469	453	408	395	358	348	317	297
	9	817	778	699	666	566	540	460	439	399	382	349	336	309	285
	10	811	766	693	653	559	527	453	426	391	369	341	323	302	273
	11	807	755	688	641	553	514	446	414	384	357	333	311	296	262
	12	803	744	684	631	548	503	439	402	377	345	326	300	291	252
	13	800	735	680	621	543	493	434	391	371	334	319	288	287	242
	14	797	727	677	612	539	483	429	381	365	324	313	278	283	234
	15	795	720	674	604	535	474	424	371	360	314	308	268	279	226
	16	793	714	671	597	532	466	421	363	356	305	303	259	276	219
	17	791	708	669	591	530	459	417	355	352	297	299	250	273	213
	18	790	703	667	585	527	453	414	348	348	289	295	242	271	207
	19	789	699	666	580	525	447	411	341	345	282	291	235	269	202
	20	787	695	664	575	523	442	409	335	342	275	288	228	267	197
	22	786	688	662	567	520	433	405	324	337	264	282	216	263	189
	24	784	683	660	561	518	425	401	316	333	255	277	206	261	182
	26	783	678	659	556	516	419	399	308	330	246	273	198	259	177
	28	782	675	657	551	514	413	396	302	327	240	270	190	257	172
	30	781	672	656	548	513	409	395	297	325	234	267	184	255	169
	32	781	669	656	545	511	405	393	292	323	229	265	179	254	165
	34	780	667	655	542	510	402	392	288	321	224	263	174	253	163
	36	780	665	654	540	510	399	390	285	320	221	262	170	252	160
	38	779	664	654	538	509	397	389	282	319	218	260	167	252	158
	40	779	662	653	536	508	395	389	280	318	215	259	164	251	157

F_y = 50 ksi

Table 1. (continued)
Torsional Buckling Design Strength in Axial Compression
$\phi_c P_n$, kip

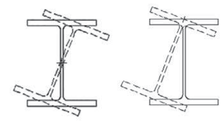

TB CAFTB

Shape	W8×											
lb / ft	24		21		18		15		13		10	
Design	TB	CAFTB	TB	CAFTB	TB	CAFTB	TB	CAFTB	TB	CAFTB	TB	CAFTB
Unbraced Length $K_z L$ (ft) 0	319	319	277	277	237	237	200	200	173	173	129	129
6	284	276	238	224	200	188	156	136	131	113	97.2	84.1
7	275	264	229	211	191	175	149	122	123	99.9	89.5	73.1
8	267	252	221	198	183	163	142	110	116	88.4	82.5	63.0
9	259	240	214	185	176	151	136	100	110	78.4	76.3	54.1
10	252	228	208	174	169	140	131	90.9	105	69.7	70.9	46.4
11	246	217	202	164	163	130	127	83.2	101	62.2	66.2	40.5
12	240	207	198	154	158	121	124	76.6	97.2	56.4	62.2	36.1
13	235	197	193	146	153	112	121	71.0	94.0	51.8	58.7	32.6
14	230	189	190	139	149	105	119	66.6	91.3	48.2	55.8	29.9
15	226	181	187	132	145	98.5	116	63.0	89.0	45.3	53.2	27.7
16	222	174	184	126	142	92.7	115	60.1	87.1	42.9	50.9	25.9
17	219	167	181	121	139	87.3	113	57.7	85.4	41.0	49.0	24.4
18	216	161	179	117	137	82.8	112	55.6	83.9	39.3	47.4	23.1
19	214	156	178	113	135	79.0	111	53.9	82.6	37.9	46.0	22.0
20	212	151	176	109	133	75.8	110	52.5	81.5	36.7	44.8	21.1
22	208	142	173	103	130	70.6	108	50.1	79.6	34.8	42.9	19.7
24	205	135	171	97.9	127	66.7	107	48.3	78.1	33.4	41.5	18.6
26	202	130	169	94.2	125	63.6	106	46.9	77.0	32.2	40.3	17.7
28	200	125	168	91.2	123	61.1	105	45.8	76.0	31.3	39.5	17.0
30	198	120	167	88.8	122	59.2	104	44.9	75.3	30.6	38.7	16.5
32	197	117	166	86.8	120	57.6	103	44.2	74.6	30.0	38.2	16.0
34	195	114	165	85.2	119	56.2	103	43.6	74.1	29.5	37.7	15.6
36	194	112	164	83.9	119	55.1	103	43.1	73.6	29.1	37.3	15.3
38	193	110	163	82.7	118	54.2	102	42.6	73.2	28.7	36.9	15.1
40	193	108	163	81.7	117	53.3	102	42.3	72.9	28.5	36.6	14.8

Experimental Investigation of Mechanical Properties of ASTM A992 Steel at Elevated Temperatures

JINWOO LEE, MOHAMMED A. MOROVAT, GUANYU HU, MICHAEL D. ENGELHARDT and ERIC M. TALEFF

ABSTRACT

This paper presents the results of a detailed experimental study into the mechanical properties of ASTM A992 structural steel at elevated temperatures. Critical testing issues, including temperature measurement, temperature control, and extensometer use, along with the testing equipment and procedures are briefly explained. Tensile steady-state temperature tests are conducted on samples of ASTM A992 steel at temperatures up to 1000 °C. Full stress-strain curves, representing steel coupons tested to fracture at elevated temperatures, are generated. Important mechanical properties such as yield stress, tensile strength, proportional limit, elastic modulus and elongation are obtained from the stress-strain curves. Results are compared with elevated-temperature properties specified by Eurocode 3 and by the AISC *Specification*. When defined as the stress at 2% total strain, the measured yield stress values agree reasonably well with the corresponding values from Eurocode 3 and the AISC *Specification*. However, for more conventional definitions of yield stress, such as the 0.2% offset yield stress, the agreement is poor. It is observed that the yield stress of steel at elevated temperatures up to about 600 °C is highly dependent on the manner in which yield stress is defined. The effects of displacement loading rates on steel strength and static yielding behavior are also investigated. It is shown that the displacement rate has a large impact on the steel strength at elevated temperatures, especially at temperatures higher than 600 °C. Further work is needed to fully characterize the time-dependent effects on the elevated-temperature stress-strain response of structural steel. Additionally, this paper presents results of Charpy V-Notch (CVN) tests on ASTM A992 steel at elevated temperatures.

Keywords: ASTM A992 steel, mechanical properties, retention factors, elevated temperatures, structural-fire engineering, fire safety.

INTRODUCTION

A key element in predicting the response of a steel structure to fire is knowledge of the elevated-temperature mechanical properties of structural steel. The properties of steel at high temperatures can be drastically different from those at room temperature. Computing the strength of steel members subjected to fire requires information on the yield stress, tensile strength, proportional limit and modulus of elasticity of steel at elevated temperatures. Advanced analysis methods, such as finite element analyses, require a more complete description of the elevated-temperature mechanical properties of steel, including data on the shape of the entire stress-strain curve as well as information on time-dependent effects such as strain rate effects and creep.

Considerable data on the elevated-temperature properties of structural steel have been published, including Harmathy and Stanzak (1970), Skinner (1972), United States Steel (1972), DeFalco (1974), Fujimoto et al. (1980, 1981), Cooke (1988), Kirby and Preston (1988), Lie (1992), Kelly and Sha (1999), Li et al. (2003), Luecke et al. (2005), Chen and Young (2006), Outinen (2006), Hu et al. (2009), and others. Nonetheless, significant gaps still exist in the database of elevated-temperature properties of structural steel. For example, ASTM A992 steel (see ASTM A992, 2011), the most common grade of structural steel used for wide-flange shapes in the United States, has not been widely examined at elevated temperatures. In addition, most previous publications on mechanical behavior of structural steel at high temperatures only report the initial portion of the stress-strain curve, leaving uncertainty on the elevated-temperature behavior of structural steel at large strains or the elevated-temperature ductility of structural steel. Further, elevated-temperature related properties such as static yielding behavior and the effect of loading rates have not yet been adequately studied. Further, the literature on high-temperature tension testing provides little information on the challenges in conducting such experiments. This is an important issue because testing techniques at elevated temperatures can have a significant effect on the test results.

Jinwoo Lee, Ph.D., P.E., S.E., Department of Civil and Architectural Engineering, Division of Nuclear Power Plant Design, Korea Electric Power Corporation E&C, Kyunggido, Republic of Korea. E-mail: jinwoo@kepco-enc.com

Mohammed A. Morovat, Ph.D. Candidate, Department of Civil, Architectural and Environmental Engineering, University of Texas at Austin, Austin, TX. E-mail: morovatma@mail.utexas.edu

Guanyu Hu, Ph.D., P.E., Engineer, 2H Offshore Engineering, Houston, TX. E-mail: huguanyu@gmail.com

Michael D. Engelhardt, Ph.D., P.E., Dewitt C. Greer Centennial Professor, Department of Civil, Architectural and Environmental Engineering, University of Texas at Austin, Austin, TX (corresponding). E-mail: mde@mail.utexas.edu

Eric M. Taleff, Ph.D., Professor, Department of Mechanical Engineering, University of Texas at Austin, Austin, TX. E-mail: taleff@mail.utexas.edu

Table 1. Chemical Composition of the Tested Specimens (Weight %)												
Coupon	**Source**	**Thickness**	**C**	**Cr**	**Mo**	**V**	**Ni**	**Mn**	**Si**	**P**	**S**	**Cu**
MA	W30×99; web	0.505 in.	0.081	0.09	0.034	0.065	0.11	1.41	0.21	0.019	0.022	0.39
MB	W30×99; web	0.525 in.	0.079	0.09	0.026	0.027	0.13	0.97	0.20	0.014	0.024	0.38
MC	W4×13; flange	0.345 in.	0.080	0.10	0.026	0.002	0.09	0.91	0.23	0.011	0.025	0.24

This paper presents results of a study on the elevated-temperature properties of ASTM A992 steel. Full-range stress-strain curves for this grade of steel at elevated temperatures up to 1000 °C are presented here, with a description of the testing equipment and procedures. The important mechanical properties of structural steel, including yield stress, tensile strength, proportional limit, elastic modulus and elongation, are obtained from the stress-strain curves. Results are compared with elevated-temperature properties specified by Eurocode 3 (2006) and by the AISC *Specification for Structural Steel Buildings*, hereafter referred to as the AISC *Specification* (2010). This paper also presents observations on the effect of cross-head displacement rate in tension tests at elevated temperatures. Test results for cross-head rates of 0.01 in./min and 0.1 in./min are presented. The static yielding behavior of ASTM A992 steel under elevated temperatures (300 to 800 °C) is also studied. Moreover, Charpy V-Notch (CVN) impact values are obtained to evaluate energy absorption capacity of ASTM A992 structural steel at elevated temperatures. Finally, this paper briefly discusses issues and difficulties that arise in performing and interpreting the results of such experiments. It should also be pointed out that a more complete account of this study is reported in a publication by Lee (2012).

EXPERIMENTAL PROGRAM

Equipment

Tension Tests at Elevated Temperatures

A 22-kip-capacity MTS 810 test frame equipped with MTS 647 water-cooled, hydraulic wedge grips was used to conduct the tension tests. The heating system consisted of the furnace, the furnace temperature controller and the data acquisition system for monitoring and recording furnace air temperature and coupon temperatures.

An MTS model 653 furnace (Figure 1a) was used as the heating device. The furnace generates heat using electrical coils and is separated into upper, middle and lower heating zones that can be individually controlled using an MTS model 409.83 temperature controller. Three thermocouples are located inside the furnace to measure the furnace air temperature.

Coupon temperatures were monitored and controlled using a separate data recording system as shown in Figure 1b. Three K-type thermocouple wires were used to measure the surface temperature at different locations along the gauge length of the coupon. The experimental set-up and a schematic diagram of the heating system used in the experimental program are shown in Figure 1b. An MTS model 632.54E-11 air-cooled high-temperature extensometer with 1-in. gauge length (with a limit strain of −5 to +10%) was used to measure strain. In order to capture the entire stress-strain relationship, throughout the course of the tests, the 1-in. gauge-length extensometer was reset when it approached the 10% limit. The procedure used for resetting the extensometer and for assembling the final stress-strain curves is described in Lee (2012).

Charpy Impact Tests at Elevated Temperatures

The Charpy V-Notch (CVN) tests were carried out at elevated temperatures by using a Tinius Olsen standard Charpy impact test machine. The heating system for the Charpy tests consisted of a small Thermolyne type 48000 bench-top muffle furnace, a temperature controller and a portable Oakton model 90600-40 thermometer.

Specimens

Tension Tests at Elevated Temperatures

In order to better assess the behavior of ASTM A992 steel at high temperatures considering the possible variability in steel material, specimens were cut from different wide-flange sections from different heats of steel. Specimens designated as MA and MB were cut from the web of W30×99 sections of two different heats of steel, and those designated as MC were cut from the flanges of a W4×13 section. Details of the dimensions of the specimens, in accordance with ASTM A370 (2012), are shown in Figure 2. The coupons were prepared so that their longitudinal dimension (18 in.) was along the rolling direction of the wide-flange sections. Moreover, though not specified by ASTM A370, the 18-in. length of the coupon was selected to create enough clearance between the furnace and the grips of the testing machine. The results of chemical analyses of the steels used in this research are presented in Table 1.

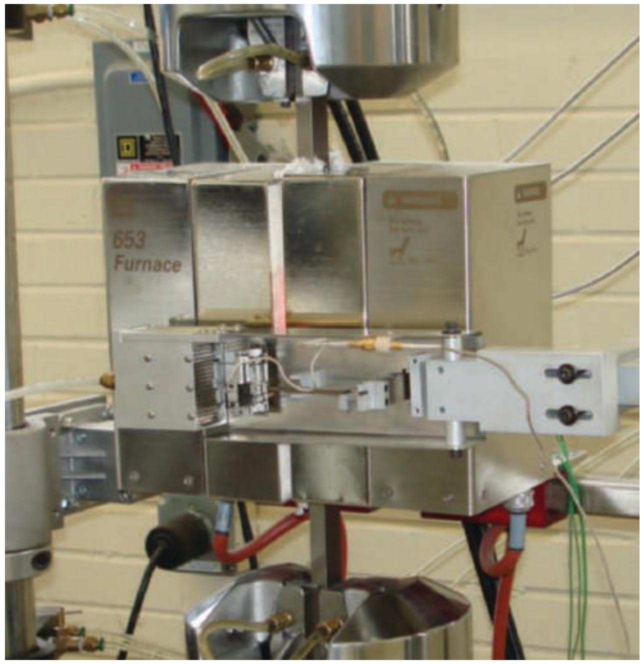

(a) Grips, wedges and furnace

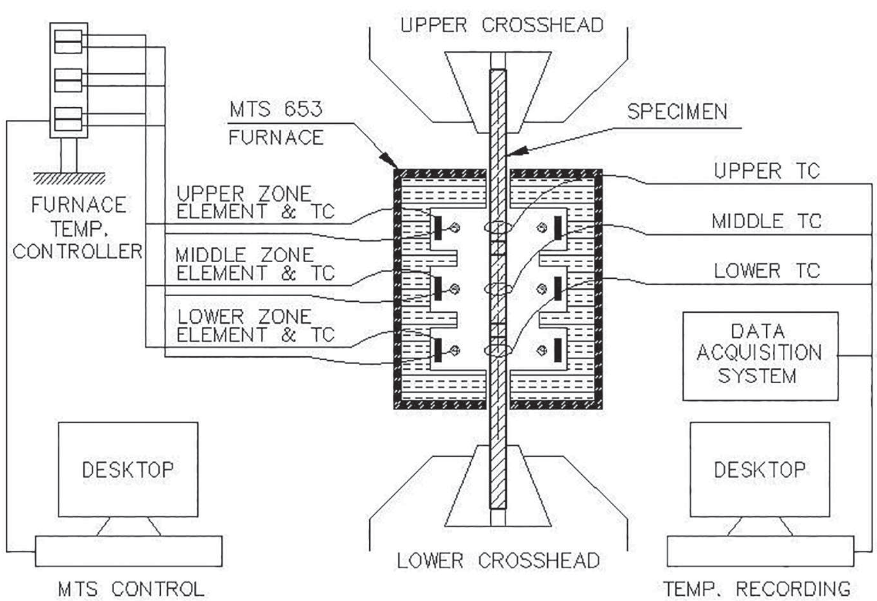

(b) Schematic diagram of heating system

Fig. 1. Test set-up consisting of the test machine and heating system.

Charpy Impact Tests at Elevated Temperatures

CVN test specimens were cut from material MB according to ASTM A370 (2012). Specimens used in the Charpy impact tests at elevated temperatures were bar-type specimens, 10 mm × 10 mm × 55 mm (0.39 in. × 0.39in. × 2.2 in.), with the V-notch machined in the center.

Procedure for Tension Tests at Elevated Temperatures

Overall Test Approach

High-temperature material tests on structural steel are usually conducted either under steady-state temperature conditions or under transient-state temperature conditions. In steady-state temperature tests, specimens are heated up to a specified temperature and then loaded to failure while maintaining the same temperature. During the initial heating process, the load is maintained at zero to allow free expansion of the specimen. The results of steady-state temperature tests are stress-strain curves at specified temperatures. Steady-state temperature tests can be carried out either as displacement or as load controlled. The resulting stress-strain curves can vary with the displacement or loading rate used in the test. In transient-state temperature tests, however, the specimens are loaded to a target stress level at ambient temperature and then heated up to failure while keeping the stress constant. Temperature and strain readings are recorded during these tests. After the test, thermal elongation is subtracted from the total strain. Finally, the results of a series of transient-state temperature tests conducted at different stress levels are converted into stress-strain curves at constant temperatures (Outinen, 2006). The resulting stress-strain curves can vary with the heating rate used in the test. A review of the literature and critical assessment of available data on high-temperature testing on structural steel indicates that for comparable loading and heating rates, the results from these two test methods are usually similar (Kirby and Preston, 1988; Outinen, 2006). Moreover, it can be interpreted that a primary reason for differences in the temperature-dependent stress-strain curves obtained from these two test methods is the influence of strain rate and creep at elevated temperatures. The influence of creep on tensile stress-strain behavior of structural steel at elevated temperatures and interpretation of such stress-strain data will be discussed briefly later in this paper.

The deciding factors on whether to choose steady-state or transient-state temperature test methods therefore come down to a matter of preference, type of equipment and how well the loading rate or temperature rate can be controlled. Based on the capabilities of the available test equipment, steady-state temperature tests, for temperatures from 20 to 1000 °C, were conducted in the investigation reported herein.

Besides being thermally steady-state, all tests were displacement-controlled, in which cross-head displacement rates were maintained at a constant value throughout a test. Specifically, two cross-head displacement rates were used: 0.01 in./min (slow test) for coupons made of MA, MB and MC materials, and 0.1 in./min (fast test) for coupons made of MA material.

Temperature Measurement and Control

Temperature measurement is a critical factor in elevated-temperature testing. Having a uniform temperature distribution over the gauge length of the steel coupon is crucial in order to accurately evaluate mechanical properties of steel at a specific temperature.

K-type thermocouple wires were used to measure the temperature at different locations along the gauge length of the coupon. Due to the fact that the thermocouple extension wire measures the temperature at the first contact point of its two dissimilar metals, this first contact point has to touch the surface of the steel coupon and maintain the initial position without moving during the test. Therefore, to have a reliable temperature measurement, thermocouple extension wires should be firmly attached to the surface of specimens. In addition, to be protected from radiation from the furnace

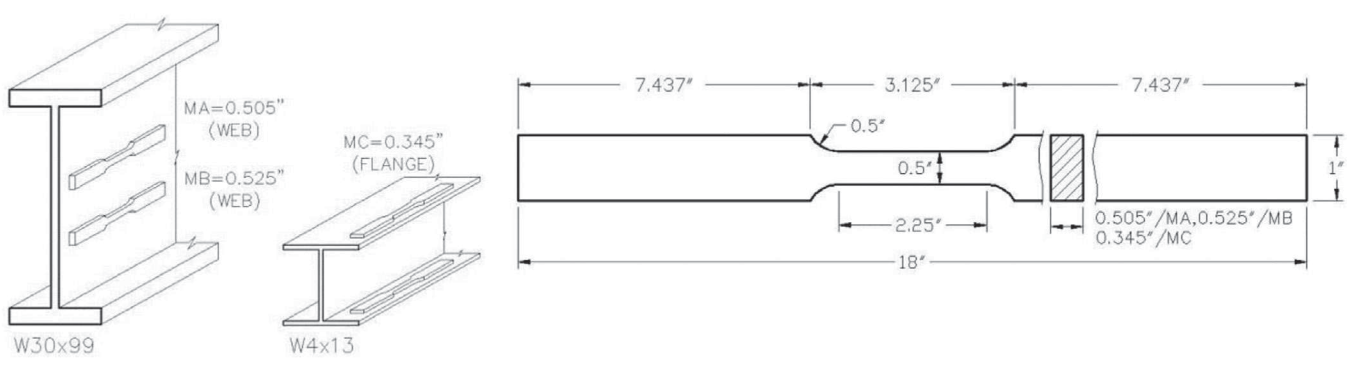

Fig. 2. Coupon specimens—designations and dimensions.

heating elements, the thermocouple wires were wrapped by Type 321 stainless steel tool wrap (Lee, 2012).

Note that considerable experience in elevated-temperature coupon testing was required before repeatable results were obtained. The investigators initially encountered significant difficulties in controlling the temperature of the coupons. It was found that a uniform air temperature in the three zones of the furnace resulted in a significant variation in steel temperature over the gauge length of the coupon. These problems were exacerbated as the coupon lengthened during testing and moved through different temperature zones in the furnace. Consequently, considerable trial-and-error experimentation was required before developing furnace control techniques that resulted in uniform steel temperatures over the height of the gauge section and throughout the duration of a test.

Load and Strain Measurement

The loading applied to the specimens was controlled and recorded by the load cell in the MTS test machine. The measured load was then used to calculate stress. The stress reported in this is engineering stress, which is equal to the measured load divided by the measured initial cross-sectional area of the coupon's reduced section.

Strains were measured using the 1-in. gauge-length MTS high-temperature extensometer described earlier. In addition to the extensometer, punch marks were placed on the specimen with initial 1-in. spacing. By measuring the initial distance between the punch marks and the final distance between punch marks (after fracture of the coupon), the strain at fracture—that is, the elongation—was determined. The initial and final distances between punch marks were measured when the coupon was at room temperature.

The strain recorded from the extensometer and the strain reported is engineering strain, based on the initial 1-in. gauge length of the extensometer. The extensometer contacts the coupon through ceramic rods, which extend outside of the furnace. Because the investigators were interested in capturing the full stress-strain curve up through fracture, which can occur at strains exceeding the 10% strain limit of the extensometer, a technique was developed for resetting the extensometer each time its 10% strain limit was reached and then reassembling the full stress-strain curves (Lee, 2012).

It should be emphasized here that testing steel coupons at elevated temperatures introduces a number of experimental difficulties that are not encountered in ambient-temperature testing. Specialized equipment is needed and considerable care and experience is required in temperature control, temperature measurement and strain measurement techniques. A more complete account of issues related to high-temperature testing of steel is reported in Lee (2012). The need for specialized equipment and specialized test techniques, and the need for considerable experience, have likely contributed to the paucity of elevated-temperature stress-strain data for structural steel.

Testing Procedure for Charpy Impact Tests at Elevated Temperatures

To perform CVN tests at elevated temperatures, CVN specimens were first heated up to the target temperatures in an electric furnace, as described previously. In general, the target temperatures were achieved within 20 min and were maintained thereafter for about an hour. Next, heated specimens were positioned in the Charpy impact machine to complete the tests. It is important to note that there is a loss in the specimens' temperature as they are taken out of the furnace and set down in the Charpy impact machine. To compensate for such temperature losses, the specimens were initially heated to temperatures about 5% more than the target temperatures.

EXPERIMENTAL RESULTS

In this section, experimental data are presented in the form of stress-strain curves for tension tests at elevated temperatures. Effects of different parameters such as variability in the steel material, elevated temperature, cross-head displacement rate and static yielding phenomenon on the tensile stress-strain behavior are illustrated and discussed. Data from the Charpy impact tests at elevated temperatures are also provided.

Specimens Following Tests at Elevated Temperatures

The necking and elongation patterns of representative coupons from elevated-temperature tension tests on material MA are shown in Figure 3. It can be observed that at temperatures of 800 and 900 °C, the necking shows a trend of distributing more along the length of the coupon's reduced section. Coupons tested at 300 °C exhibited a characteristic blue color after testing. Similarly, coupons tested at very high temperatures, above about 700 °C, exhibited a black and very rough surface appearance. Fracture surfaces in coupons tested at lower temperatures exhibited sharp corners at failure locations.

The fracture surfaces and deformation patterns of the specimens from elevated-temperature Charpy impact tests are shown in Figure 4. As can be seen from this figure, at temperatures above 700 °C, specimens bent but did not break at the location of the notches.

Stress-Strain Curves

Effect of Elevated Temperature

To illustrate the effect of elevated temperatures on tensile properties of ASTM A992 steel, stress-strain curves are

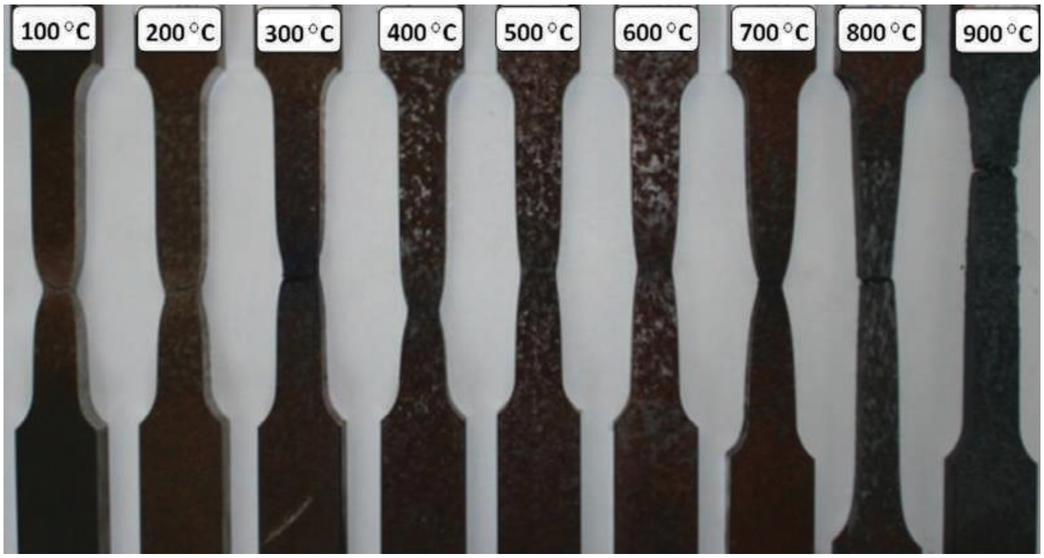

Fig. 3. Material MA coupons after elevated-temperature tests.

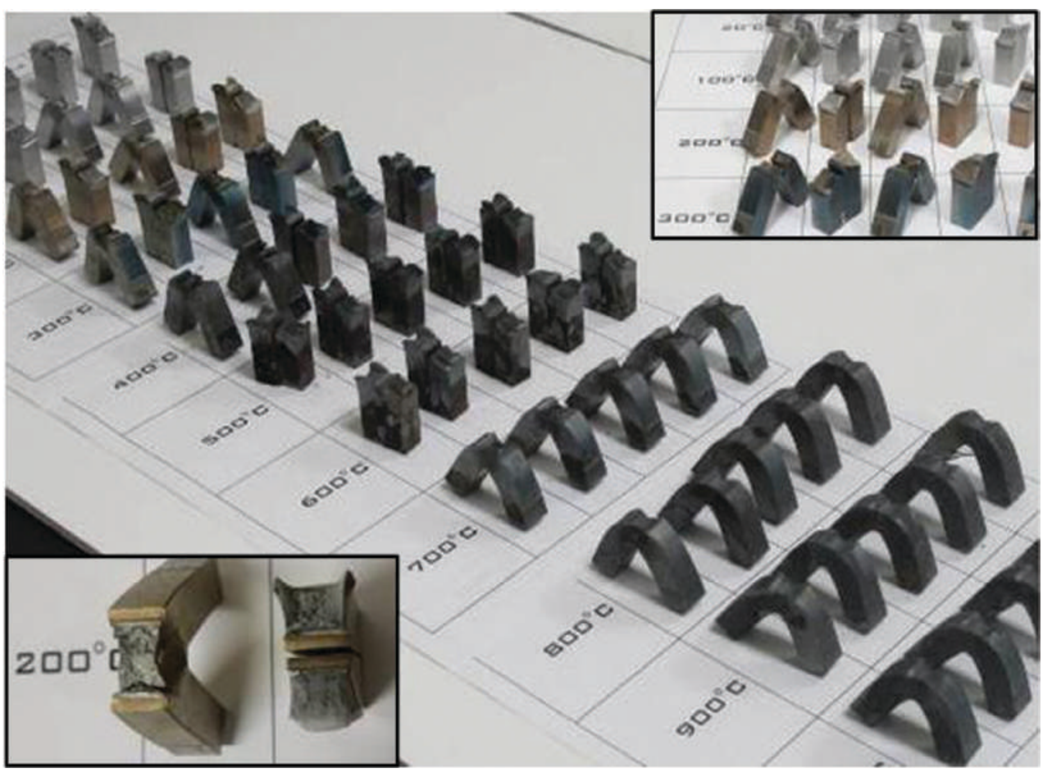

Fig. 4. Material MB specimens after Charpy impact tests at elevated temperatures.

presented for different designations of steel materials; MA, MB and MC in Figures 5, 6 and 7, respectively. In these figures, stress-strain curves are plotted up to 80% strain, which includes strains from the start of loading to the fracture of the coupons at different temperatures, except for materials MA and MB at 800 °C, for which the strains at fracture are 128% and 120%, respectively. All stress-strain curves presented in Figures 5, 6 and 7 are for a cross-head displacement rate of 0.01 in./min. As illustrated in Figures 5a, 6a and 7a, for each material, the tensile strength increases compared to the corresponding one at room temperature, at temperatures of 200 and 300 °C. At higher temperatures, progressive loss in the tensile strength can be clearly observed. Another important property, ductility, as measured by the final elongation of the coupons, exhibits a small reduction up to 500 °C, then increases in the range of 600 to 800 °C and then reduces again at 900 °C. On the other hand, ductility, as measured by the strain at which the tensile strength is developed, shows a dramatic decrease with increasing temperature from 400 to 700 °C. Furthermore, Figures 5b, 6b and 7b plot the initial parts of the stress-strain curves up to 0.5% strain for each material. These figures clearly show that the yield stress and modulus of elasticity decrease with temperature.

As observed in previous tension tests reported in the literature, these data show that the fundamental shape of the stress-strain curve changes as temperature increases. At 400 °C and above, the steel no longer exhibits a well-defined yield plateau and shows significant nonlinearity at low levels of stress and strain. Likewise, as described earlier, the strain corresponding to the maximum engineering stress (tensile

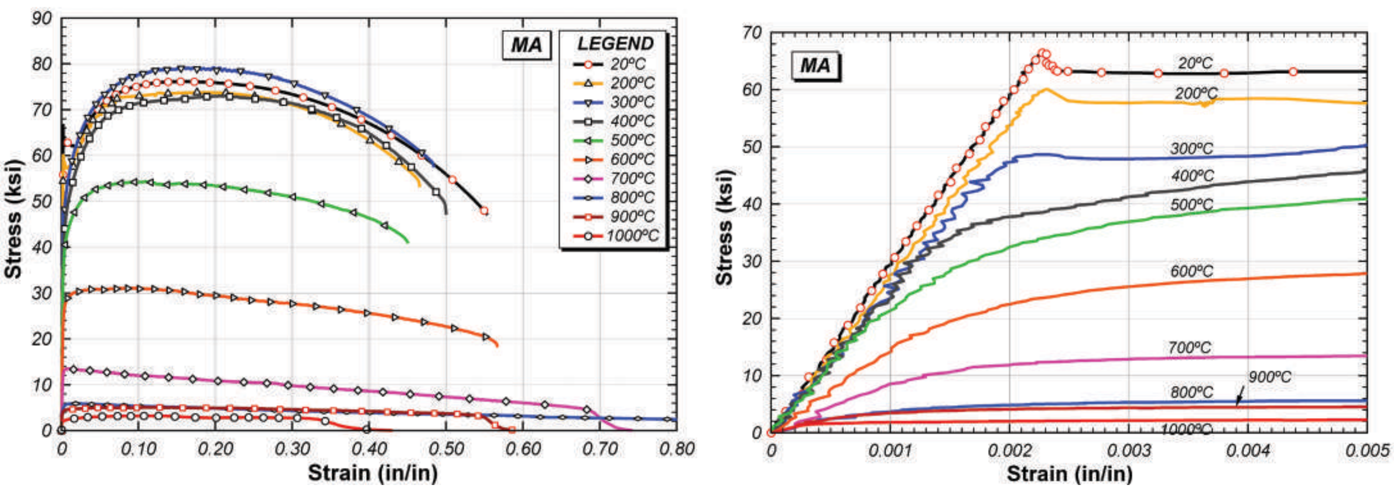

(a) Full-range stress-strain curves

(b) Initial portion of stress-strain curves

Fig. 5. Stress-strain curves for material MA at elevated temperatures.

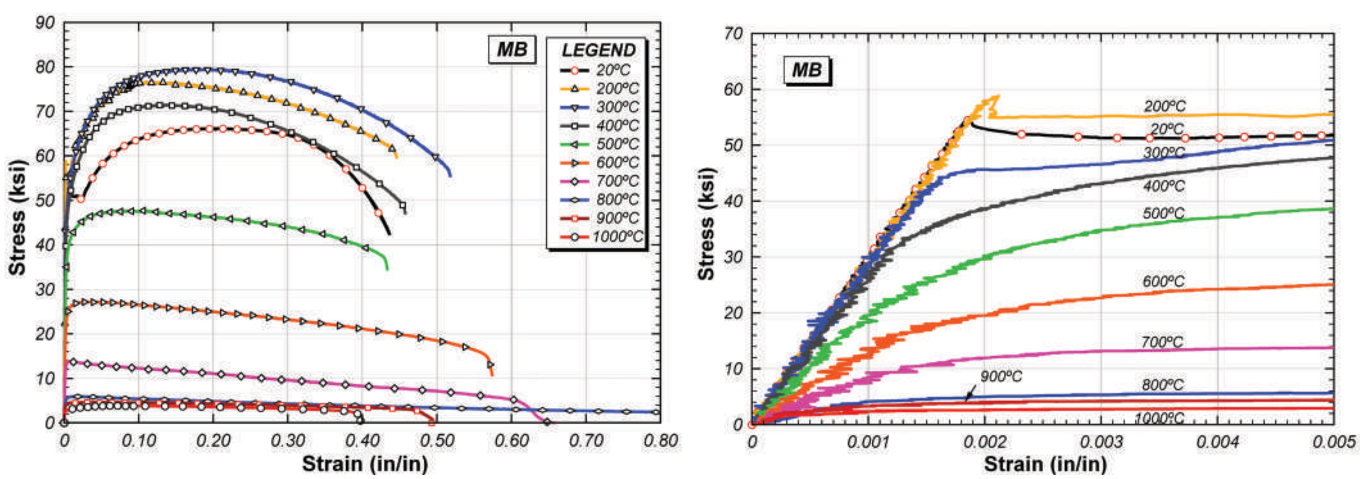

(a) Full-range stress-strain curves

(b) Initial portion of stress-strain curves

Fig. 6. Stress-strain curves for material MB at elevated temperatures.

strength) decreases rapidly as temperature increases, and the stress-strain curve subsequently shows a long, gradual decline.

At ambient temperature, the initial portion of the stress-strain curve is often modeled using a simple elastic–perfectly plastic approximation, in which the response is linear-elastic up to yield and then follows a plateau. Simple elastic–perfectly plastic stress-strain models may be less appropriate at elevated temperatures due to early nonlinearity in stress-strain curves, as seen in Figures 5, 6 and 7. This early nonlinearity may be particularly significant when considering stability phenomena, wherein tangent stiffness is a critical material property.

Effect of Material Variability

Figure 8 illustrates the effect of material variability by presenting stress-strain curves at specific temperatures for materials designated as MA, MB and MC. Stress-strain curves presented in Figure 8 are for a cross-head displacement rate of 0.01 in./min. As is clear from this figure, there is appreciable difference in material stress-strain response among these three materials, which are all classified as ASTM A992 steel. More specifically, it can be observed from this figure that materials MA and MB, both from the web of W30×99 sections of different heats, show similar stress-strain behaviors at elevated temperatures. The difference in behavior of materials MA and MB at room temperature may be attributed to the difference in chemistry, especially in terms of molybdenum and manganese contents. It can also be observed that the stress-strain curves of material MC, which is from the flange of a W4×13 section, are very different from those of materials MA and MB at elevated temperatures. Of particular interest is the comparison among these three materials at 200 °C, where very large strain hardening and a very large increase in tensile strength are seen in the stress-strain behavior of material MC. At first, this behavior was suspected to be experimental error. However, several coupons of MC material were tested at 200 °C, and this same behavior was consistently observed. These observations suggest that there may be considerable variability in stress-strain response for a particular grade of steel, and this variability should be considered in any attempt at developing general stress-strain material models for structural steel at elevated temperatures.

Some additional interesting trends can be observed from these data. For example, a phenomenon in which the stress-strain curves are not smooth in the strain hardening range, but rather exhibited a number of sudden stress jumps, can be observed at 200 °C for all materials (Figure 8b). At first, this was believed to be slipping of the extensometer. However, this effect was observed repeatedly in tests at 200 °C and thus did not appear to be experimental error. A review of the literature suggests this may be a metallurgical phenomenon known as the Portevin-LeChatelier effect (Dieter, 1986). In addition, the stress-strain curves at 1000 °C (Figure 8j) show multiple peaks rather than just one, a characteristic that cannot be seen in the stress-strain behavior at any other temperature considered in this test program. This phenomenon, which is known as dynamic recrystallization, has been reported in the literature on properties of metals at elevated temperatures (Humphreys and Hatherly, 2004).

Effect of Cross-Head Displacement Rate

Loading rate can have a significant effect on the measured stress-strain curves of structural steel, and this effect appears to be more pronounced at elevated temperatures. To address the influence of loading rates on tensile test results at elevated temperatures, the tensile tests were carried out with two different cross-head displacement rates. Figure 9 shows the comparison of stress-strain curves for cross-head

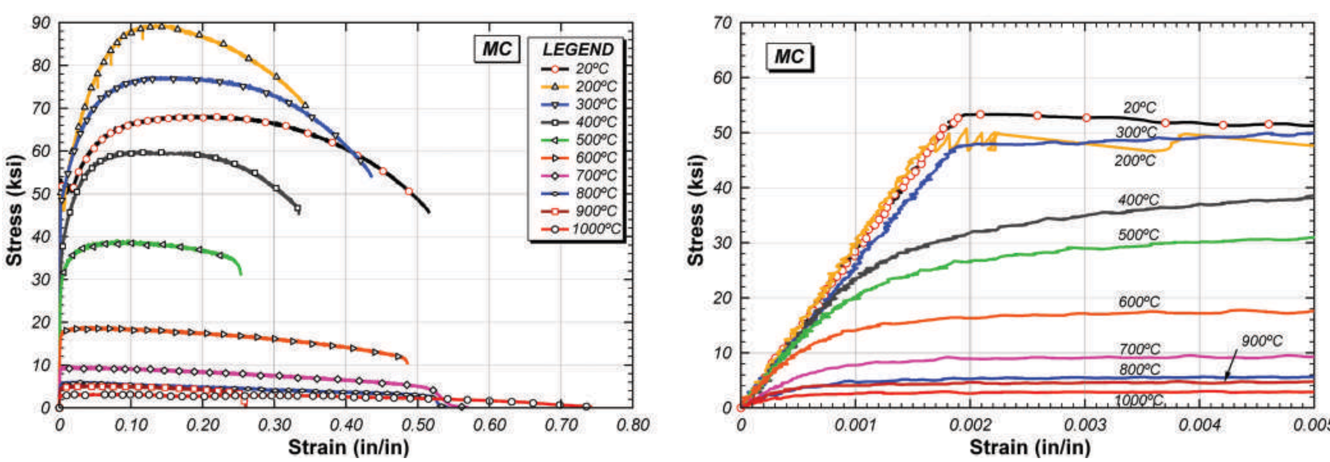

(a) Full-range stress-strain curves

(b) Initial portion of stress-strain curves

Fig. 7. Stress-strain curves for material MC at elevated temperatures.

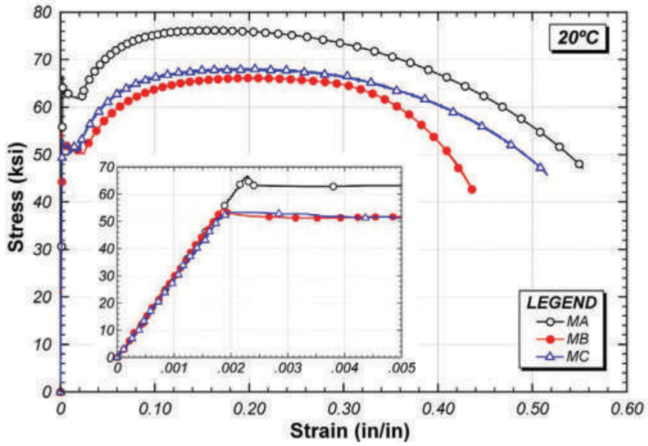

(a) Room temperature

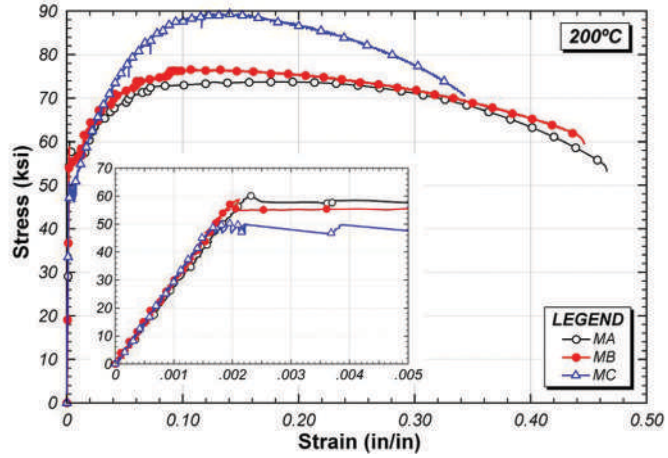

(b) 200 °C

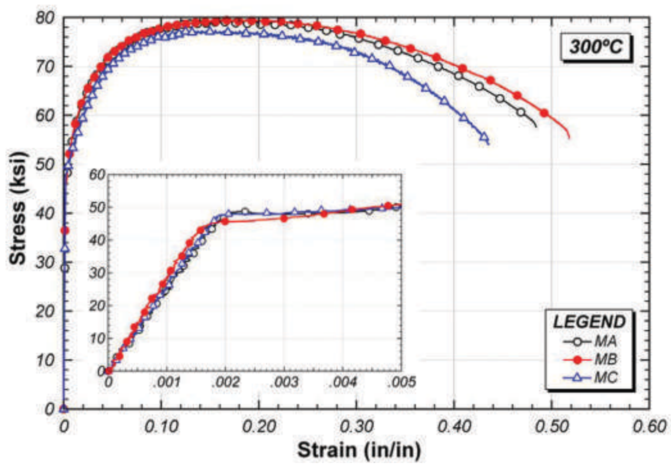

(c) 300 °C

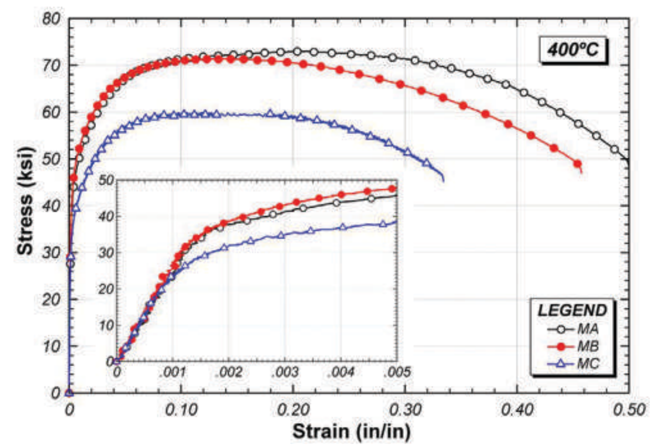

(d) 400 °C

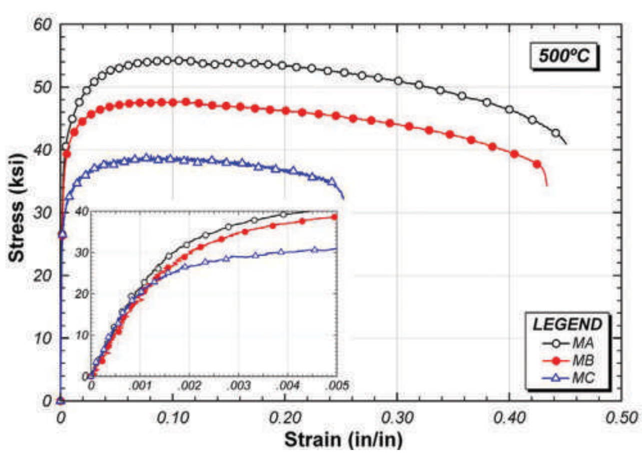

(e) 500 °C

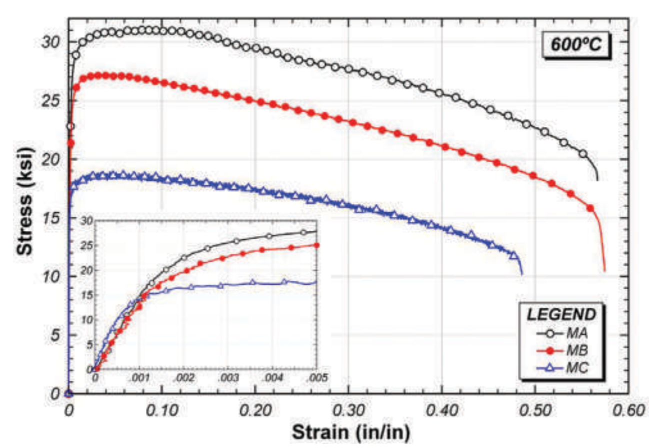

(f) 600 °C

Fig. 8. Comparison of elevated-temperature stress-strain curves for three different ASTM A992 materials.
(continued on next page)

displacement rates of 0.01 in./min and 0.1 in./min at each temperature for temperatures up to 900 °C (for the material designated as MA. Figure 9j plots and compares the full stress-strain curves measured using the two displacement rates for the entire range of tested temperatures. Similarly, the initial portions of the stress-stain curves are plotted up to 2% strain in Figure 10. As can be seen from these figures, at lower temperatures up to 400 °C, there is little difference in the stress-strain curves from the two different displacement rates. Some of the differences observed in the shape of stress-strain curves at these temperatures are likely related to the inherent material variability from one coupon specimen to another. It is at 500 °C and above that the differences between the two cross-head displacement rates become more significant. For instance, at temperatures higher than 500 °C, the displacement rate of 0.1 in./min results in yield and tensile strengths 30 to 40% higher than those obtained at 0.01 in./min. These data suggest the importance of controlling and reporting loading rates in elevated-temperature tests on structural steel materials, members and connections, and in considering rate effects in overall analysis and design of steel structures for fire conditions.

Effect of Static Yielding

In ambient temperature testing, static yield stress values are often measured in coupon tests to provide a zero-strain rate evaluation of yield stress. Static yield values are useful in research for comparing member and material tests at comparable strain rates (SSRC, 1987) and are useful in the development of design rules that properly account for loading-rate effects (Beedle and Tall, 1960). Static yield stress values at ambient temperature are obtained by stopping the machine cross-heads and holding the cross-heads at a fixed displacement for 3 to 5 min and then reading the value of stress. In the elevated temperature tests reported here, static yielding was examined by suspending cross-head movement during tension tests for periods of either 30 min or 3 min and then measuring the subsequent stress relaxation. These

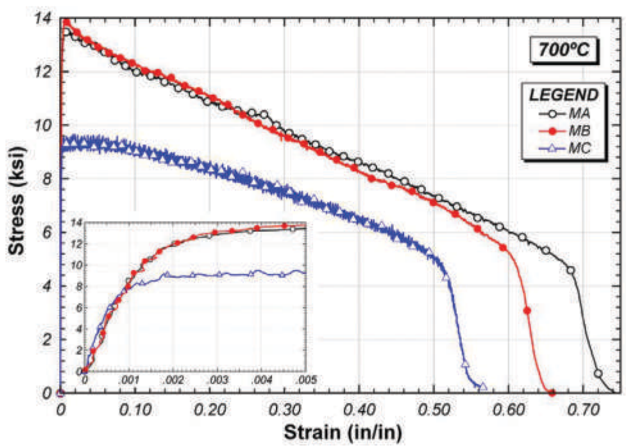

(g) 700 °C

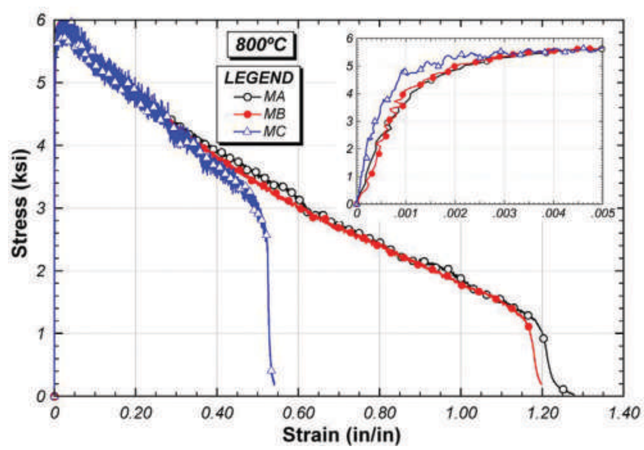

(h) 800 °C

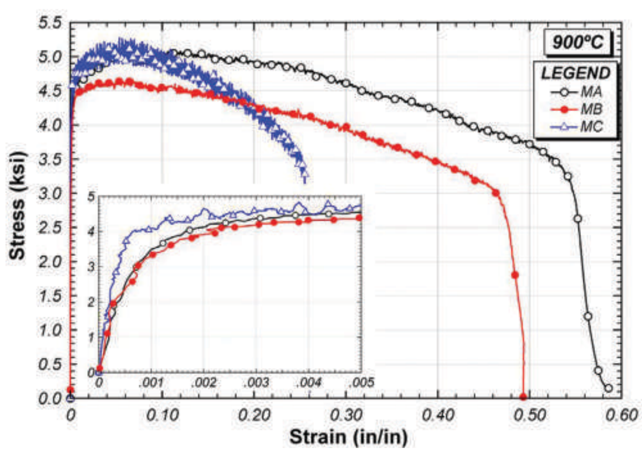

(i) 900 °C

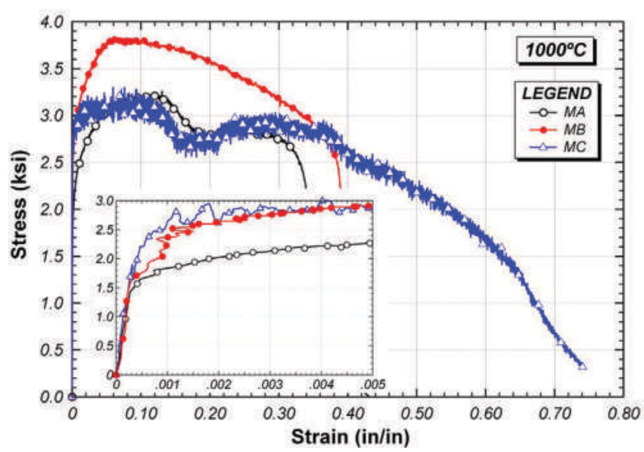

(j) 1000 °C

Fig. 8. Comparison of elevated-temperature stress-strain curves for three different ASTM A992 materials.
(continued from previous page)

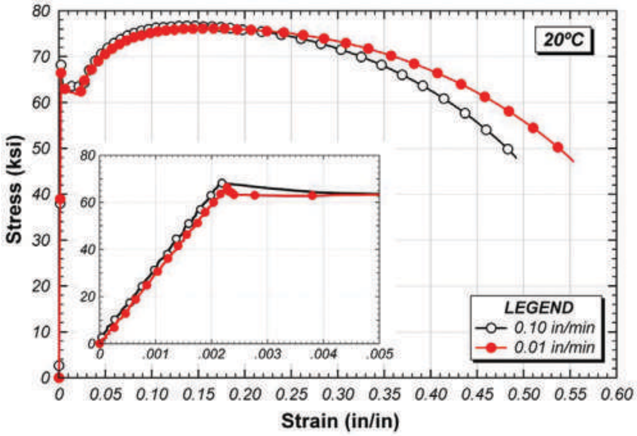

(a) Room temperature

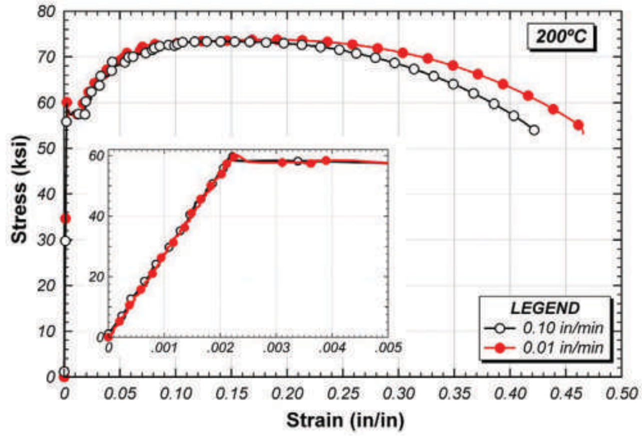

(b) 200 °C

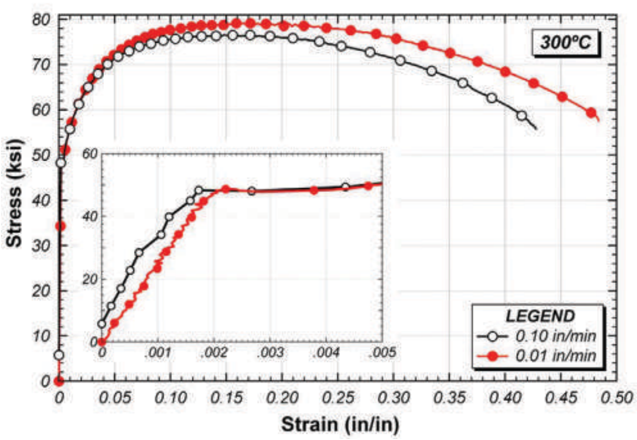

(c) 300 °C

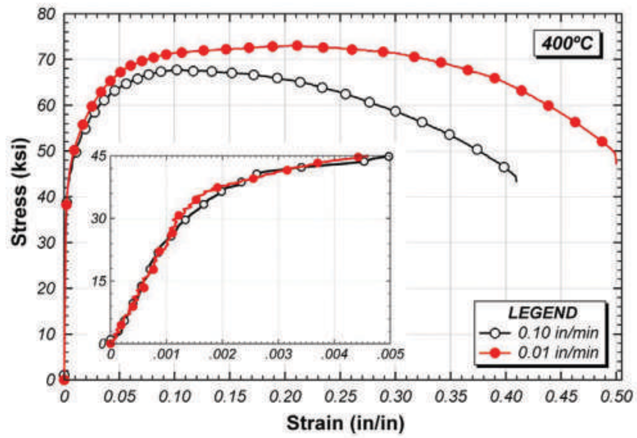

(d) 400 °C

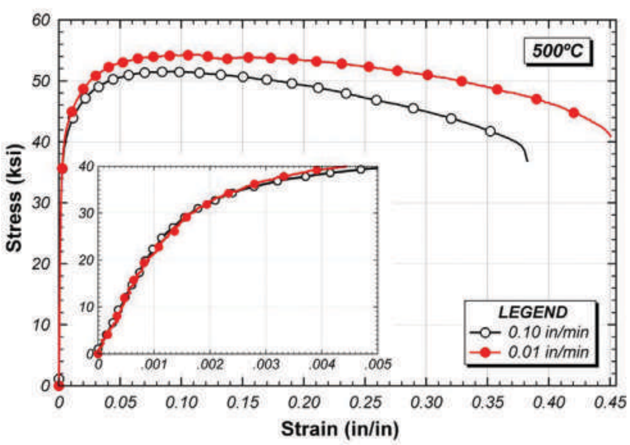

(e) 500 °C

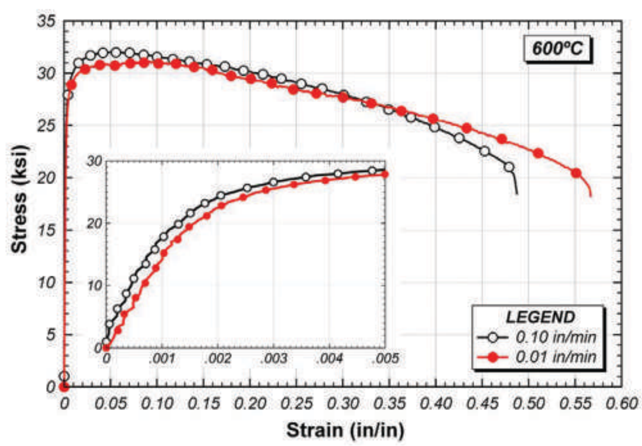

(f) 600 °C

Fig. 9. Comparison of elevated-temperature stress-strain curves for different cross-head displacement rates.
(continued on next page)

static yielding tests were conducted during the slow tests (0.01 in./min) on material MA at different temperatures. The resulting stress-strain curves are shown in Figure 11. Compared with dynamic yielding, static yielding produced significantly lower values of steel strength at high temperatures. For example, at 800 °C, the steel strength almost dropped to zero after a 30-min cross-head hold. The significant difference between static and dynamic yielding reflects the influence of creep and relaxation at high temperatures. Interestingly, at 300 °C, such static yielding behavior tests increased the tensile strength of the coupon, which may be due to strain aging phenomenon at that temperature. The data in Figure 11 further illustrate the importance of rate effects on the effective strength of steel at elevated temperatures and the influence of creep. These factors are often neglected in describing the high-temperature stress-strain response of structural steel but appear to be very important phenomena that merit further investigation. The effect of creep on tensile stress-strain behavior of structural steel at elevated temperatures and interpretation of such stress-strain data will be discussed in more detail later in this paper.

Charpy Impact Tests

Charpy V-Notch impact tests were conducted on samples of steel from material MB that were subjected to elevated temperatures up to 1,000 °C. Results of these tests are listed in Table 2 as impact energies in foot-pounds (ft-lb). As can be seen from Table 2, the results show a significant reduction in CVN values with temperature for temperatures up to 600 °C and then a sharp increase at 700 °C. At temperatures higher than 700 °C, CVN values again start to decrease almost linearly with temperature.

ANALYSIS OF EXPERIMENTAL DATA

In this section, analyses and further discussions of the experimental data are provided along with comparisons of key mechanical properties derived from the stress-strain curves

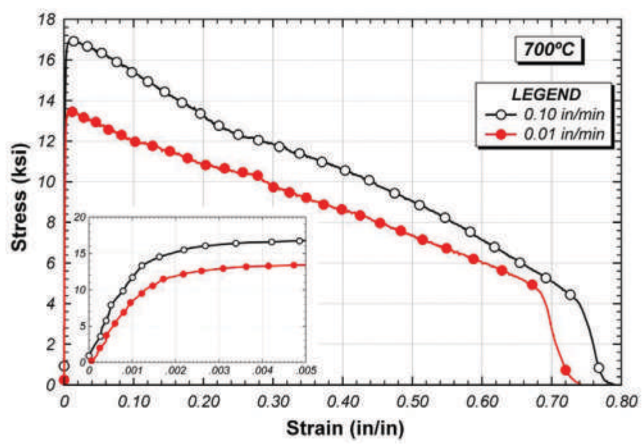

(g) 700 °C

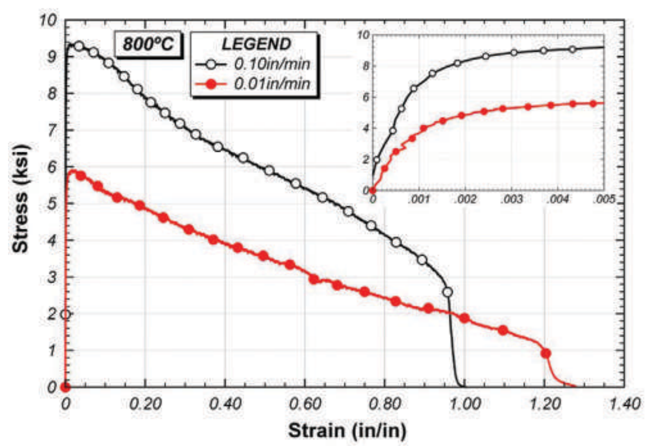

(h) 800 °C

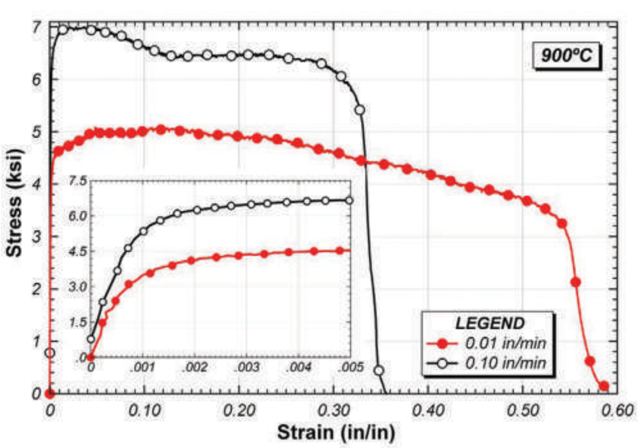

(i) 900 °C

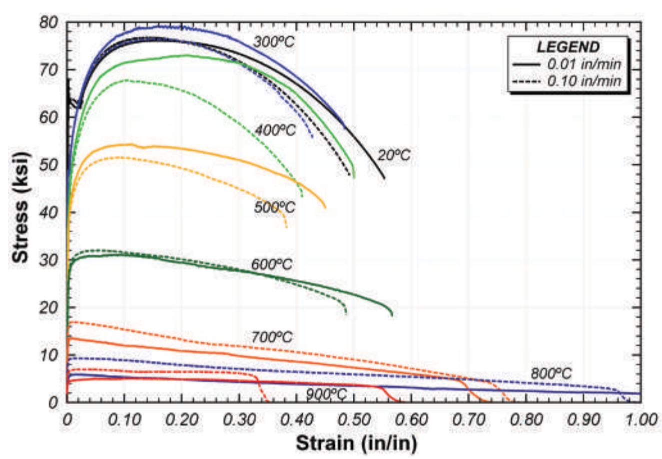

(j) Full stress-strain curves at different temperatures

Fig. 9. Comparison of elevated-temperature stress-strain curves for different cross-head displacement rates.
(continued from previous page)

Table 2. CVN Impact Energy for ASTM A992 Steel at Elevated Temperatures (ft-lb)										
Temperature (°C)	20	200	300	400	500	600	700	800	900	1000
CVN value	238	233	209	143	69	59	183	134	103	64

at elevated temperatures. These properties include the yield stress, tensile strength, proportional limit, elastic modulus and total elongation. Data on selected properties are also compared with the predictions from Eurocode 3 (2006) and the AISC *Specification* (2010).

General Observations

As can be observed from Figures 5, 6 and 7, the stress-strain behavior of ASTM A992 steel undergoes significant changes as temperature increases. In general terms, the steel loses strength and stiffness with increase in temperature. More specifically, at elevated temperatures, both the yield stress and the modulus of elasticity are reduced from their room-temperature values. Except for low temperatures, the tensile strength also reduces with temperature. In addition to the reduction in yield stress, tensile strength and modulus of elasticity, the shape of the stress-strain curve at high temperatures is fundamentally different from the corresponding one at ambient temperature. At high temperatures, the stress-strain curve does not exhibit a well-defined yield plateau and becomes highly nonlinear at low levels of stress. In other words, at elevated temperatures, the proportional limit occurs at a stress less than the yield stress. It should be emphasized that the greater nonlinearity exhibited by the stress-strain curves at high temperatures can have a significant influence on member behaviors governed by stability modes of failure, where stiffness is a critical material property.

Yield Stress

At temperatures above approximately 300 to 400 °C, the measured stress-strain curves do not exhibit a well-defined yield plateau. Consequently, defining yield stress becomes more subjective at elevated temperatures than at ambient temperature. For metals that do not exhibit a yield plateau, the 0.2% offset yield stress definition is widely used and is specified by ASTM E21 (ASTM, 2009) for defining the yield stress at elevated temperatures. With this method, yield stress is defined as the stress at the intersection of the stress-strain curve and the proportional line offset by 0.2% strain. This definition of yield stress is also presented graphically in Figure 12. Within the literature on elevated-temperature properties of structural steel, various definitions of yield stress have been used. In addition to the conventional 0.2% offset definition, the yield stress has also been defined as the stress corresponding to 0.5% total strain and as the stress corresponding to 2% total strain, as well as other definitions. These alternate definitions are also illustrated in Figure 12. Both Eurocode 3 (2006) and the AISC *Specification* (2010) have adopted the 2% total strain definition for the yield stress of structural steel at elevated temperatures. It is important to note that because this definition is not a standard definition for yield stress, the yield stress corresponding to the 2% total strain is called "effective yield stress" in Eurocode 3. Figure 13 shows the initial portion of a stress-strain curve from this test program for 400 °C and a cross-head displacement rate of 0.01 in./min. The values of yield stress are shown for

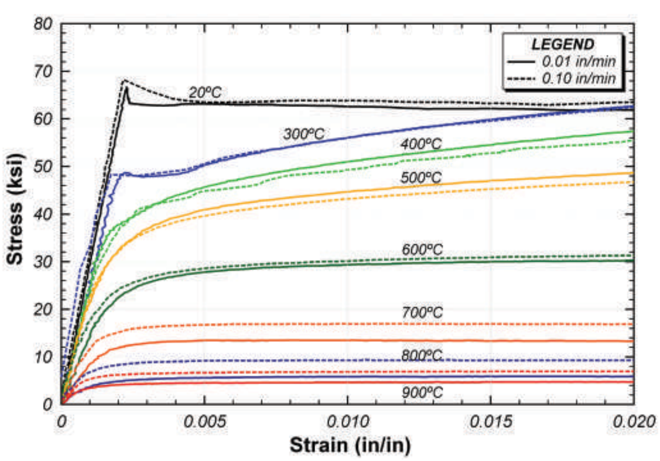

Fig. 10. Cross-head displacement-rate effects at elevated temperatures—stress-strain curves up to 2% strain.

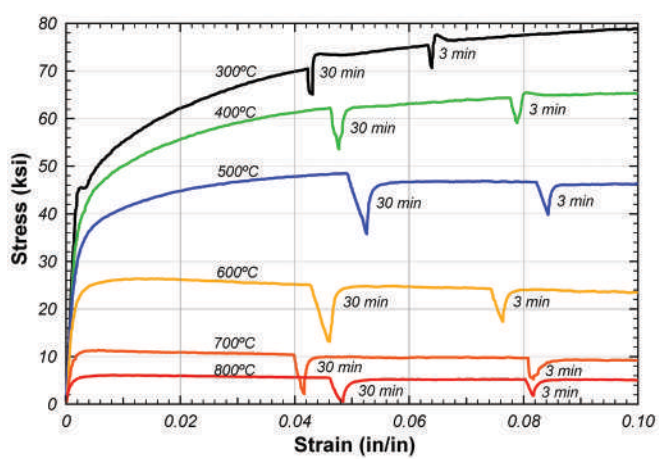

Fig. 11. Static yield phenomenon at elevated temperatures for ASTM A992 steel.

the three definitions of yield stress: 43.8 ksi for 0.2% offset strain, 45.8 ksi for 0.5% total strain and 57.5 ksi for 2% total strain definition. It is clear that the choice of the definition of yield stress can have a very large impact on the resulting value of yield stress.

Yield stress retention factors based on the data collected in this research are plotted in Figure 14. The yield stress retention factor is defined as the yield stress at a specific temperature (using stress-strain curves at 0.01 in./min cross-head displacement rate) divided by the yield stress at ambient temperature. The retention factors for yield stress based on the 0.2% offset, 0.5% total strain and 2% total strain definitions are compared with retention factors from Eurocode 3 (2006) and from the AISC *Specification* (2010) in Figure 14. Note that Eurocode 3 and the AISC *Specification* use the same retention factors for yield stress and are, therefore, plotted as a single line. As can clearly be seen from Figures 14a and 14b, for temperatures in the range of 100 to 500 °C, the yield stress retention factors from tests, based on the 0.2% offset and 0.5% total strain definitions, are significantly lower than the corresponding values specified by Eurocode 3 and the AISC *Specification*. To the contrary, Figure 14c shows a good agreement between retention factors from test data and those predicted by the codes, when the retention factors for the test data are based on the 2% total strain definition of yield stress. Similar observations can be made from Figures 14d, 14e and 14f, where yield stress retention factors are presented and compared with code predictions for materials MA, MB and MC, respectively. From these figures, it can be seen that the values of yield stress from the test data are fairly close to one another for the 0.2% offset and 0.5% total strain definitions. Further, above about 600 °C, all three definitions of yield stress give similar values. However, below 600 °C, the yield stress based on the 2% total strain definition is significantly higher than the yield stress values based on the other two definitions.

As is clear from Figure 14, the yield stress of steel at elevated temperatures up to about 600 °C is highly dependent on the manner in which it is defined. Based on Twilt and Both (1991), it appears that the yield stress retention factors for structural steel at elevated temperatures used in Eurocode 3 (2006) were adopted from British Steel Corporation data (Kirby and Preston, 1988). However, little was found in the literature to support this definition of yield stress for structural-fire engineering design of steel structures. It seems that the most appropriate definition for yield stress of steel at elevated temperatures ultimately lies in how these values are used in design formulas, and further investigation and discussion of this issue appears justified. The design implications of different definitions for the yield stress will be discussed in more detail later in this paper.

Finally, for reference, the yield stress values evaluated using different definitions for each steel material at elevated temperatures are presented in Table 3. The yield stress data reported in Table 3 are based on tension tests conducted under the slow rate condition of 0.01 in./min.

Tensile Strength

The retention factors for tensile strength, obtained for all steel materials tested in this program, are compared with the corresponding values in Eurocode 3 (2006) and AISC *Specification* (2010) in Figure 15. In Figure 15a, the tensile strength retention factor is defined as the tensile strength measured at a specific temperature (using stress-strain curves at 0.01 in./min cross-head displacement rate) divided by the yield stress measured at ambient temperature. The data are presented in this manner because this is how the tensile strength retention factor is defined in both Eurocode 3 (2006) and the AISC *Specification* (2010). For temperatures at and above 400 °C, both Eurocode 3 and the AISC *Specification* take the elevated-temperature tensile strength

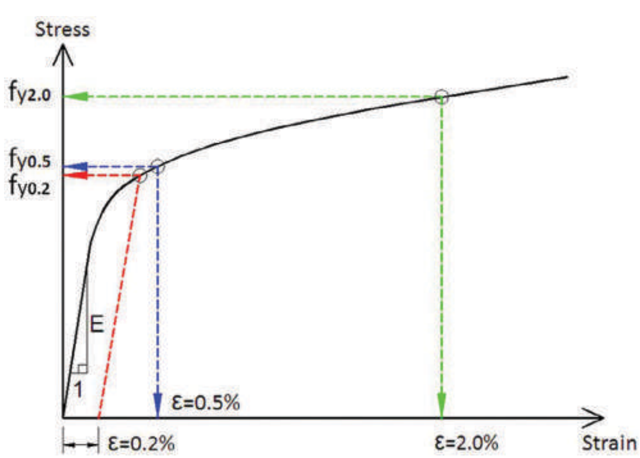

Fig. 12. Different definitions of yield stress.

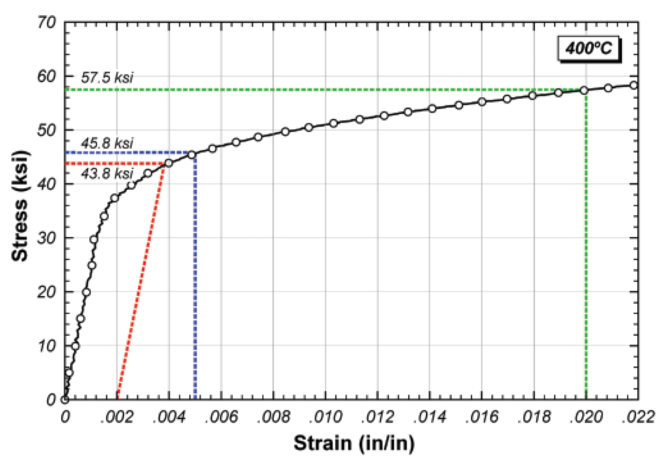

Fig. 13. Yield stress values for test at 400 °C.

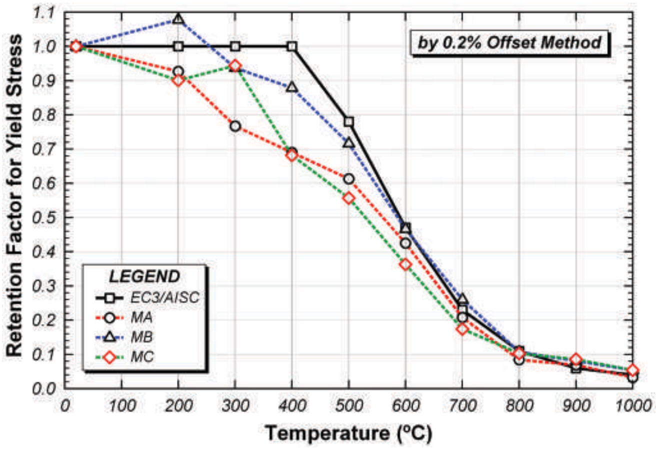

(a) 0.2% offset definition

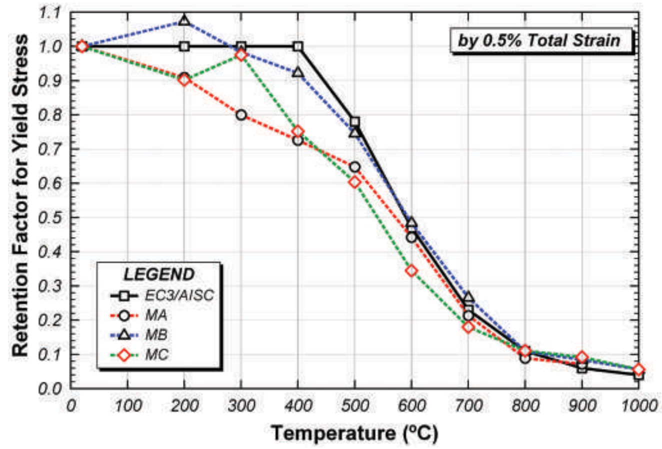

(b) 0.5% total strain definition

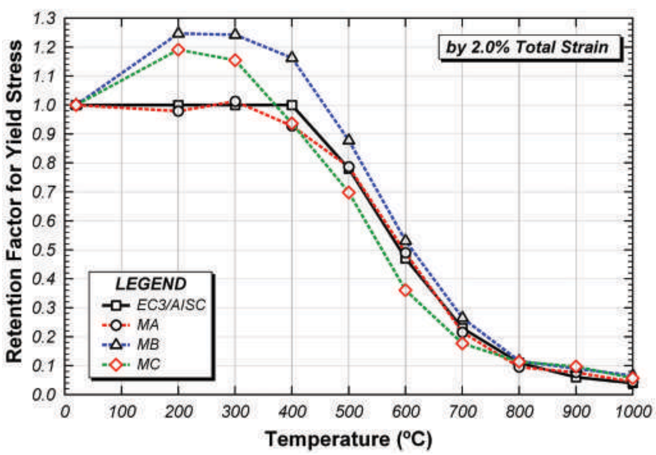

(c) 2% total strain definition

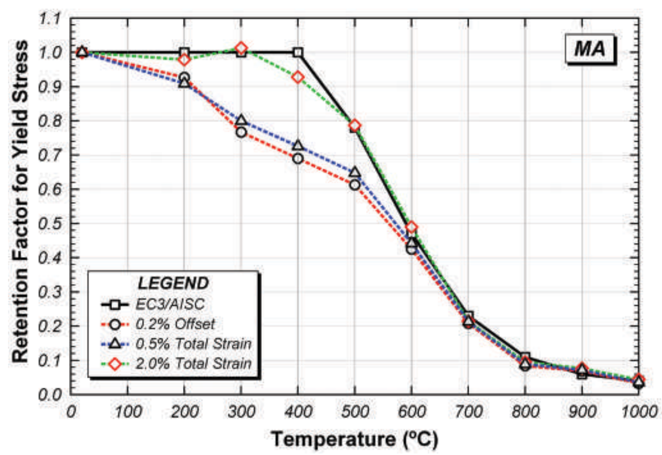

(d) Material MA: different yield stress definitions

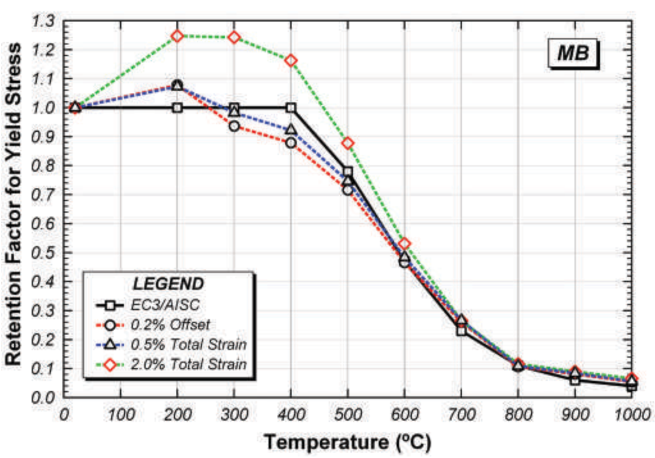

(e) Material MB: different yield stress definitions

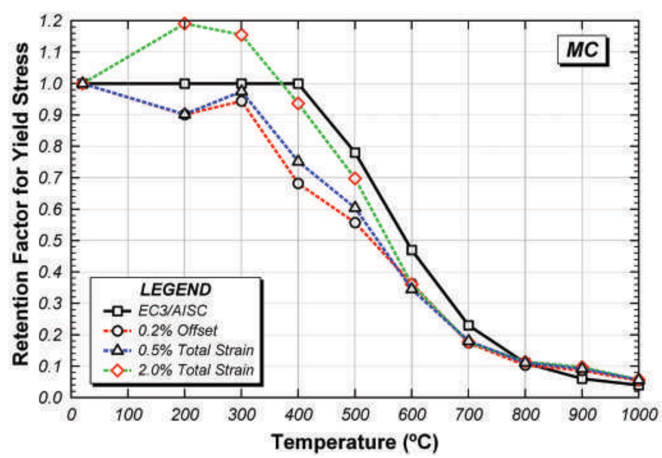

(f) Material MC: different yield stress definitions

Fig. 14. Yield stress retention factors.

Table 3. Yield Stress Values for ASTM A992 Steel at Elevated Temperatures (ksi)											
Temperature (°C)		20	200	300	400	500	600	700	800	900	1000
MA	0.2% offset	63.1	58.5	48.4	43.5	38.7	26.8	13.1	5.3	4.4	2.1
	0.5% total strain	63.2	57.4	50.5	45.8	41.0	27.9	13.5	5.6	4.6	2.3
	2.0% total strain	61.9	60.6	62.8	57.5	48.7	30.3	13.3	5.9	4.7	2.7
MB	0.2% offset	51.4	55.4	48.2	45.2	36.8	24.0	13.3	5.5	4.1	2.8
	0.5% total strain	51.7	55.5	50.8	47.7	38.6	25.1	13.8	5.7	4.4	2.9
	2.0% total strain	50.9	63.4	63.2	59.2	44.6	27.0	13.5	5.9	4.6	3.4
MC	0.2% offset	51.8	46.7	48.9	35.4	28.8	16.8	9.0	5.3	4.5	2.8
	0.5% total strain	51.3	46.3	50.0	38.6	31.0	17.7	9.2	5.7	4.7	2.9
	2.0% total strain	51.6	61.4	59.6	48.3	36.0	18.6	9.2	5.9	5.0	3.0

equal to the elevated-temperature yield stress, or elevated-temperature effective yield stress as defined by Eurocode 3.

Figure 15b shows the tensile strength retention factors from the tests, where the retention factor is defined as tensile strength measured at a specific temperature divided by the tensile strength measured at ambient temperature (using stress-strain curves at 0.01 in./min cross-head displacement rate). This seems to be a more conventional definition of tensile strength retention factor. For reference, the tensile strength values obtained for each steel material at elevated temperatures are shown in Table 4. Comparing the elevated-temperature tensile strength values listed in Table 4 with the elevated-temperature yield stress values based on the 2% total strain definition listed in Table 3, it can be seen that the tensile strength generally exceeds the yield strength for temperatures up through and including 500 °C. For 600 °C and above, the measured tensile strength and yield strength values are essentially the same.

Elastic Modulus

The elastic modulus was determined by measuring the slope of the initial linear portion of the stress-strain curves for tests conducted at a cross-head displacement rate of 0.01 in./min. Strains were measured in the tension coupon tests using a nonaveraging type extensometer; that is, strains were measured on only one side of the coupon. Consequently, errors at small strain levels can occur due to bending of the coupon resulting in errors in the measured strain. As such, the elastic modulus values derived from the stress-strain curves may be subject to some error. Nonetheless, the elastic modulus data were still examined for general trends.

The variation of elastic modulus with temperature is plotted in Figure 16 for all steel materials tested in this program. Retention factors for elastic modulus are plotted in Figure 17, where the retention factor is defined as the elastic modulus measured at a specific temperature divided by

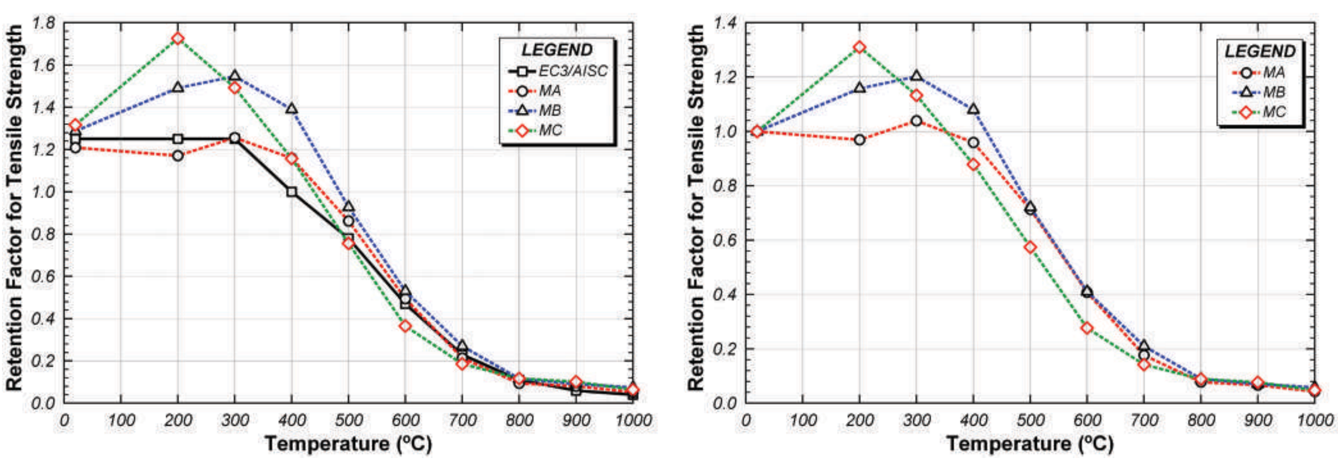

(a) Using $(f_{u,T}/f_{y,20°C})$ definition

(b) Using $(f_{u,T}/f_{u,20°C})$ definition

Fig. 15. Tensile strength retention factors.

Table 4. Tensile Strength at Elevated Temperatures (ksi)										
Temperature (°C)	20	200	300	400	500	600	700	800	900	1000
MA	76.2	73.8	79.2	73.1	54.3	31.1	13.5	5.9	5.1	3.3
MB	66.2	76.6	79.5	71.5	47.7	27.2	13.9	5.9	4.7	3.9
MC	68.3	89.4	77.4	60.0	39.2	18.9	9.7	6.1	5.3	3.3

the elastic modulus at ambient temperature. Compared to Eurocode 3 (2006) and the AISC *Specification* (2010) in Figure 17, the experimental predictions of retention factors for elastic modulus show the same overall changing trend at elevated temperatures, albeit the reductions in the modulus values with temperature are less severe than predictions by Eurocode 3 and by AISC *Specification*. The elastic modulus data are more scattered among the three steel samples in comparison with the results shown earlier for the yield and tensile strength retention factors (referring to Figures 14 and 15), especially at temperatures at and above 600 °C. It is not clear whether this variability in elastic modulus values for different steel materials is an intrinsic material variability or, in fact, is an experimental error.

Proportional Limit

The proportional limit was determined by estimating the highest stress at which the curve in a stress-strain diagram is a straight line. At room temperature, the proportional limit is about the same as the yield stress. However, at high temperatures, proportional limits are usually significantly lower than yield stress. Figure 18 plots the calculated values of proportional limits for all steel materials at elevated temperatures, using stress-strain curves measured at a cross-head displacement rate of 0.01 in/min.

Retention factors for proportional limit at elevated temperatures are also calculated and compared with the corresponding ones in Eurocode 3 (2006) and in the AISC *Specification* (2010), as shown in Figure 19. In general, reasonable agreement can be found between experimental retention factors for proportional limit and those predicted by Eurocode 3 and by the AISC *Specification*.

It is important to note that compared with other mechanical properties considered here, the proportional limit shows a higher rate of reduction with increasing temperature (see Figures 14, 15, 17 and 19). This observation is important because the tangent modulus reduces rapidly after exceeding the proportional limit (Morovat et al., 2010, 2011). The rapid reduction of tangent modulus at elevated temperatures is particularly significant in stability related problems.

Elongation at Fracture

Figure 20 plots the elongation of the steel coupons with temperature, for coupons tested at a cross-head displacement rate of 0.01 in/min. As seen in this figure, the elongation for materials MA and MB is relatively constant for temperatures up to 500 °C; then shows a sharp increase up to 800 °C; and finally a sharp decrease at 900 °C, almost to its corresponding value at room temperature. The reason the maximum elongation occurs at 800 °C is most probably related to the

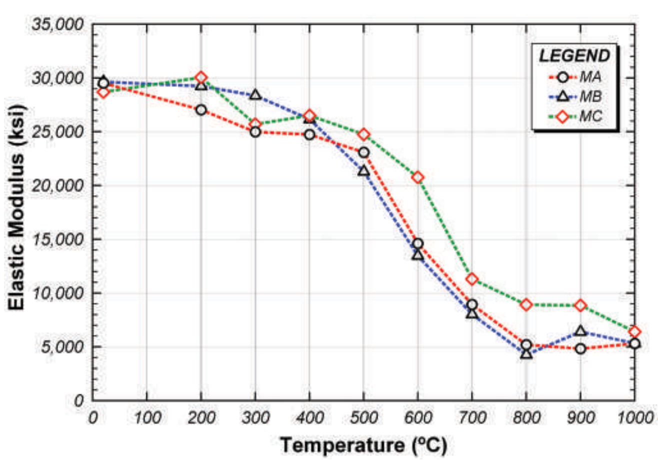

Fig. 16. Changes in elastic modulus with temperature.

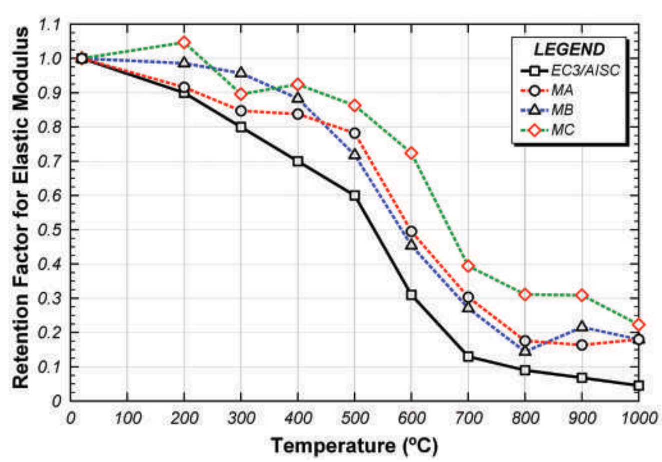

Fig. 17. Elastic modulus retention factors.

phase change around the eutectoid point for low-carbon steel at about 727 °C. Due to the phase change from ferrite (α-Fe) to austenite (γ-Fe), the elongation continuously increases up to the eutectoid point. In the case of material MC, the same trend can be observed, although with less variation that seen for materials MA and MB. The primary difference in the trend of elongation can be seen in the temperature range of 900 to 1000 °C, where material MB sees a drop in elongation while material MC experiences a rise in elongation.

Eurocode 3 (2006) does not provide retention factors for elongation, and as a result, no comparison with Eurocode 3 is provided here. However, Eurocode 3 provides equations for stress-strain curves where, irrespective of the temperature, a constant value of 20% is suggested for the elongation of steel at elevated temperatures. Stress-strain curves from Eurocode 3 will be discussed and compared with experimental results later in this paper.

Strain Corresponding to the Tensile Strength

Figure 21 plots the strain at which the tensile strength is developed, for coupons tested at a cross-head displacement rate of 0.01 in/min. As seen in this figure, the strain at the tensile strength shows a dramatic decrease with increasing temperature from 400 to 800 °C. For all three material samples, the lowest values of strain at the development of the tensile strength occurred at temperatures of 700 to 800 °C. At these temperatures, the strains at the development of the tensile strength were on the order of 1 to 2%, representing a very large reduction from the ambient temperature values, which were on the order of 16 to 18%. This trend further reinforces previous observations that the basic shape of the stress-strain curve for steel can be very different at elevated temperatures compared to ambient temperature.

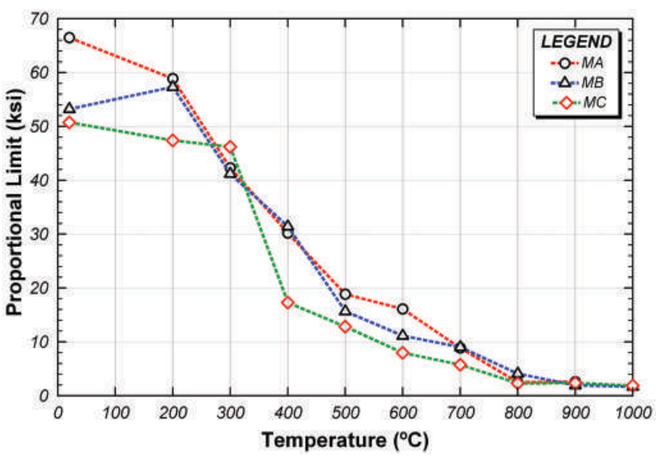

Fig. 18. Changes in proportional limit with temperature.

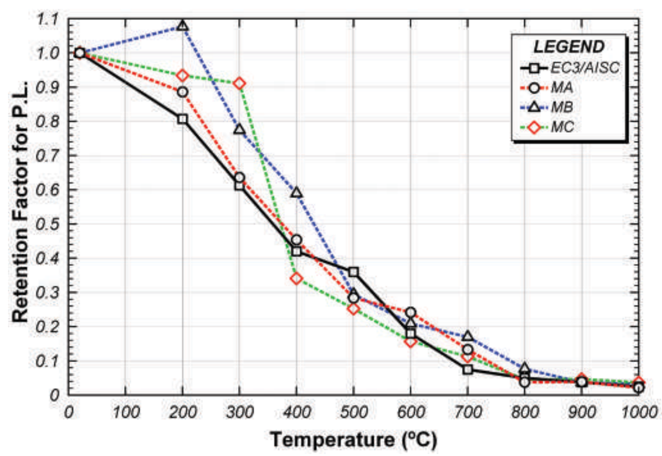

Fig. 19. Proportional limit retention factors.

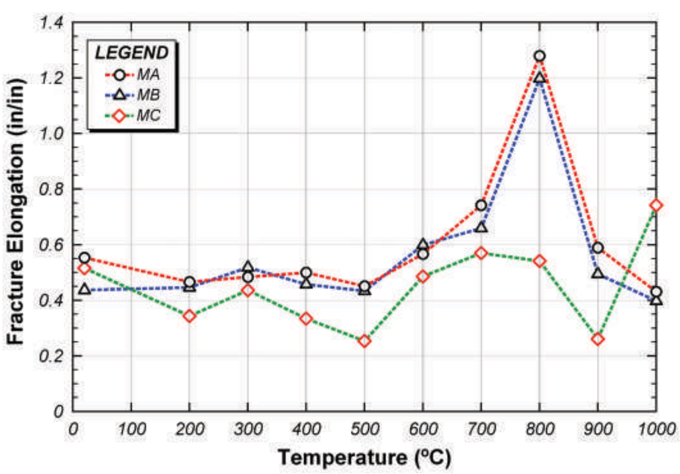

Fig. 20. Changes in elongation with temperature.

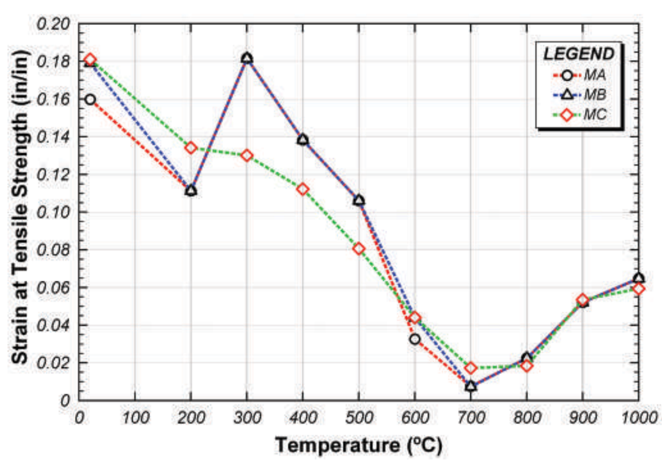

Fig. 21. Changes in strain corresponding to tensile strength with temperature.

Shape of Stress-Strain Curves

The use of advanced analysis methods, such as finite element analysis, to predict the response of steel structures to fire requires a more complete description of the elevated-temperature mechanical properties of steel, including data on the shape of the stress-strain curves at elevated temperatures. Eurocode 3 (2006) provides equations to predict the stress-strain curves for structural steel at elevated temperatures for use in advanced analysis. Generally speaking, these equations divide stress-strain curves into four sections and include both rising and descending portions of the stress-strain curves. In addition, these stress-strain curves do not include strain hardening, thereby assuming the yield and tensile strengths to be the same. Eurocode 3 has additional curves that include strain hardening at lower temperatures, although these curves are not considered in this paper.

In Figure 22, stress-strain curves from tests conducted at a cross-head displacement rate of 0.01 in./min are compared against the corresponding curves predicted by Eurocode 3 (2006) at several representative temperatures. It can be seen that at strains smaller than 15%, the Eurocode's simplified stress-strain relationships match the test data quite well. However, at strains larger than 15%, the Eurocode 3 model displays a faster stress drop and a smaller total elongation and ductility. It is also important to note that while the typical shapes of the stress-strain curves of Eurocode 3 are similar for all temperatures higher than 400 °C, the actual curves obtained from tests vary with temperature significantly. Furthermore, as can be seen in Figure 22, all the stress-strain curves terminate at 20% strain. In other words, in Eurocode 3, a temperature-independent value of 20% is considered for the final elongation of steel at elevated temperatures. This is not the case for experimental stress-strain curves, where final elongation changes significantly with temperature.

It should be noted that stress-strain curves presented in Figure 22 correspond to the tests conducted at the lower displacement rate (0.01 in./min). When the Eurocode 3 (2006) equations are compared with stress-strain curves from tests conducted at the higher displacement rate (0.1 in./min), the correlation is not as good as that seen in Figure 22.

INTERPRETATION OF HIGH-TEMPERATURE STRESS-STRAIN DATA

This section provides more in-depth discussion on two major aspects of the behavior of ASTM A992 steel at elevated temperatures that have direct implications in the design of steel structures for fire: definition of yield stress and treatment of time-dependent effects.

Definition of F_y for Use in Design Equations at Elevated Temperatures

As noted before in the discussion of retention factors for yield stress at elevated temperatures, different definitions of yield stress can result in significantly different values of yield stress, especially at temperatures below 600 °C. Three definitions were considered earlier for yield stress, corresponding to the stress at 0.2% offset strain, 0.5% total strain and 2% total strain. As shown earlier in Figure 13, for a test conducted at 400 °C, these three definitions resulted in yield stress values of 43.8, 45.8 and 57.5 ksi. Clearly, the definition adopted for yield stress has a very large impact on the resulting yield stress value. As also noted earlier, Eurocode 3 (2006) and the AISC *Specification* (2010) define the elevated-temperature yield stress (effective yield stress in Eurocode 3) as the stress at a total strain of 2%. A review of past test programs on the elevated-temperature properties of structural steel showed that a number of different definitions for yield stress were adopted by various authors (Kirby and

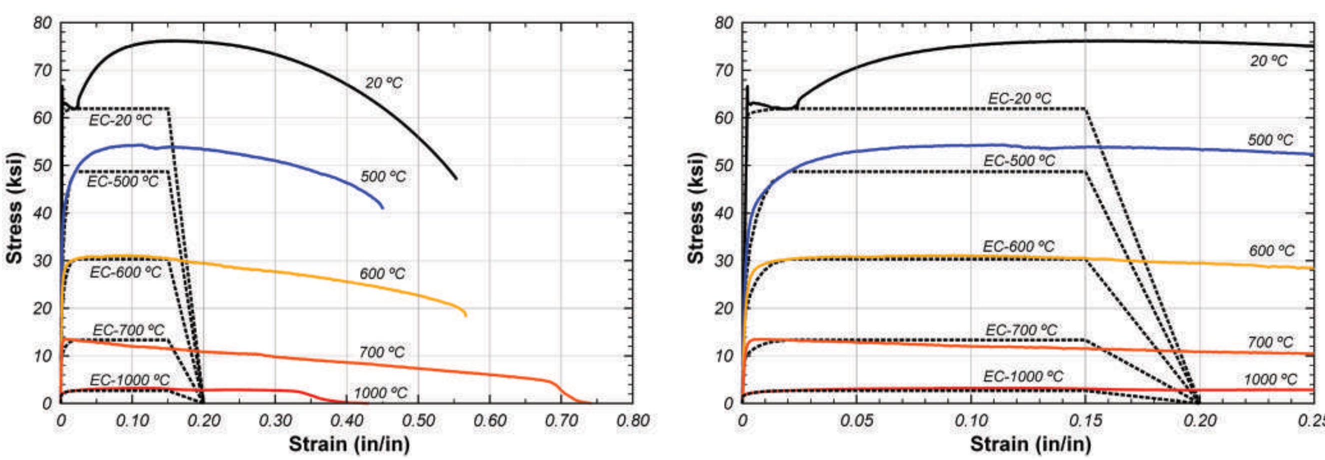

(a) Complete stress-strain curves *(b) Stress-strain curves up to 25% strain*

Fig. 22. Experimental stress-strain curves compared to stress-strain curves from Eurocode 3 (2006).

Preston, 1988) and that at least some of the apparent variability in elevated-temperature yield stress values reported in the literature was due to variations in the definition of yield stress.

To consider the most appropriate definition of elevated-temperature yield stress in design, it is instructive to consider how yield stress values are used in calculations of member strength. In general, yield stress is used in computing member strength based on yield limit states and based on stability limit states. For yield limit states at ambient temperature, the value of yield stress is used to compute, for example, the plastic moment capacity of a wide-flange cross-section, $M_p = Z\ F_y$, the plastic shear capacity of a cross-section, $V_p = 0.6F_y\, A_{web}$, and the plastic axial capacity of a cross-section, $P_y = A\ F_y$. In these equations, Z is the plastic section modulus, A_{web} is the web area, A is the total cross-sectional area, and F_y is the minimum specified yield stress at ambient temperature (50 ksi for ASTM A992 steel, 36 ksi for ASTM A36 steel, etc.). When computing member strength at elevated temperatures for yield limit states, both Eurocode 3 (2006) and the AISC *Specification* (2010) use their own specific formulas for ambient temperature but replace F_y with $F_{y(T)}$, where $F_{y(T)}$ is the value of yield stress at temperature T. The value of $F_{y(T)}$ is determined by multiplying the ambient value of F_y by the yield stress retention factor for temperature T. Thus, the corresponding elevated-temperature cross-section strength values are simply $M_{p(T)} = ZF_{y(T)}$, $V_{p(T)} = 0.6\ F_{y(T)}\, A_{web}$, and $P_{y(T)} = \mathrm{A}\ F_{y(T)}$.

To better gauge the design implications of different definitions for the yield stress when computing elevated-temperature strength based on yield limit states, a simply supported beam was analyzed using finite element analysis at elevated temperatures using the stress-strain curves obtained in this testing program. The model is shown as insets in Figure 23 and consists of a 30-ft-long W18×60 beam with two equal concentrated, symmetrically applied loads. The model was developed on the finite element analysis program Abaqus (2011). The beam was analyzed at 400 °C and at 600 °C. For each temperature, the measured stress-strain curve for material MC was used as input to Abaqus.

Figure 23 shows the results of the Abaqus analysis. Analysis results are plotted as moment in the beam (computed as the applied load P multiplied by 120 in.) versus mid-span displacement. Results are plotted for 400 and 600 °C. Also shown in each plot is the computed plastic moment capacity of the beam, $M_{p(T)} = ZF_{y(T)}$. Three different values of $M_{p(T)}$ are shown on each plot, corresponding to three different definitions of $F_{y(T)}$. Thus, these plots provide a comparison of the estimated actual bending capacity of the beam based on Abaqus analysis, and the bending capacity as would be computed in a design calculation; that is, $M_{p(T)} = ZF_{y(T)}$. Among the three yield stress definitions, the value of $M_{p(T)}$ based on yield stress at 2% total strain appears to provide the best estimate of the bending capacity predicted by the Abaqus analysis. When this bending capacity is achieved, the predicted mid-span displacement of the 30-ft-long beam is about 25 to 30 in. for both temperatures. While this deflection is quite large, it can be argued that in an extreme fire scenario, such deflections may be considered acceptable, as long as the beam can safely support its load. On the other hand, if the design objective is to limit deflections of the beam in a fire scenario to relatively small values, perhaps to allow for easier repair, then adopting the 0.2% offset strain definition for yield stress may be more reasonable. For this example, if $M_{p(T)}$ is computed using the 0.2% offset definition of yield stress, the predicted deflection of the 30-ft-long beam is about 5 in. for both temperatures. Thus, the most appropriate definition of yield stress for calculating elevated-temperature member strength for yield limit states is a matter of judgment and structural performance requirements.

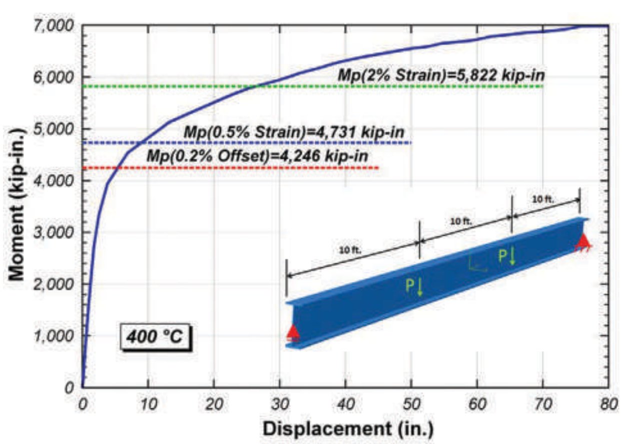

(a) Beam response at 400 °C

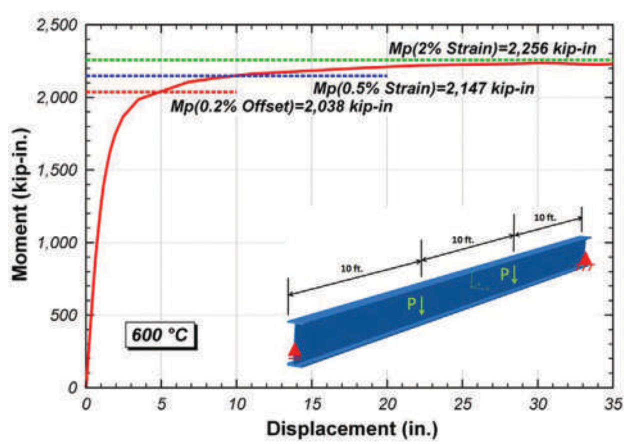

(b) Beam response at 600 °C

Fig. 23. The load-carrying capacity of a steel beam at elevated temperatures.

However, in the view of the authors, the definition of yield stress based on 2% total strain, as currently used in Eurocode 3 (2006) and the AISC *Specification* (2010), seems to provide a reasonable basis for design.

As noted earlier, values of yield stress are also used when computing member strength based on stability limit states (e.g., when computing column buckling capacity). Buckling capacity is more closely related to material stiffness than to material strength, and ambient-temperature formulas for column capacity depend on both E and F_y of the steel. However, to predict column capacity at elevated temperatures, it is not possible to use ambient-temperature formulas for column buckling and simply replace E and F_y at ambient with the corresponding values $E_{(T)}$ and $F_{y(T)}$ at the temperature of interest (Takagi and Deierlein, 2007; Ho, 2010). This is because of the highly nonlinear shape of the stress-strain diagram and the substantial difference between yield stress and proportional limit for steel at elevated temperatures. That is, the fundamental shape of the stress-strain diagram for steel at elevated temperatures is very different than the shape at ambient, and this difference has a large impact on buckling behavior. Thus, design formulas for buckling at elevated temperatures must consider values of modulus of elasticity, proportional limit, and yield stress at elevated temperatures, and the formulas must be calibrated or fit to either experimental or numerical predictions of column buckling capacity. Such a calibration can be done using any of the possible definitions of yield stress. For example, equations for flexural buckling of columns and lateral torsional buckling of beams at elevated temperatures provided in the AISC *Specification* (2010) use the value of yield stress at 2% total strain, based on calibration to numerical buckling predictions by Takagi and Deierlein (2007). Thus, when choosing a definition of yield stress at elevated temperatures for use in computing buckling capacities, any of the definitions of elevated-temperature yield stress can be used, as long as the buckling formula has been appropriately calibrated to the chosen definition of yield stress.

In summary, the definition adopted for the yield stress of steel at elevated temperatures can have a large impact on the value of yield stress, and in turn, can have a large impact on the member strength calculations. At present, Eurocode 3 (2006) and the AISC *Specification* (2010) define elevated-temperature yield stress as the stress at a total strain of 2%. It should be further noted that Eurocode 3 (2006) refers to the 2% total strain as the yield strain and the yield stress corresponding to the 2% total strain as the effective yield stress. Based on the previous discussion, this definition of yield stress appears to provide a reasonable basis for member strength calculations at elevated temperatures. Note that when the response of a steel structure to fire is determined using advanced analysis, such as by finite element analysis, the actual elevated-temperature stress-strain curve can be used in the analysis, and there is no particular need to define a yield stress. Finally, for the three samples of ASTM A992 steel tested in this research program, the yield stress retention factors based on the 2% total strain definition match reasonably well with the yield stress retention factors defined in Eurocode 3 (2006) and the AISC *Specification* (2010).

Time Effects on Stress-Strain Behavior of Steel at Elevated Temperatures

Time-dependent or creep effects can have significant impact on the behavior of structural steel at elevated temperatures (Morovat et al., 2012; Lee, 2012). In general, time-dependent effects can be explicitly accounted for by conducting specific material characterization tests at elevated temperatures. One common way to characterize time-dependent effects on the

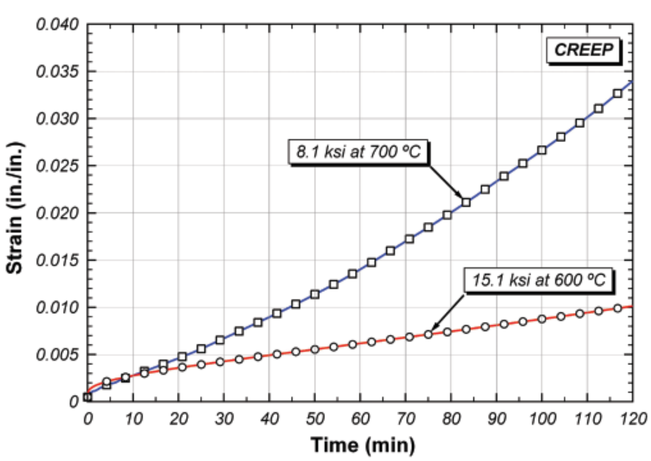

Fig. 24. Representative creep curves for material MC.

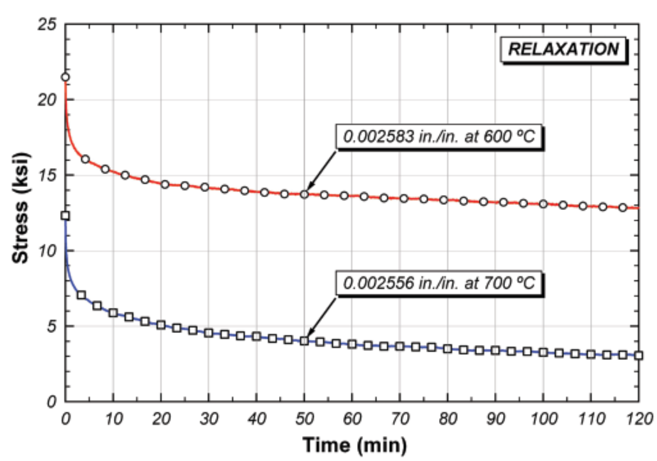

Fig. 25. Representative relaxation curves for material MC.

behavior of structural steel at high temperatures is to conduct creep tests, in which the steel coupons are subjected to constant stress and temperature and strain is measured as a function of time. Representative results of such tests, known as creep curves, for material MC are shown in Figure 24. Another common way to study the time-dependency of steel material behavior at high temperatures is to conduct relaxation tests, in which the steel coupons are subjected to constant strain and temperature, and stress is measured as a function of time. Sample results of such tests, known as stress relaxation curves, for material MC are shown in Figure 25.

Data like those shown in Figures 24 and 25 clearly show the significant time dependency of steel material behavior at elevated temperatures. As described earlier in this paper, an apparent difference between stress-strain predictions from steady-state and transient-state temperature tests is in the way they treat the rate- or time-dependent effects. In steady-state temperature tests, rate effects are considered using load or displacement rates, while in transient-state temperature tests, such effects are taken into account using heating rates. Stress-strain curves obtained at two different displacement rates and shown in Figure 9 are examples of how the rate-dependent effects are considered in the steady-state temperature tests. As mentioned previously, these curves clearly indicate the significance of rate or time effects on the stress-strain behavior of structural steel at elevated temperatures, especially at temperatures at or above 500 °C. What is even more significant about the stress-strain curves in Figure 9 is that they represent the complexities involved in interpreting the results of tensile tests at elevated temperatures for use in design. Another difficulty in choosing stress-strain curves most representatives of the structural steel behavior at high temperatures is that there is no clear basis on how to compare the results from steady-state and transient-state temperature tests at elevated temperatures.

Based on the preceding discussion, it seems that the interpretation of material test results in designing steel structures for fire safety should consider how the effect of creep should be treated in analysis. If creep is explicitly considered in the analysis using high-temperature creep models for structural steel (e.g. Harmathy, 1967; Fields and Fields, 1989; Lee, 2012; Morovat et al., 2012), the basic stress-strain curves should probably have the least amount of creep present in them, and testing at higher strain rates is perhaps more appropriate. On the other hand, for some design problems, considering creep in just a very approximate way may be acceptable, and the lower loading rates, which implicitly include a significant amount of creep, are perhaps more justifiable. Unfortunately, while some studies suggest testing rates at which creep becomes significant in tension tests at elevated temperatures (Cooke, 1988; Kirby and Preston, 1988; Outinen, 2006), it is not clear how fast tension tests should be performed so that they become time-independent or how slowly they should be run in order to include an appropriate amount of creep in the structural response analysis. Consequently, the interpretation of tensile stress-strain data at elevated temperatures is somewhat influenced by the treatment of rate effects and time effects. This is an area that merits additional research, particularly at high temperatures where time-dependent effects become more important.

CONCLUSIONS

Results of an experimental program on the mechanical properties of ASTM A992 structural steel at elevated temperatures have been presented along with testing techniques and procedures. Steady-state temperature tests were conducted on steel coupons in tension at temperatures up to 1000 °C. In addition to elevated-temperature mechanical properties in tension, Charpy V-Notch (CVN) impact values were obtained to evaluate energy absorption capacity at elevated temperatures.

As a result of the tension tests, full-range stress-strain curves at elevated temperatures were obtained. The effect of loading rates on the steel strength at high temperatures was also examined by comparing the results of tension tests conducted at the cross-head displacement rates of 0.01 in./min and 0.1 in./min. Further, static yielding behavior was investigated in this study. It is shown that the displacement rate has a large impact on the steel strength at elevated temperatures, especially at temperatures higher than 600 °C.

The yield stress, tensile strength, elastic modulus and proportional limit obtained from the tensile stress-strain curves at elevated temperatures were compared with values specified by Eurocode 3 (2006) and the AISC *Specification* (2010). The measured values of yield stress agree reasonably well with Eurocode 3 and the AISC *Specification*, when yield stress is defined as the stress at 2% total strain. Elevated-temperature values of tensile strength, modulus of elasticity and proportional limit measured in these tests also agree reasonably well with predictions in Eurocode 3 and in the AISC *Specification*.

The data collected in this testing program also showed that the definition adopted for the yield stress of steel at elevated temperatures can have a large impact on the value of yield stress, and in turn, can have a large impact on the member strength calculations. At present, Eurocode 3 (2006) and the AISC *Specification* (2010) define elevated-temperature yield stress as the stress at a total strain of 2%. Based on analysis and discussion provided in this paper, this definition of yield stress appears to provide a reasonable basis for member strength calculations at elevated temperatures. It should be emphasized, however, that the question of how to define yield stress of structural steel requires further analysis and discussion within the design community.

ACKNOWLEDGMENTS

The research reported herein was conducted as part of research projects on “Elevated Temperature Performance of Beam End Framing Connections,” “Creep Buckling of Steel Columns Subjected to Fire” and “Elevated Temperature Performance of Shear Connectors for Composite Beams,” all supported by the National Science Foundation (NSF awards 0700682, 0927819 and 1031099, respectively). Elevated temperature material tests were conducted using equipment procured through an NSF Major Research Instrumentation Grant (NSF award CMS-0521086, “Acquisition of a High-Temperature Testing Facility for Structural Components and Materials”). The support of the National Science Foundation and of former NSF Program Directors M.P. Singh and Douglas Foutch is gratefully acknowledged. The authors are also grateful to Gerdau-Ameristeel for donating materials for this research. The authors would especially like to thank Matthew Gomez of Gerdau-Ameristeel for his support of this research. Finally, special thanks are due to the technical staff at the Ferguson Structural Engineering Laboratory at the University of Texas at Austin for their extensive assistance with the this testing program. Any opinions, findings and conclusions or recommendations expressed in this paper are those of the authors and do not necessarily reflect the views of the National Science Foundation.

REFERENCES

Abaqus (2011), Abaqus Version 6.11 User’s Manual, Dassault Systèmes Simulia Cor., Providence, RI.

AISC (2010), *Specification for Structural Steel Buildings*, Standard ANSI/AISC 360-10, American Institute of Steel Construction, Inc., Chicago, IL.

ASTM A370-12 (2012), *Standard Test Methods and Definitions for Mechanical Testing of Steel Products*, American Society for Testing and Materials, West Conshohocken, PA.

ASTM A992-11 (2011), *Standard Specification for Structural Steel Shapes*, American Society for Testing and Materials, West Conshohocken, PA.

ASTM E21-09 (2009), *Standard Test Methods for Elevated Temperature Tension Tests of Metallic Materials*, American Society for Testing and Materials, West Conshohocken, PA.

Beedle, L. and Tall, L. (1960), “Basic Column Strength,” *Journal of the Structural Division*, ASCE, Vol. 86, No. 7, pp. 139–173.

Chen, J., and Young, B. (2006), “Stress-Strain Curves for Stainless Steel at Elevated Temperatures,” *Engineering Structures*, Vol. 28, No. 2, pp. 229–239.

Cooke, G.M.E. (1988), “An Introduction to Mechanical Properties of Structural Steel at Elevated Temperatures,” *Fire Safety Journal*, Vol. 13, No. 1, pp. 45–54.

DeFalco, F.D. (1974), “Investigation of the Compressive Response of Modern Structural Steels at Fire Load Temperatures,” PhD Dissertation, Department of Civil Engineering, University of Connecticut.

Dieter, G.E. (1986), *Mechanical Metallurgy*, 3rd ed., McGraw-Hill, New York, NY.

Eurocode 3 (2006), *Design of Steel Structures. Part 1-2: General Rules.* Structural Fire design, EN 1993-1-2, European Committee for Standardization, CEN.

Fields, B.A. and Fields, R.J. (1989), “Elevated Temperature Deformation of Structural Steel,” Report NISTIR 88-3899, National Institute of Standards and Technology, Gaithersburg, MD.

Fujimoto, M., Furumura, F., Ave, T. and Shinohara, Y. (1980), “Primary Creep of Structural Steel (SS41) at High Temperatures,” *Trans. of Architectural Institute of Japan*, Vol. 296, pp. 145–157.

Fujimoto, M., Furumura, F. and Ave, T. (1981), “Primary Creep of Structural Steel (SM50A) at High Temperatures,” *Trans. of Architectural Institute of Japan*, Vol. 306, pp. 148–156.

Harmathy, T.Z. (1967), “A Comprehensive Creep Model,” *Journal of Basic Engineering, Transactions*, ASME, Vol. 89, No. 3, pp. 496–502.

Harmathy, T.Z. and Stanzak, W.W. (1970), “Elevated-Temperature Tensile and Creep Properties of Some Structural and Prestressing Steels,” *Fire Test Performance,* ASTM STP 464, American Society for Testing and Materials, pp. 186–208.

Ho, C. (2010), “Analysis of Thermally Induced Forces in Steel Columns Subjected to Fire,” MS Thesis, Department of Civil, Architectural and Environmental Engineering, University of Texas at Austin.

Hu, G., Morovat, M.A., Lee, J., Schell, E. and Engelhardt, M.D. (2009), “Elevated Temperature Properties of ASTM A992 Steel,” *Proc. Structures Congress*, ASCE, Austin, April 30–May 2, 2009.

Humphreys, F.J. and Hatherly, M. (2004), *Recrystallization and Related Annealing Phenomena*, 2nd ed., Elsevier Science Ltd, Oxford.

Kirby, B.R. and Preston, R.R. (1988), “High Temperatures Properties of Hot-rolled Structural Steels for Use in Fire Engineering Design Studies,” *Fire Safety Journal*, Vol. 13, No. 1, pp. 27–37.

Kelly, F.S. and Sha, W. (1999), "A Comparison of the Mechanical Properties of Fire-Resistant and S275 Structural Steels," *Journal of Constructional Steel Research*, Vol. 50, No. 3, pp. 223–233.

Lee, J. (2012), "Elevated Temperature Properties of Steel for Structural Fire Engineering Analysis," PhD Dissertation, Department of Civil, Architectural and Environmental Engineering, The University of Texas at Austin.

Li, G.Q., Jiang, S.C., Yin, Y.Z., Chen, K. and Li, M.F. (2003), "Experimental Studies on the Properties of Constructional Steels at Elevated Temperatures," *Journal of Structural Engineering*, ASCE, Vol. 129, No. 12, pp. 1717–1721.

Lie, T.T. (Ed.). (1992), *Structural Fire Engineering*, ASCE Manuals and Reports on Engineering Practice No. 78, American Society of Civil Engineers, New York, NY.

Luecke, W.E., McColskey, J.D., McCowan, C.N., Banovic, S.W., Fields, R.J., Foecke, T., Siewert, T.A. and Gayle, F.W. (2005), "Federal Building and Fire Safety Investigation of the World Trade Center Disaster—Mechanical Properties of Structural Steels," Report NCSTAR 1-3, National Institute of Standards and Technology, Gaithersburg, MD.

Morovat, M.A., Lee, J., Hu, G. and Engelhardt, M.D. (2010), "Tangent Modulus of ASTM A992 Steel at Elevated Temperatures." *Proc. Sixth International Conference on Structures in Fire* (SiF 10), Michigan State University, East Lansing, Michigan, June 2–4, 2010.

Morovat, M.A., Engelhardt, M.D., Taleff, E.M. and Helwig, T.A. (2011), "Importance of Time-Dependent Material Behavior in Predicting Strength of Steel Columns Exposed to Fire," *Applied Mechanics and Materials*, Vol. 82, pp. 350–355.

Morovat, M.A., Lee, J., Engelhardt, M.D., Taleff, E.M., Helwig, T.A. and Segrest, V.A. (2012), "Creep Properties of ASTM A992 Steel at Elevated Temperatures," *Advanced Materials Research*, Vols. 446–449, pp. 786–792.

Outinen, J. (2006), *Mechanical Properties of Structural Steel at Elevated Temperatures and After Cooling Down*, Helsinki University of Technology, Laboratory of Steel Structures, Finland.

Skinner, D.H. (1972), "Measurement of High Temperature Properties of Steel," BHP Melbourne Research Laboratories, Report MRL 6/10, The Broken Hill Proprietary Company Limited Australia.

SSRC (1987), *Technical Memorandum No. 8: Standard Methods and Definitions for Tests for Static Yield Stress*, Structural Stability Research Council.

Takagi, J. and Deierlein, G.G. (2007), "Strength Design Criteria for Steel Members at Elevated Temperatures," *Journal of Constructional Steel Research*, Vol. 63, pp. 1036–1050.

Twilt, L. and Both, C. (1991), *Stress-Strain Relationships of Structural Steel at Elevated Temperatures: Analysis of Various Options & European Proposal*, SA 112 Part F: Mechanical Properties, TNO Building and Construction Research, Delft, The Netherlands.

United States Steel (1972), *Steels for Elevated Temperature Service*, United States Steel Corporation, Pittsburgh, PA.

Structural Fire Engineering: Overview and Application Examples of Appendix 4 of the AISC Specification

JOHN GROSS, NESTOR IWANKIW and MATTHEW JOHANN

ABSTRACT

This paper presents an overview of current conventional practices for providing passive fire protection of building structures and describes alternative engineering approaches covered in Appendix 4 of the 2010 AISC *Specification*, ANSI/AISC 360-10. The concept of structural fire engineering is discussed, along with guidance and design references that are available to support performance-based structural fire engineering analyses. The roles and responsibilities typically assumed by design team members and other stakeholders in a structural fire engineering project are presented, as are considerations associated with peer reviews and approval by authorities having jurisdiction. The paper concludes with a series of four design examples that demonstrate a range of structural fire engineering applications for steel buildings.

Keywords: fire, structural fire engineering, performance-based fire design, fire engineering, AISC *Specification* Appendix 4.

INTRODUCTION

Beginning with the 2005 edition, Appendix 4 of the AISC *Specification for Structural Steel Buildings* has addressed structural design for fire conditions by analysis. By providing performance objectives and design requirements, guidance for the characterization of fires and their effects on steel members, and permitted methods of analysis, Appendix 4 supports the pursuit of structural fire engineering strategies that fall outside of the more traditional, prescriptive, code-based fire resistance design approach.

This article provides a general overview of prescriptive and performance-based structural fire-resistance design approaches and discusses how Appendix 4 of the 2010 AISC *Specification* can be used to support the latter. Four examples are included to demonstrate a range of possible structural fire engineering applications.

CURRENT PRACTICES

Building fire protection is achieved through either active or passive measures, or by a combination of both. Active measures, such as sprinkler systems, are intended to control the development and growth of fires. Passive measures are intended to protect structural elements from damage or collapse and to prevent the spread of fires. Examples of passive measures include sprayed fire-resistant materials (SFRMs) and construction of separating elements that prevent the transmission of heat and hot gases. By choosing and designing appropriate materials, assemblies and architectural arrangements, building designers can meet building code requirements for providing a prescribed level of fire resistance for the selected type of construction, occupancy and layout (height and area).

The term *fire resistance* refers to the ability of a given structure (or portion thereof) to maintain physical and thermal stability for some duration during a fire and to meet the acceptance criteria of the fire test standard(s) referenced by the applicable building code. This time period may be used for occupant evacuation, property protection and fire department response, depending on the type of the building, stakeholders' requirements and/or nature of the emergency event.

Model building codes, upon which the majority of jurisdictions in the United States and many international authorities base their local building codes, require minimum levels of structural fire resistance based on a building's size and use, among other factors. Prescriptive fire-resistance ratings for building construction in the United States have long been based on the test methods and acceptance criteria of ASTM E119 (referenced in UL 263 and NFPA 251) (ASTM, 2012; UL, 2011; NFPA, 2006). This fire resistance is most commonly achieved through specification of structural assemblies and systems, which are comprised of structural members as well as coatings, encasements, systems and other protective measures. A given rated assembly or system is prequalified to achieve a fire-resistance time through fire testing (per ASTM E119 or its UL or NFPA counterparts) or the derivative analytical methods contained in ASCE/SEI/SFPE 29 (ASCE, 2005).

John Gross, Ph.D., P.E., Research Structural Engineer, National Institute of Standards and Technology, Gaithersburg, MD. E-mail: john.gross@nist.gov

Nestor Iwankiw, Ph.D., P.E., S.E., Senior Engineer, Hughes Associates, Inc., Chicago, IL (corresponding). E-mail: niwankiw@haifire.com

Matthew Johann, P.E., Senior Fire Engineer, Arup USA, Inc., Cambridge, MA. E-mail: matt.johann@arup.com

Prescriptive approaches such as these are usually conservative, and they can be easily implemented by a design team and enforced by building officials. Thus, they have had a generally successful and long history of providing for public life safety. However, prescriptive fire-resistance approaches are based on physical fire tests or calculation methodologies with limitations. Also, size-constrained assemblies for laboratory tests are considered in isolation rather than as part of a larger structural system. Furthermore, because these standardized fire test methods evaluate only the relative performance of particular assemblies subjected to standard fire exposures, they do not provide information regarding how the tested construction assembly, or a slightly different variant of it, might respond to a real fire as part of a structural system within a building. For these reasons, alternative methods based on the available scientific and engineering knowledge, modern computational tools and past experimental or event outcomes provide the only other recourse for some design conditions.

OVERVIEW OF APPENDIX 4

Appendix 4 of the 2010 AISC *Specification* is designed to support flexible approaches to structural fire resistance by providing methodologies and criteria to support evaluation of structural response to real fire exposures. Appendix 4 is organized into three main sections:

- Section 4.1: General Provisions
- Section 4.2: Structural Design for Fire Conditions by Analysis
- Section 4.3: Design by Qualification Testing

Section 4.1 (General Provisions) provides information regarding the performance objectives that should be used to determine if an assembly's performance is acceptable. It also defines the load combinations that should be used when evaluating structural performance under fire conditions.

Section 4.3 (Design by Qualification Testing) provides the engineer with the traditional option of using established fire testing protocols, such as ASTM E119 (ASTM, 2012), to determine the fire-resistance rating of a structural member or assembly.

The heart of Appendix 4 lies in Section 4.2 (Structural Design for Fire Conditions by Analysis). It is in this section that alternative methods, parameters and criteria are presented to guide performance-based structural fire engineering analysis. Key portions of Section 4.2 are described here.

Design-Basis Fire

An important aspect of an engineering evaluation of structural fire resistance is the definition of the design-basis fire(s). The selection of the design-basis fire(s) is usually performed by the fire protection engineer. If the bounding (worst-case) fire conditions against which the performance of a structure is evaluated are not accurately and fully described, the resulting conclusions will likely not be correct. Considerations and approaches are provided to help the engineer effectively describe the design-basis fire exposure, such as the fire compartment size and thermal characteristics of its boundaries, combustible fuel load density and ventilation conditions.

Material Strength and Properties at Elevated Temperatures

As construction materials are heated in a fire, their strength and mechanical properties degrade. Appendix 4 provides methodologies and material property data for structural steel and concrete for use in evaluating strength, modulus of elasticity and thermal expansion at elevated temperatures.

Structural Design Requirements

Criteria for providing structural integrity are given in terms of strength requirements and deformation limits. These are evaluated in the context of changing material properties at elevated temperatures and load combinations as defined earlier in the section. A structural system is required to be able to withstand local damage without experiencing loss of global stability. Connections must be designed to support the forces developed during the design-basis fire.

Methods of Analysis

Methods of analysis supported by Appendix 4 fall into two categories: simple and advanced. The simple methods are intended to predict the fire-induced response of individual members in tension, compression, flexural and composite floor action.

Advanced methods include approaches such as computational fluid dynamics modeling to describe temperature exposures, finite element modeling to evaluate heat transfer with structural members, and local and global structural frame response to predicted temperatures.

STRUCTURAL FIRE ENGINEERING

Performance-based structural fire engineering provides opportunities for engineers to seek innovative ways to meet code-required fire-resistance requirements. Prescriptive provisions do not typically support new or "outside-of-the-box" design solutions, and standard furnace testing of unique assemblies, even if feasible due to laboratory and furnace size constraints, can be a costly and time-consuming addition to a project. The structural fire engineering approaches supported by Appendix 4 can alleviate these challenges but may require more complex analyses of fire resistance with which some structural engineers may not be accustomed.

Performance-based approaches are common in the fire protection engineering community, especially for the design of smoke management systems. The Society of Fire Protection Engineers (SFPE) defines performance-based design as "an engineering approach to fire protection design based on: (1) agreed upon fire safety goals and objectives; (2) deterministic and/or probabilistic analysis of fire scenarios; and (3) quantitative assessment of design alternatives against the fire safety goals and objectives using accepted engineering tools, methodologies and performance criteria" (SFPE, 2007).

Available Guidance

Performance-based design, by definition, is flexible. The required methodology for one project may or may not be appropriate for another. Many factors influence the choice of engineering tools, performance measures and solutions. Because of this, specific analysis methodologies are difficult to document in codes and standards. Instead, the fire protection community has developed guidance for the overall approach to performance-based design. Four documents are available:

- ASCE/SEI 7-10, Section 1.3.1.3, Performance Based Procedures (ASCE, 2010)
- *SFPE Engineering Guide to Performance-Based Fire Protection* (SFPE, 2007)
- *SFPE Code Official's Guide to Performance-Based Design Review* (SFPE, 2004)
- *Guidelines for Peer Review in the Fire Protection Design Process* (SFPE, 2009)

These documents can be used to define an appropriate process for addressing a given structural fire engineering challenge, including definition and agreement of goals and objectives, documentation of the analysis and approval of the proposed solutions and associated justifications.

Additional methodology and data references specific to structural fire engineering are discussed later in this article.

Professional Roles and Responsibilities

The SFPE notes that "the team approach is essential to the success of a performance-based design" (SFPE, 2007). This team comprises building owners, architects, engineers, building and fire officials and others who may have a role in the project. Depending on the complexity of a proposed approach, performance-based design may require greater collaboration than is typical of a more conventional design project.

Structural fire engineering requires collaboration among five stakeholders.

Fire Protection Engineers

Because structural fire engineering will usually not rely on the fire exposure specified for standardized furnace testing, specialized knowledge in the calculation of real building fire exposures is required. Fire protection engineers are responsible for defining and interpreting the level of fire safety required by the code and for translating that information to appropriate performance criteria. They will also define the thermal environment to which the structure is exposed, including the combustible content, ventilation or wind effects, heat energy, flame shape and height, fire duration and affected area(s). This task may involve computer-based fire modeling or more simple hand calculations and may consider the effects of suppression systems, fire department activities and passive fire protection systems.

In many cases, the fire protection engineer will also characterize the transfer of heat into the structural member, the corresponding material temperature rise and the resulting thermal effects to the member. Fire protection engineers must be able to effectively convey the effects of material temperatures in a form that structural engineers can use to evaluate the response of the structure.

Fire protection engineers are also generally responsible for documenting these aspects of the performance-based design and supporting the approvals process.

If the structural fire engineering approach involves comparing unique or untested members or assemblies to conventional members that have been tested, fire protection engineers may be responsible for documenting this comparison and substantiating compliance.

Structural Engineers

The structural engineer's initial role in the structural fire engineering process is to assist the fire protection engineer in defining critical members for analysis. Analysis of every member in a structure would be inefficient and is generally unnecessary. The engineers should evaluate possible fire exposures, structural load paths, and any redundancies in order to determine the members or subassemblies that represent a limited number of critical cases.

After the results of the thermal exposure analysis are available, the structural engineer may consider them in a number of ways. If various members will reach temperatures that will substantially reduce their strength or stiffness, the structural engineer may evaluate the impact of these reductions on the response of the local and global structural systems. The structural engineer may also need to determine the ways in which the restraint of thermal expansion may affect a structure. If individual members are shown, through the fire analysis, to exceed failure criteria, then the structural engineer's role may be to consider load redistributions and structural redundancies in order to verify if these "local" failures can be tolerated to avoid progressive (disproportionate) collapse.

Through collaboration with the fire protection engineer, the structural engineer may also propose and evaluate changes to the structure to help withstand the predicted thermal exposures. Examples of this include increasing the size of given members, revising the framing layout and/or member design or using alternative framing connections, each of which could improve fire resistance.

Architects

Solutions developed through the performance-based design may impact the architecture of a building. The architect must be involved in this process in order to provide feedback regarding the acceptability of any proposed design alternatives. For example, while increasing the size of a concrete column will improve structural fire resistance, it may narrow an adjacent corridor to a width that may not be acceptable.

The architect (and building owner) must also provide details regarding interior finish materials, furnishings and the proposed uses of individual spaces. This information is required by the fire protection engineer for development of fire scenarios for evaluation of thermal exposures.

Owners

The building owner is the most directly affected stakeholder in the performance-based fire design approach and also has most to gain or lose. Thus, owners must be fully briefed beforehand on the critical reasons and benefits for utilizing this alternative approach, as well as its uncertainties, challenges and risks. The latter may include project schedule delays, budget extras and design revisions. The initial performance-based design plan may not be found totally acceptable, and certain changes may be required due to various considerations raised by other members of the project team, consultants, peer reviewers or the building officials. Good communication and coordination among the owner, the entire project team and the building authorities throughout this endeavor are paramount.

The building owner should remain fully committed to supporting the performance-based design approach during its execution and, accordingly, must manage the responsible professional members of the project team. In the same "buy-in" perspective, the owner could help influence the building official to be receptive to the new concepts and innovation resulting from this effort.

Building Officials

The building official's primary responsibility is to ensure that the goals and objectives of the laws, codes, standards and ordinances adopted by the jurisdiction are appropriately implemented in the design and construction of a building or structure. When a design uses an alternative approach, this responsibility can become more challenging and ambiguous. Therefore, the building official must determine if the appropriate skills are available within his or her office to properly contribute to the review and approval process when considering the proposed alternative design. If not, an external reviewer or peer review may be needed, or the design team may be required to petition a higher code authority, such as a state appeals board.

During the design process, the building official should be given the opportunity to actively contribute to discussions regarding overall strategy for performance-based or alternative approaches. The building official should promptly voice any concerns regarding the alignment of the proposed strategies and design approaches with the goals and objectives of the building and fire codes and impose any special requirements that must be implemented in order to meet the intent of the codes. This participatory approach represents a departure from the traditional role of the building official which has historically been more focused on post-design review.

Coordination with Authorities

A typical building or fire official may never have been presented with a performance-based approach to structural fire resistance, even though current building codes in the vast majority of jurisdictions contain provisions than will allow for this type of alternative design approach. Performance-based fire design remains uncommon because guidance for such an approach has been limited until relatively recently and also because it is not often applied on more common projects, such as residential and smaller commercial buildings. To date, the main applications of performance-based fire design have been on larger, more monumental projects with unique architectural or structural features or unusual fire exposures or risks.

This fact should not discourage building owners and engineers from pursuing a performance-based approach to structural fire resistance. However, the design team must address the needs and concerns of the officials at an early stage and throughout the design process. Authority buy-in is critical because if a building official is faced with evaluating a performance-based design at the final review stage, and if he or she disagrees with any of the underlying assumptions, methodologies or conclusions, the outcome can be disastrous. This scenario may result in costly redesigns (with associated delays) or complete abandonment of the performance-based approach. Ignoring concerns until late in the design can also damage the working relationship between the owner and the building official.

The building and fire officials are stakeholders in every building project within their jurisdiction. Their opinions, interpretations and goals need to inform the performance-based design from start to finish. They should be briefed on the intent to pursue an alternative approach once the feasibility of that approach is well understood by the design team, and they should be involved in stakeholder meetings early on. Authorities may influence decisions regarding fire scenarios, performance criteria, choice of structural members to be analyzed, analysis methodologies and documentation requirements. They may also require a peer review, which must be anticipated.

The SFPE Code Official's Guide to Performance-Based Design Review (SFPE, 2004) is intended to assist building and fire officials with the process of reviewing a performance-based design. This extensive guide includes many frequently asked questions, the answers to which can greatly inform both the approving authorities and the other project stakeholders. The engineer must understand the content of this document to be fully prepared to address the needs of the officials.

Peer Reviews

Often, when advanced analysis techniques are employed, one or more of the project stakeholders (frequently the building owner or the authority having jurisdiction) may not be suitably trained or experienced to evaluate the work and recommendations of the engineer, or they may not have resources available to review such a design. This is particularly true for structural fire engineering, which is historically relatively uncommon in the United States. In these cases, the stakeholder may require a peer review of the performance-based design. A peer review can provide an independent professional opinion regarding the appropriateness of the assumptions, methodologies and conclusions of a performance-based design.

The SFPE and ASCE publish guidelines for peer review of fire protection and performance-based designs (SFPE, 2009; ASCE, 2010), and this general approach can be a good fit for performance-based structural fire engineering. The document describes what the scope of a peer review should include, how the review should be conducted and what documentation should be produced. It also addresses such concerns as confidentiality and intellectual property.

A peer review can affect a project's schedule in several ways. The review itself takes time, especially if the analysis and resulting design are complex and involve advanced calculation tools. Also, the review may call for changes to the methodology or final outcome of the analysis. Because of these concerns, it is most efficient if the reviewer becomes involved in the process well before the final design review.

DESIGN REFERENCES

While Appendix 4 includes valuable information needed for structural fire engineering assessments, additional references may be required, depending on the type of analysis being pursued. One study by AISC (AISC, 2005) provided in-depth information regarding available references to support structural fire engineering. The following six additional references identify more sources for a wide range of information needed when carrying out structural fire engineering analyses.

SFPE S.01: *Engineering Standard on Calculating Fire Exposures to Structures*

SFPE recently published its first standard, SFPE S.01: *Engineering Standard on Calculating Fire Exposures to Structures* (SFPE, 2011). It provides methodologies for describing thermal boundary conditions (heating effects) for structural elements exposed to both local and fully developed compartment fires. These types of natural (nonstandard) fire analyses will typically be performed by a fire protection engineer.

ASCE/SEI/SFPE 29-05: *Standard Calculation Methods for Structural Fire Protection*

ASCE/SEI/SFPE 29-05 (ASCE, 2005) provides simple empirical calculation methods for evaluating the structural fire resistance of individual members of multiple common construction materials. These methods are based on well-established equivalencies to results of standard fire resistance testing, but these methods cannot address effects of nonstandard fires, structural framing continuity, connections or member sizes/layouts that are outside the tested data base range.

SFPE Handbook of Fire Protection Engineering

The *SFPE Handbook of Fire Protection Engineering* (SFPE, 2008) includes chapters on "Methods for Predicting Temperatures in Fire Exposed Structures," "Structural Fire Engineering of Building Assemblies and Frames" and "Analytical Methods for Determining Fire Resistance of Steel Members." Heat transfer calculation approaches are discussed in depth. Advanced methodologies and performance-based approaches are discussed in concept, though technical content focuses on simple methods of predicting structural response to fire.

Eurocodes

The structural Eurocodes devote significant attention to fire-related issues. Each code includes a substantial amount of information on design for particular fire design case. For steel structures, Eurocode 1 (Basis of Design and Actions on Structures), Eurocode 3 (Design of Steel Structures) and

Eurocode 4 (Design of Composite Steel and Concrete Structures) apply (CEN, 2009a; CEN, 2009b; CEN, 2008b).

The Eurocodes support both prescriptive and performance-based design approaches, as well as consideration of individual members and whole frames. They discuss methods for characterizing fire exposures, predicting temperature-dependent thermal and mechanical properties using comprehensive mathematical expressions, choice of methodology and verification. Extensive tabulated data are included.

AISC *Design Guide 19*

While most of AISC *Design Guide 19* (AISC, 2003) explains and illustrates the conventional prescriptive approach to fire-resistive design of structural steel, one chapter introduces some basic computations for structural fire engineering. This guide contains many example problems and design aids, including tabulation of W/D properties for the standard steel shapes, and is an excellent beginning resource for practitioners less familiar with the subject.

NIST *Best Practice Guidelines for Structural Fire Resistance of Concrete and Steel Buildings*

The *NIST Best Practice Guidelines* (NIST, 2010) offer insights and recommendations for critical fire exposure variables, analysis-design of steel and concrete structures at high temperatures, risk and reliability of engineered structures when subjected to fire events, and general practical application considerations. The *Guidelines* provide a compact synthesis and guide on the overall existing state of the art in 2010 from a U.S. perspective.

EXAMPLES

The following four design examples are intended to demonstrate the application of various structural fire engineering techniques. They range from the comparatively elementary Example 1, which illustrates steel shape substitutions based on their weight to heated perimeter (W/D) property, to more complex problems. The focus of these examples is the effect of a fire on the structural performance of various types of members and on development of thermal restraint. In-depth discussion of the methodologies to calculate fire exposures to the structural elements and heat transfer are outside the scope of this paper, and the given information is only provided as direct input data for the examples. For actual project work of this type, a fire protection engineer would usually be tasked with performing the requisite fire/heating analyses and providing the final material temperature results to the structural engineer. The reader may reference SFPE S.01: Engineering Standard on Calculating Fire Exposures to Structures (SFPE, 2011) and the other noted references for additional information in this regard.

Since the 1970s, ASTM E119 and UL 263 have differentiated between restrained and unrestrained fire resistance ratings for beams in prescriptive design. In many cases, the required fire protection material thickness for thermally unrestrained beams is greater than for their thermally restrained counterparts with the same rating time. This thermal restraint classification, as defined in ASTM E119, can be quite different than the typical member end restraint connotation in structural engineering. Consequently, it has been a frequent source of confusion and interpretation questions over the decades. Section 4.3.2 of Appendix 4 of the 2010 AISC *Specification* provides specific guidance for structural steel beams and girders that support concrete slabs and are integrally connected by bolts or welds to adjacent steel framing: These can be considered as restrained (thermally) for purposes of such prescriptive fire resistance applications. Examples 1 and 3 illustrate some of the implications and effects of these fire-resistance rating distinctions.

For the purposes of these examples, various elevated material temperatures are provided as given information assumed to be properly determined either from tests or suitable analyses. Also, for similar practical reasons, computerized structural solutions are not fully described but are only presented as final results. These examples are intended to convey the capabilities of performance-based fire design approaches, their typical assumptions and computational steps, and the resulting sensitivity of the structural design to the fire and thermal exposures that have been postulated.

In many cases, agreement on the design basis fire scenario(s) may present the most critical project issue, followed by resolution of uncertainties in thermal properties of fire protection materials and in the fire response of member connections. For such instances, parameter variation and iterative sensitivity studies may be necessary to envelope the realistically expected performance range of the structure. As previously described, the entire project team and building official should review all analysis and design details prior to implementation.

Example 1: Shape Substitutions for Beams and Columns

Access to the *UL Fire Resistance Directory* (UL, 2013) in its published or online form is encouraged to enable a better understanding of this example, in particular the nature and details of the referenced fire resistive assemblies.

Problem Statement—Beams

A standard 2-hr fire resistive rating is required for a building floor system, which has been designated a “restrained” assembly. UL D902 (UL, 2013) is the specified rated floor assembly for this construction. The steel floor deck is to consist of all fluted, 2-in.-deep units, topped with 3¼ in. of lightweight concrete.

For the W24×84 steel beams in this floor system, compute the minimum contour thickness of spray-applied fire-resistive material (SFRM) required for a 2-hr unrestrained beam rating consistent with UL D 902, assuming Type 300 is the selected SFRM protection product.

Note: In accordance with ASTM E119 and the cited UL assembly listing, selection of a 1-hr unrestrained beam protection would also have been acceptable for the specified 2-hr restrained assembly rating, and would have accordingly resulted in a lower fire protection material thickness requirement.

Approach and Solution

The W/D steel shape property represents its ratio of weight to heated perimeter as the effective thermal inertia of the member. Shapes with larger W/D values are more resistant to heating effects than those with lower W/D values for identical exposure and fire protection cases. This shape parameter frequently recurs in the theoretical and design equations for steel fire resistance. AISC *Design Guide 19* (AISC, 2003) includes a tabulation of W/D properties for all the standard steel shapes.

The W24×84 beams (W/D = 1.14 lb/ft/in.) are substantially larger and heavier than the minimum W8×28 size (W/D = 0.80 lb/ft/in.) in the UL listing; hence, the proposed beam size complies with this requirement of UL D902. The easiest, but most conservative, thickness of the SFRM (of the type prescribed in the listing) can be simply taken as 11⁄16 in. as provided within the UL D902 assembly listing for the 2-hr protection of the minimum W8×28 beam size.

However, some efficiency and cost savings can be achieved by using the substitution equations given in the references (UL, 2013; ASCE, 2005; SFPE, 2008) and the 2012 *International Building Code* (ICC, 2012). This simple calculation adjusts the minimum required SFRM thickness on the basis of W/D for the actual beam shape to be protected, rather than the minimum size prescribed in the rated assembly. The required protective material thickness for the actual beam, t_2, is calculated based upon the thickness listed for the minimum beam size in the UL listing, t_1 = 11⁄16 (or 0.688 in.), and the W/D ratios of the two beam sizes, as follows:

$$
\begin{aligned}
t_2 &= \frac{W_1/D_1 + 0.6}{W_2/D_2 + 0.6}(t_1) \\
&= \frac{0.8 + 0.6}{1.14 + 0.6}(0.688) \\
&= 0.553 \text{ in. or approximately } 9/16 \text{ in.}
\end{aligned}
$$

Thus, a minimum 9⁄16-in. SFRM contour thickness could be used for the W24×84 beams in the 2-hr floor construction, resulting in a material thickness reduction of ⅛ in. relative to the baseline UL D902 assembly listing. While this material and cost savings may be marginal for the spraying of relatively few beams, it can quickly compound when multiplied over the many floors in a multi-story building.

This beam substitution equation must only be used within its stated limits of application, as given in the cited references.

Problem Statement—Columns

A 2-hr fire resistive rating is required for a built-up steel column (doubly symmetric I-shape), with MK-5 SFRM protection along its contour. UL X772 (UL, 2013) is the referenced rated assembly to be used.

For this given steel shape, compute W/D and the minimum required SFRM thickness.

Consider a doubly symmetric, built-up (nonstandard) I-shape column with the following dimensions:

- Total depth of I shape (d): 18 in.
- Flange width (b_f): 8 in.
- Flange thickness (t_f): 0.75 in.
- Web thickness (t_w): 0.5 in.

Approach and Solution

The weight per unit length, W, is calculated as follows:

$$W = \left[2b_f t_f + \left(d - 2t_f\right)t_w\right]\left[\frac{490 \text{ lb/ft}^3}{144 \text{ in.}^2/\text{ft}^2}\right] = 68.9 \text{ lb/ft}$$

The heated perimeter of the column, D, is calculated as follows, assuming that it in fully surrounded by fire, which induces the greatest heating effects.

$$D = 4b_f + 2d - 2t_w = 67 \text{ in.}$$

W/D then equals (68.9 lb/ft)/(67 in.) = 1.028 lb/ft/in.

Other partial-heating exposures can be represented by suitably modifying D for the conditions to be considered; for example, for a perimeter column that will have one flange face not subjected to the fire, the heated perimeter would decrease and slightly increase the W/D value relative to the all-around exposed case.

The UL X772 assembly includes the following formula for computation of the minimum required MK-5 SFRM thickness, h, as a function of W/D given a required fire resistance period, R:

$$h = \frac{R}{1.05\left(W/D\right) + 0.61} = \frac{2}{1.05\left(1.028\right) + 0.61} = 1.184 \text{ in.}$$

Practical round-up of this answer provides the required 1³⁄₁₆-in. thickness for this shape and the given conditions. One could also approximately check the accuracy of this solution by observing that the UL X772 listing itself required a minimum 1⅛-in. SFRM thickness for 2-hr protection of a W10×49 with $W/D = 0.83$.

This column equation must only be used within its stated limits of application, as given in the *UL Directory* (UL, 2013). Other column assemblies and SFRM products will have different curve-fitted formulas for this design purpose.

Example 2: Bending Strength of a Simply Supported Composite Beam

Problem Statement

A floor system has 2-in.-deep steel deck units, topped with 3¼ in. of 3,000-psi lightweight concrete. Simply supported and fully composite W16×26 beams—ASTM A992 steel, spaced 8 ft on center (o.c.), spanning 35 ft (see Figure 1) and running perpendicular to the deck flutes—have been designed for a uniformly distributed dead load of 60 psf and a live load of 100 psf (nominal, unfactored loads). Check only the adequacy of this beam's positive bending design strength for both ambient and fire conditions, assuming that ambient serviceability (deflections or floor vibrations) is to be separately assessed. Use the ultimate strength (fully yielded) model for both conditions. The shear connector design for full composite beam action is done conventionally and is assumed to be similarly effective at the elevated fire temperatures, consistent with the simple member analysis provision of Section 4.2.4.3.b of Appendix 4 of the 2010 AISC *Specification*.

The worst-case fire exposure for the strength limit state results in an average steel temperature of 1300 °F at the bottom flange and 600 °F at the top flange (much cooler due to its proximity to and heat shielding by the floor slab), as determined from past tests or heat transfer analysis (provided information).

Approach and Solution

First check factored loads and full composite beam design strength at ambient.

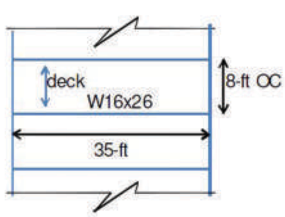

Fig. 1. Beam layout.

- 60 psf nominal dead load × 8 ft o.c. = $w_D = 0.480$ kips per lineal foot (klf)
- 100 psf nominal live load × 8 ft o.c. = $w_L = 0.800$ klf
- Beam span (L) = 35 ft
- Steel yield stress (ambient) (F_Y) = 50 ksi
- Concrete compressive stress (ambient) (f_c') = 3 ksi
- $w_u = 1.2w_D + 1.6w_L = 1.86$ klf

The required ambient strength for maximum positive bending at mid-span, M_u is calculated as follows:

$$M_u = \frac{w_u}{8}L^2 = 284.2 \text{ k-ft}$$

The design strength, ϕM_n, from conventional stress block calculations or from AISC *Manual* tables for Y2 = 4½ in., is 356 k-ft. The entire W16×26 member is fully yielded in tension at this limit state, $F_y = 50$ ksi. Because ϕM_n exceeds M_u, the composite beam has adequate strength for ambient design.

Next, check factored loads and full composite beam design strength for the design basis fire. The ASCE 7-10 load combination for an extreme event (fire) is:

$$w_{uf} = 1.2w_D + 0.5w_L = 1.0 \text{ klf}$$

Note that this required load combination for fire case is quite different from that used for ambient design conditions in terms of its live load component.

The required beam strength at the fire limit state is calculated as:

$$M_{uT} = \frac{w_{uf}}{8}L^2 = 149.4 \text{ k-ft}$$

For the composite beam design strength at elevated temperatures, use the given maximum average steel temperatures for this fire exposure to accordingly reduce the steel yield stress for thermal degradation (see 2010 AISC *Specification* Appendix 4, Table A-4.2.1). Because the beam web temperature is not explicitly given, assume a linear thermal gradient between the bottom and top flanges, which results in an average web temperature of:

$$(1300 \text{ °F} + 600 \text{ °F})/2 = 950 \text{ °F}$$

Consider the entire steel beam section to again be yielded in flexural tension.

Subdivide the steel beam into three distinct thermal regions (bottom flange, web and top flange) and assign the given average steel temperatures from the fire uniformly to each area (1300 °F, 950 °F and 600 °F, respectively) to correspondingly reduce the yield stress from ambient. Application of the web average 950 °F across the full web depth is a crude initial idealization, which will subsequently be refined.

Because the compressive stress block in the concrete slab is at the top of the floor and the heat transfer analyses have shown it to be much cooler than the steel beam temperatures (much less than 600 °F, the top flange temperature), the concrete strength is assumed to remain at its unreduced ambient value.

Use k_y retention factors from Table A-4.2.1 of the 2010 AISC *Specification* and interpolate as necessary to determine reduced yield strengths for each portion of the beam.

- At the top flange (600 °F), F_{tf} = 1.0, F_y = 50 ksi (no reduction due to temperature)
- At the web (950 °F), F_w = 0.73, F_y = 36.5 ksi
- At the bottom flange (1300 °F), F_{bf} = 0.255, F_y = 12.8 ksi

Cross-sectional areas are as follows for the W16×26 beam:

- Top flange area (A_{tf}) = 1.9 in.^{2}
- Web area (A_w) = 3.8 in.^{2}
- Bottom flange area (A_{bf}) = 1.9 in.^{2}

Assuming the entire steel beam is in tension due to composite action, summation of steel beam tensile yield forces, with high-temperature reductions, gives:

$$F_T = F_{tf}A_{tf} + F_wA_w + F_{bf}A_{bf} = 257.9 \text{ kips}$$

Impose force equilibrium of steel tension with a concrete compression block of $0.85f'b$ and solve for the depth of the concrete stress block at the top of the slab, a. The effective concrete width, b, is equal to the beam spacing, which is 8 ft or 96 in.

$$a = \frac{F_T}{0.85f'_cb} = 1.05 \text{ in.}$$

Because a = 1.05 in. is less than the concrete slab topping height of 3¼ in. and the plastic neutral axis is above the steel beam, the original assumption of the entire steel beam acting only in flexural tension has been confirmed. The composite beam flexural resistance is computed from the summation of moments (by parts) generated by the steel flange and web area tension relative to the center of the concrete compression block $(a/2)$, as shown in Figure 2.

- Vertical distance between concrete and top flange centroids (L_{tf}) = 4.89 in.
- Vertical distance between concrete and beam web centroids (L_w) = 12.57 in.
- Vertical distance between concrete and bottom flange centroids (L_{bf}) = 20.25 in.

$$M_{nT} = F_{tf}A_{tf}L_{tf} + F_wA_wL_w + F_{bf}A_{bf}L_{bf}$$

$$\phi M_{nT} = 0.9\frac{M_{nT}}{(12 \text{ in./ft})} = 202.4 \text{ k-ft}$$

The design strength during fire is therefore 202.4 k-ft, which represents approximately a 43% reduction from the ambient case.

Because $\phi M_{nT} > M_{uT}$ = 149 k-ft, the composite beam has adequate strength for the given fire exposure based on this simple idealization of the fire-induced temperature effects in the web.

A slightly more refined bending model and analysis follow, which subdivides the steel web into two parts—upper and lower halves—with corresponding average temperatures for each. This improved web discretization will more accurately reflect the beam's effective web bending due to the vertical steel temperature variations along its height. The average temperature in the bottom half of the web is 1125 °F and that for the top half is 775 °F (see Figure 3). Consideration of the beam flanges as single individual areas at one temperature is generally sufficient because the thermal gradient through the relatively thin flange thickness has inconsequential effects.

The axial force balance remains unchanged from before, with a = 1.05 in., as does the resistance of both flanges. The only difference appears in the bending moment summation of the two web half-areas, as follows, wherein the additional subscripts for the variables F and L refer to the top and bottom halves of the web area.

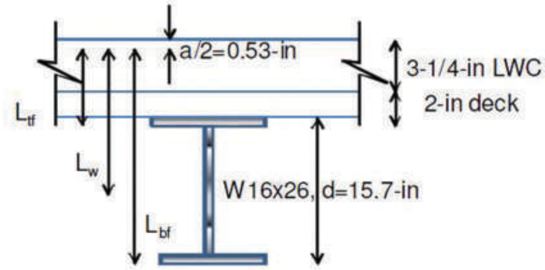

Fig. 2. Assembly cross section.

Again use k_y retention factors from Table A-4.2.1, with interpolation as necessary.

- At the top half of the web (775 °F), $F_{tw} = 0.97F_y = 48.5$ ksi
- At the bottom half of the web (1150 °F), $F_{bw} = 0.43F_y = 21.5$ ksi
- Vertical distance between concrete and beam top web centroids (L_{tw}) = 8.82 in.
- Vertical distance between concrete and beam bottom web centroids (L_{bw}) = 16.32 in.

The following two-part M_{web} expression now replaces the previous single $F_w A_w L_w$ term, with the flange model remaining the same.

$$M_{web} = F_{tw} A_w \frac{L_{tw}}{2} + F_{bw} A_w \frac{L_{bw}}{2} = 1.5\times10^3 \text{ k-in.}$$

$$M_{nT} = F_{tf} A_{tf} L_{tf} + M_{web} + F_{bf} A_{bf} L_{bf}$$

$$\phi M_{nT} = 0.9 \frac{M_{nT}}{(12 \text{ in./ft})} = 182.6 \text{ k-ft}$$

The revised ϕM_{nT} value of 182.6 k-ft is approximately 10% less than the 202.4 k-ft value computed previously and about a 49% reduction from ambient.

Because $\phi M_{nT} > M_{uT}$, the composite beam again demonstrates adequate strength for the given fire exposure, with approximately 23% reserve bending strength (183/149). One additional computational iteration could be attempted with additional web subdivisions to confirm the satisfactory convergence of this bending moment solution at a value exceeding the required strength.

As a side note, if the steel beam temperature had resulted from a lumped mass heat transfer analysis, Section 4.2.4.3b.4 of Appendix 4 of the 2010 AISC *Specification* would have required a prescribed (conservative) temperature distribution through the cross-section to be used in the determination of its moment resistance, with the lumped mass temperature assumed over the bottom half of the steel beam shape (flange and web), then linearly decaying at no more than 25% through the upper web half to the top flange. Because this problem identified specific steel temperature inputs for both beam flanges, this more general provision may be considered to be superseded by the given thermal profile input.

If the more severe maximum uniform temperature profile had been imposed for the bottom half of the W16×26 (1300 °F through lower beam $d/2$, then linearly varying to 600 °F in the steel top flange), the concrete compressive stress block depth is reduced to $a = 0.84$ in. For these modified thermal conditions, the composite beam design strength ϕM_{nT} additionally decreases to 137 k-ft, which is now about 8% less than the required 149 k-ft moment. A slightly larger beam size or an incremental increase in the initial steel beam fire protection thickness would decrease the fire heating effects and enhance the member's design strength to compensate for this strength differential.

The most conservative assumption of a uniform maximum 1300 °F temperature over the entire steel beam results in the lower bound composite beam design strength of approximately 85 k-ft, which would likewise have required a redesign.

This problem illustrates the basic structural limit state model for this type of design problem and the effects of variations in the temperature distribution through the steel beam depth on the composite member design strength. As demonstrated, the critical heating parameter is not only the maximum steel temperature in the bottom flange, but also the thermal gradient along the beam web. The fidelity of the prior heat transfer analysis and/or empirical data used as the

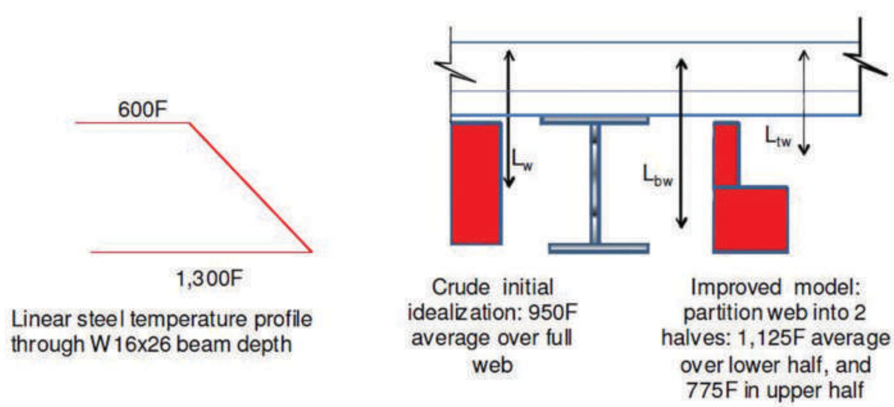

Fig. 3. Influence of refined consideration of web temperature distribution.

thermal input for these structural calculations should help guide selection of the most appropriate and bounding steel beam temperature distribution for the design fire exposure.

Example 3: Restrained Beam

Problem Statement

This example illustrates an application of advanced analysis to better understand, assess and design for thermally restrained or unrestrained conditions, as defined in ASTM E119 (ASTM, 2012) and UL 263 (UL, 2011).

A W16×40 ASTM A992 member has been chosen through ambient temperature design for a 30-ft span. The simply supported beam is noncomposite to the floor deck above and can be assumed to be continuously braced for lateral torsional buckling. The building is subdivided by full-height (slab-to-structure) fire barriers that align with the column grid such that a fire in one compartment will not directly heat beams in an adjacent compartment, assuming the fire barriers do not fail. The flexural resistance of this beam design when exposed to elevated temperatures during a fire is to be reviewed for an interior bay (restrained condition) and for an exterior bay (assumed to be unrestrained). The uniformly distributed dead load is 0.48 kips/ft and the uniformly distributed live load is 0.80 kips/ft.

Approach

Based on a load combination for fire of $1.2D + 0.5L$ per ASCE 7-10 and Appendix 4 of the 2010 AISC *Specification*, the maximum required moment at center span (M_u) is 110 kip-ft.

Per Section 4.2.4.3b.(3) of Appendix 4, the hottest bottom flange temperature is conservatively taken as being representative of the temperature of the rest of the cross-section.

W16×40 section properties:

$A = 11.8 \text{ in.}^2$ $\quad$ $t_f = 0.505 \text{ in.}$

$d = 16 \text{ in.}$ $\quad$ $I_x = 518 \text{ in.}^4$

$t_w = 0.305 \text{ in.}$ $\quad$ $Z_x = 73 \text{ in.}^3$

$b_f = 7 \text{ in.}$

Per the user note to Specification Section F2, W16×40 is a compact section.

Ambient temperature material properties for ASTM A992 steel:

$F_y = 50 \text{ ksi}$

$E = 29{,}000 \text{ ksi}$

F_y and E are temperature dependent per Table A-4.2.1 of Appendix 4. The coefficient of thermal expansion is 7.8×10^{-6}/°F at temperatures greater than 150° F (AISC, 2010). The 30-ft-long beam expands as its temperature increases as shown in Figure 4.

Unrestrained Case—Exterior Bay

In the proposed structural design, the exterior wall provides minimal lateral restraint against the axial expansion of the beam, which is ignored such that the beam is conservatively assumed to behave as simply supported without development of significant second-order moments due to P-Δ effects as a result of the applied loading and heating. The moment capacity of the beam is:

$$R_f = \phi_b M_{n,fire} = \phi_b F_y k_y Z_x$$

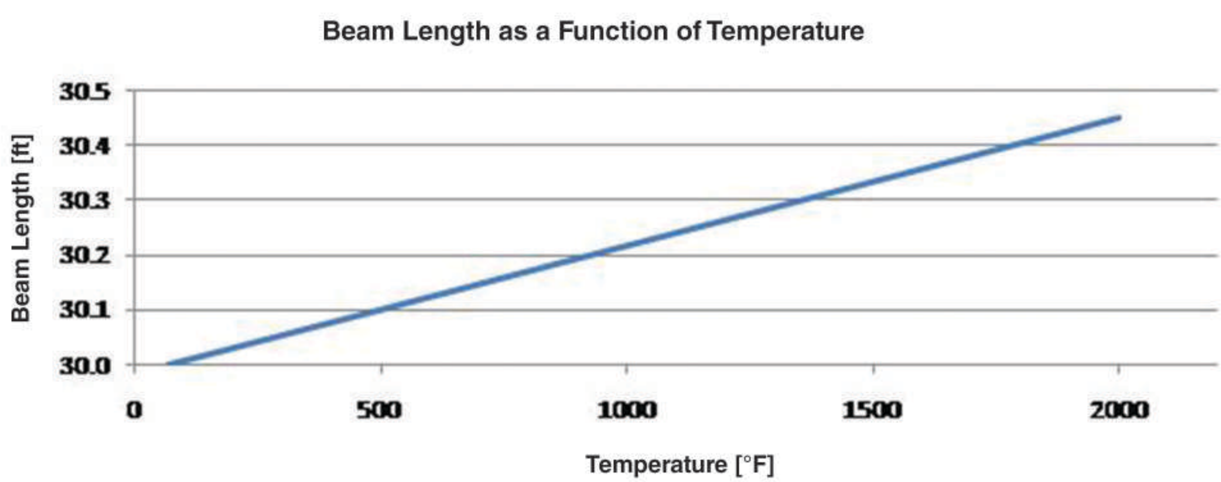

Fig. 4. Thermal expansion.

where R_f is the flexural resistance during fire, $\phi_b = 0.9$ and k_y is the temperature-dependent strength reduction factor obtained from Table A.4.2.1 from Appendix 4.

Restrained Case—Interior Bay

If a fire occurs in an interior compartment and the compartment's fire barriers do not fail, only the structural members in the interior bay will experience high temperatures, and the structure of the surrounding bays will provide restraint against fire-induced axial forces in the heated beams. The level of restraint will vary based upon the design of the structure. For this example, 75% restraint is used given that the frame is bolted (nonsliding connection) but the floor construction is not composite with the beams.

When thermal expansion (as discussed earlier) is induced by elevated temperatures but the ends of the beam are restrained against this expansion, high axial thrust forces can develop at the supports. Depending on the design of the connection, this thrust force can result in second-order moments that either increase or reduce the moment-carrying capacity of the member as long as the end connections do not fail. For this example, the connection is designed with consideration of this condition such that the thrust force occurs below the centroid of the beam and the connection has sufficient capacity to resist this force at elevated temperatures—a case that can result in improved moment capacity. The axial force, P, induced by thermal expansion is calculated as follows:

$$P = Ek_E A\alpha\Delta T$$

where

P = axial force, kips
k_E = temperature-dependent reduction factor for E
A = cross-sectional area, in.^{2}
α = coefficient of thermal expansion
L = beam length, in.
ΔT = temperature rise above ambient, °F

The critical buckling load for the W16×40 with a 30-ft unbraced length is calculated using the Euler formula and changes as the beam is heated given the temperature dependence of the modulus of elasticity. Figure 5 compares the calculated axial force due to thermal restraint with the critical buckling load. The critical buckling load will only be surpassed above 1800 °F (indicated in Figure 5 by the "x" denoting the intersection of the curves); otherwise, the restraining axial thrust reaction can be included in the beam's flexural strength.

Local member buckling at the connections should be reviewed because it might be an important factor given the high axial loads concentrated at the bottom flange. At elevated temperatures, this complex behavior is best reviewed through computer modeling, which is beyond the scope of this example.

The second-order moments induced by restraint of thermal expansion can be calculated as follows:

$$M_{axial\ thrust} = P\Delta$$

where P is the axial thrust force at the connection and Δ is the eccentricity associated with the location of the thrust

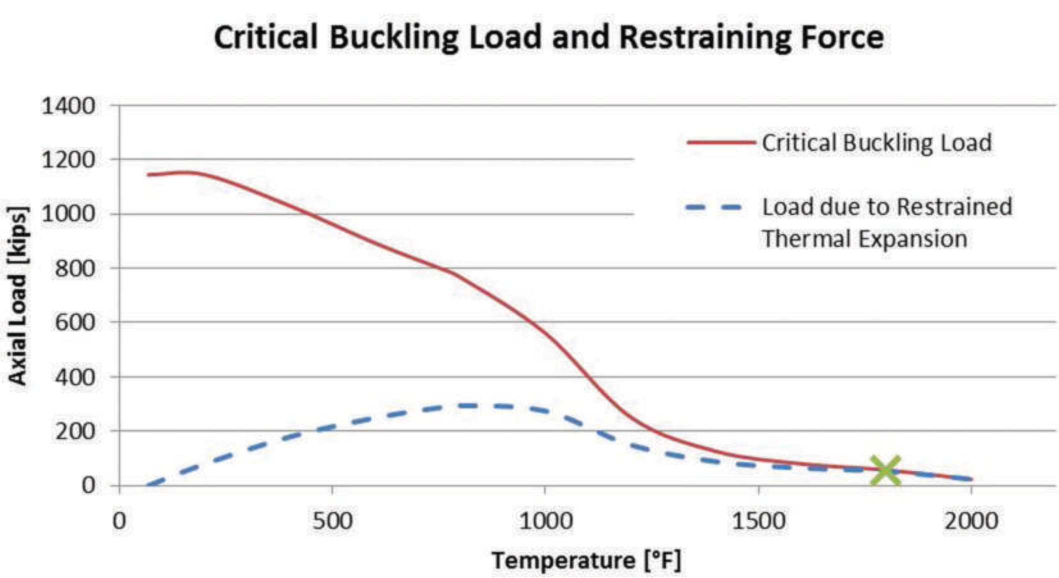

Fig. 5. Critical buckling load and restraining force for W16×40.

force relative to the centroid of the top flange of the beam. The value of Δ will change as the beam deforms and deflects due to the reduction of the modulus of elasticity at elevated temperatures. For steel temperatures not more than 1800 °F, the total flexural resistance, R_f, of this restrained beam then becomes:

$$R_f = M_{gravity} + M_{axial\ thrust}$$

Summary of Results

Figure 6 summarizes the total flexural capacity of the W16×40 beam as a function of temperature for the unrestrained and restrained cases. Based on flexural capacity and ignoring local buckling at the connections, the moments induced by the axial restraint condition allow the beam to sustain the applied gravity load at higher temperatures than for the unrestrained case.

As the beam continues to deflect, Δ may approach zero, reducing or eliminating the benefits of the second-order moment. At some point, the orientation of the second-order moment is reversed and the thrust force will reduce the flexural capacity of the beam, as seen in Figure 6 for temperatures above about 1600 °F.

This example has only considered an overall general temperature regime without any particular maximum exposure value. Credible design fire(s) must be used to evaluate the imposed heating demands and expected structural performance. The effects of cooling, and the resulting reduction in the length of the beam, may need to be reviewed to determine if the cooling phase might lead to failure of the connections.

Example 4: Exterior Tension Rods

Problem Statement

A new building includes a large atrium with a cable-stayed glass façade. The architectural design includes exterior steel cables or rods that span from the top of the wall (50 ft above grade) down to concrete foundations at the ground level. The original structural system utilized steel cables, and the ambient temperature design called for these members to be 3.5 in. in diameter. They are approximately 62 ft in total length and are spaced approximately 13.1 ft apart. The members span above a road surface adjacent to the building's main entrance.

The design team identified the following objectives:

- The structural members require a 1-hr fire resistance rating per the building code.
- The members should appear to be steel and should not be coated in protective material (i.e., omit applied fireproofing).
- Either cables or rods can be used.
- Large passenger vehicles (buses) should be allowed to utilize the access road.

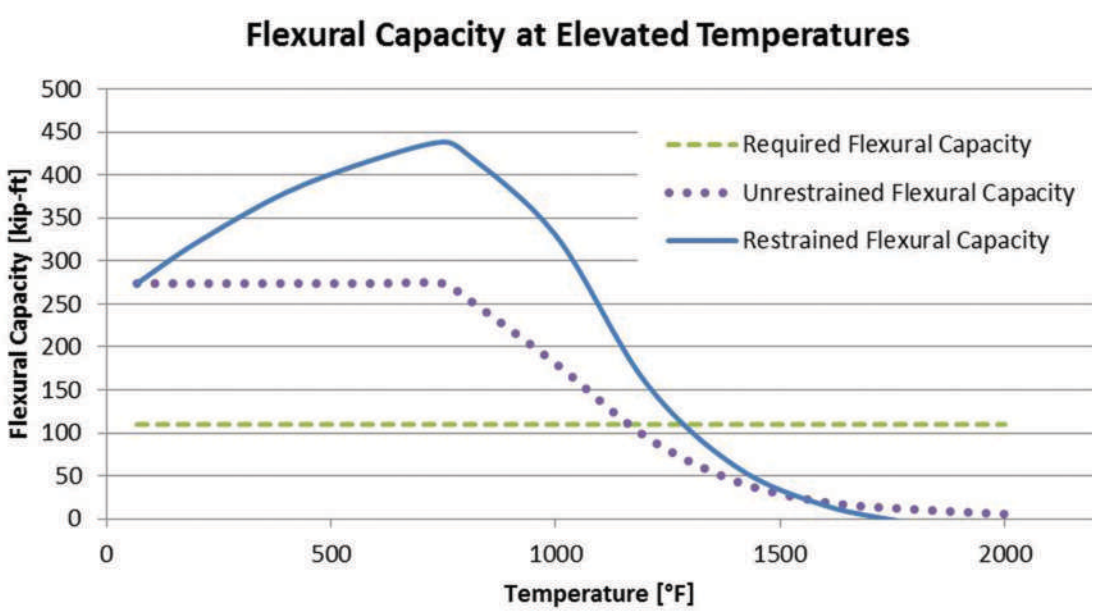

Fig. 6. W16×40 beam flexural capacity at elevated temperatures.

The fire protection engineer identified the most severe credible design fire for this case. The relevant details of this design fire are as follows:

- The fire source is a passenger bus.
- Up to four structural members (tension rods or cables) could be directly exposed to a fire engulfing the bus.
- Barriers prevent the bus from being closer than 11.8 ft to the base of the cables/rods.
- The burning rate of the bus has been determined based on the fuel load and ventilation.

Steel Temperatures

Based upon the preceding design fire description, the fire protection engineer has calculated the heat transfer from the bus fire to the adjacent members. Available research (SFPE, 2008) indicates that school bus fires may achieve peak heat release rates near 35 MW, as shown in Figure. 7.

The heat transfer analysis, which considered flame extension from the windows of the burning bus, resulted in estimates of steel temperatures along the length of the members as shown in Figure. 8, with a maximum expected steel cable/rod temperature of 1200 °F. Similar temperature profiles have been used for the four cables/rods directly adjacent to the bus (fire source) in order to represent the most severe exposure expected. The members immediately adjacent to the fire, but not directly above it, attained a maximum temperature of only 570 °F.

Reduction in Steel Strength

The loss in strength and stiffness of steel at high temperatures depends on how the steel was processed. Steel cables are typically cold worked and lose strength and stiffness at high temperatures more quickly than hot rolled steel. At 1200 °F, cold worked steel retains only 8% of its ambient strength (CEN, 2008a). Hot rolled steel retains 35% of its ambient strength at this temperature (CEN, 2008a). Figure 9 compares the loss of strength of these materials at elevated temperatures.

Thermal Expansion

Steel expands as it is heated. The coefficient of thermal expansion for the analysis was taken as a constant 7.8×10^{-6}/°F when the steel temperature is greater than 150 °F (AISC, 2010). More refined temperature-dependent representations of this coefficient exist. Taking the temperatures shown in Figure 8 as the average temperature of each 1-m-long portion of the member, the total thermal expansion of each of the four members directly above the bus fire is 4.3 in. The next adjacent members expand by approximately 1.9 in. given a maximum temperature of 570 °F and a similar profile to that shown in Figure 8.

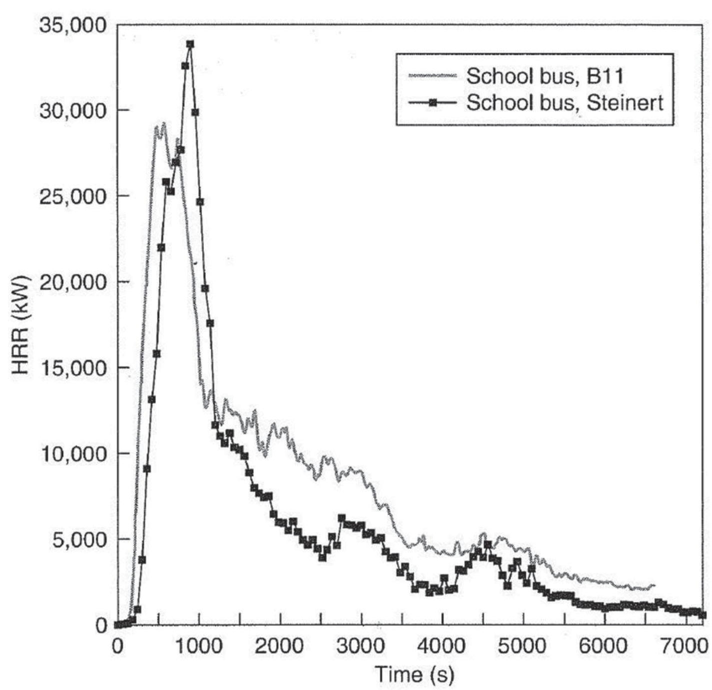

Fig. 7. School bus fire sizes (SFPE, 2008).

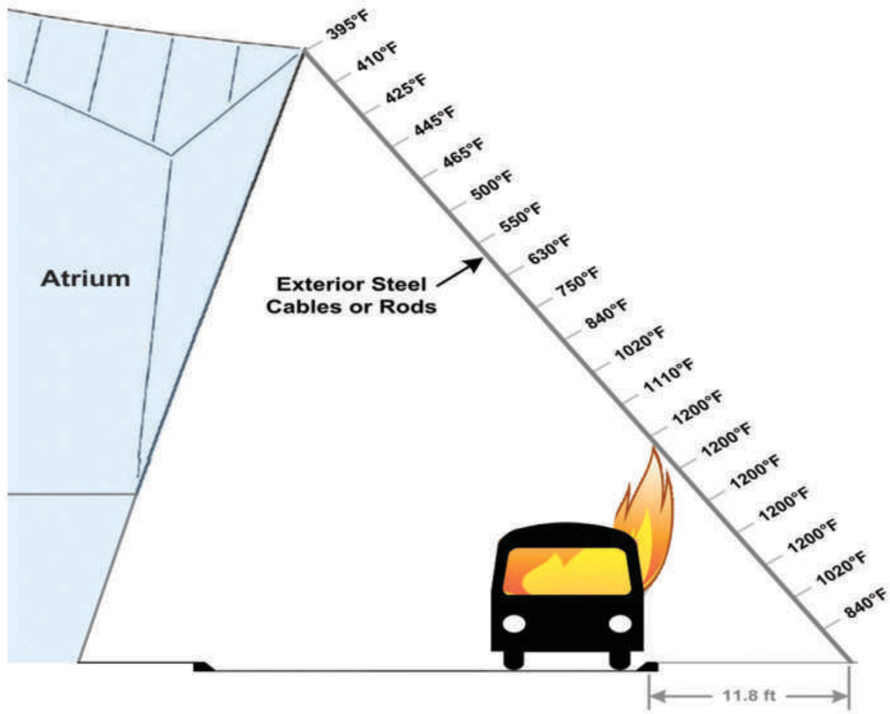

Fig. 8. Steel temperatures for tension rods/cables adjacent to bus fire source.

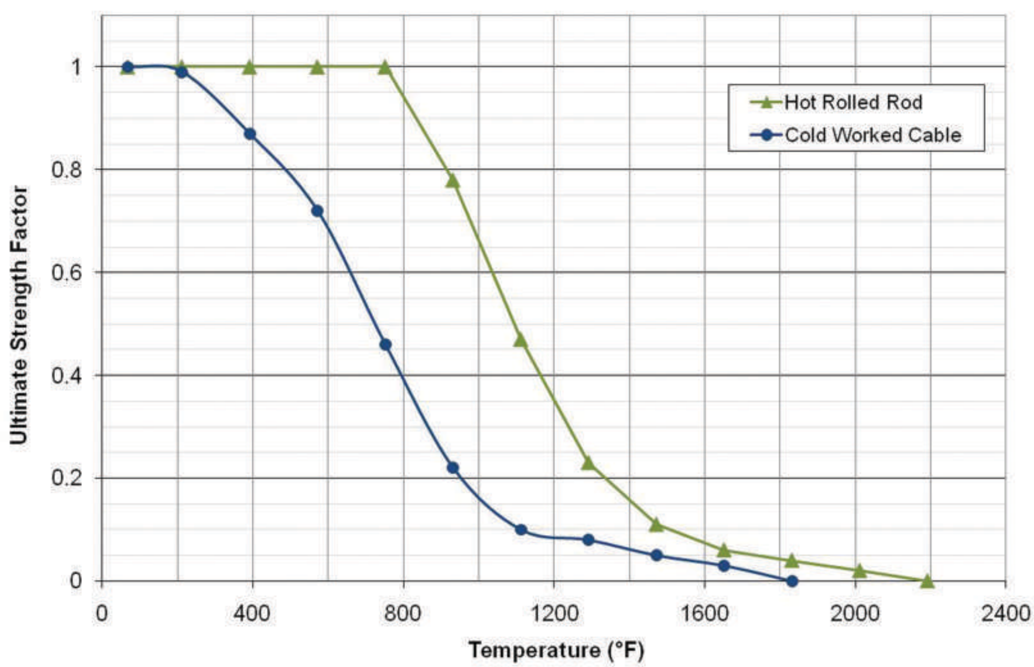

Fig. 9. Steel strength as a function of temperature.

Table 1. Structural Analysis Results				
Rod	Required Tensile Strength (kips)	Available Tensile Strength at 68 °F (kips)	Available Tensile Strength at 1200 °F (kips)	Remaining Material Safety Factor
3.5-in.-diamater Rods				
R1	112	454	159	1.4
R2	157	454	159	1.0
R3	168	454	159	0.9
R4	105	454	159	1.5
4.1-in.-diameter Rods				
R1	112	617	216	1.9
R2	157	617	216	1.4
R3	168	617	216	1.3
R4	105	617	216	2.1

Structural Analysis

Based on the steel temperature analysis discussed earlier, the design team chose to move forward using hot-rolled steel rods because they showed the most promise for meeting the goal of omitting applied fireproofing. The following load combinations were used to evaluate structural performance for the fire case (ASCE, 2010; AISC, 2010):

$$1.2D + 0.5L + 0.2S$$

$$1.2D + 0.5L + 0.2W$$

where D represents the nominal dead load, L is the nominal occupancy live load, S is the nominal snow load and W is the nominal wind load. ASTM A588 steel was chosen for this application ($F_y = 46$ ksi; $F_u = 67$ ksi).

The normal-temperature structural design of the atrium, including the exterior members discussed here, was accomplished using a finite element model given the highly complex geometry and interactions between different members. The same model was used to evaluate the effects of reduced member strength in the fire case. The model also accounted for the calculated 4.3-in. increase in the length of the four rods directly above the fire, as well as the lesser expansion of other rods in the vicinity. The complex response of the structural system to the weakening and expansion of individual members required this type of advanced analysis.

The structural engineer determined the required tensile strengths in the fire case with the four critical tension rods heated to the temperatures indicated in Table 1 summarizes the results of this analysis.

As can be seen in Table 1, the available strength in the fire case is not sufficient for rod R3 with a diameter of 3.5 in. However, a safety factor of at least 1.3 is maintained if the diameter of the rods is increased to 4.1 in. This level of performance is maintained for the 1-hr duration required by the applicable building code.

The completed structural fire engineering analysis demonstrated that increasing the diameter of the steel tension rods to 4.1 in. provides 1-hr fire resistance performance without the need for applied fire-resistive materials on the rods.

CONCLUSION

This article has presented an overview of Appendix 4 of the 2010 AISC *Specification*, with focus on its provisions for structural fire engineering. While movement to such advanced and performance-based approaches to structural fire resistance has been somewhat slow in the United States, it is further advanced in some other countries with a relative wealth of information available to support its undertaking. Building codes and referenced standards in the United States now provide means of gaining approval to use these types of approaches.

The four design examples demonstrate the types of approaches that are available with their potential outcomes and benefits. As more experience, confidence and successful project applications are developed with performance-based structural fire design, it is expected that its popularity will accordingly grow.

REFERENCES

AISC (2003), *Design Guide 19, Fire Resistance of Structural Steel Framing*, American Institute of Steel Construction, Chicago, IL.

AISC (2005), *Strategy for Integrating Structural and Fire Engineering of Steel Structures*, report prepared by Ove Arup & Partners for the American Institute of Steel Construction, Chicago, IL.

AISC (2010), *Specification for Structural Steel Buildings*, ANSI/AISC 360-10, American Institute of Steel Construction, Chicago, IL.

ASCE (2005), *Standard Calculation Methods for Structural Fire Protection*, ASCE/SEI/SFPE 29, American Society of Civil Engineers, Reston, VA.

ASCE (2010), *Minimum Design Loads for Buildings and Other Structures,* ASCE/SEI 7-10, American Society of Civil Engineers, Reston, VA.

ASTM (2012), *Standard Test Methods for Fire Tests of Building Construction and Materials*, ASTM E119-12, ASTM International, West Conshohocken, PA.

CEN (2008a), *Eurocode 2: Design of Concrete Structures. ENV 1992, Part 1-2: General Rules—Structural Fire Design*, European Committee for Standardization, Brussels.

CEN (2008b), *Eurocode 4: Design of Composite Steel and Concrete Structures. ENV 1994, Part 1-2: General Rules—Structural Fire Design*, European Committee for Standardization, Brussels.

CEN (2009a), *Eurocode 1: Actions on Structures. ENV 1991, Part 1-2: General Actions—Actions on Structures Exposed to Fire*, European Committee for Standardization, Brussels.

CEN (2009b), *Eurocode 3: Design of Steel Structures. ENV 1993, Part 1-2: General Rules—Structural Fire Design*, European Committee for Standardization, Brussels.

ICC (2012), *International Building Code (IBC),* International Code Council, Country Club Hills, IL.

NFPA (2006), *Standard Methods of Tests of Fire Endurance of Building Construction and Materials*, NFPA 251, National Fire Protection Association, Quincy, MA.

NIST (2010), *Best Practice Guidelines for Structural Fire Resistance of Concrete and Steel Buildings*, Technical Note 1681, National Institute of Standards and Technology, Gaithersburg, MD.

SFPE (2004), *SFPE Code Officials Guide to Performance-Based Design Review*, Society of Fire Protection Engineers, Bethesda, MD.

SFPE (2007), *SFPE Engineering Guide to Performance-Based Fire Protection*, 2nd edition, National Fire Protection Association, Quincy, MA.

SFPE (2008), *SFPE Handbook of Fire Protection Engineering*, 4th edition, National Fire Protection Association, Quincy, MA.

SFPE (2009), *Guidelines for Peer Review in the Fire Protection Design Process*, Society of Fire Protection Engineers, Bethesda, MD.

SFPE (2011), *Engineering Standard on Calculating Fire Exposures to Structures*, SFPE S.01, Society of Fire Protection Engineers, Bethesda, MD.

UL (2011), *Standard for Fire Tests of Building Construction and Materials*, UL 263, Underwriters Laboratories Inc., Northbrook, IL.

UL (2013), *Fire Resistance Directory,* Underwriters Laboratories, Inc., Northbrook, IL.

Current Steel Structures Research

No. 34

REIDAR BJORHOVDE

INTRODUCTION

This issue of "Current Steel Structures Research" for the *Engineering Journal* focuses on a selection of research projects from two major Canadian universities. The descriptions will not discuss all of the current projects at the schools—there are simply too many. But selected studies provide a representative picture of the research work and demonstrate the importance of the schools to Canada, as well as the United States and indeed to the efforts of industry and the profession worldwide. But the close collaboration between institutions and individuals in the two countries has always been essential, and the results have impacted industry significantly.

The universities and their many researchers and graduate students are very well known in the world of steel construction: the University of Toronto in Ontario and the École Polytechnique in Montréal, Québec. The size of their respective civil engineering faculties—especially their structural engineering groups—is indicative of their leading roles in Canadian academic research. The studies presented in the following reflect elements of specific projects as well as other long-time efforts. As has been typical of American, European and worldwide engineering research projects for years, many of the projects are multiyear efforts, and a number of them are also multipartner efforts. This calls for very careful cooperation, planning and implementation, including the education of graduate students and advanced researchers. The outcomes of the projects focus on industry needs and incorporation of results into design standards.

The researchers in Toronto and Montréal have been active for many years, as evidenced by their leading roles in research and development across North America. They have also been frequent participants in the work in other countries. A large quantity of high-quality technical papers, reports, design guides and conference presentations have been published, contributing to a collection of studies that continue to offer solutions to complex problems for designers, fabricators and erectors.

Reidar Bjorhovde, Dr.-Ing., Ph.D., P.E., Research Editor of the AISC *Engineering Journal,* Tucson, AZ. E-mail: rbj@bjorhovde.com

References are provided throughout the paper where they are available in the public domain. However, much of the work is still in progress, and in some cases reports or publications have not yet been prepared for public dissemination.

SOME CURRENT RESEARCH WORK AT UNIVERSITY OF TORONTO

Selected Projects of Professor Jeffrey A. Packer

Professor Packer has been at the University of Toronto since 1980 and is currently the Bahen/Tanenbaum Professor of Civil Engineering. He is one of the premier researchers in the world who addresses the broad area of tubular (HSS) members and structures. Thus, his research group performs experimental (small- to large-scale), numerical (nonlinear finite element analysis) and analytical research with primary focus on the behavior and design of steel structures. His current tubular structures research emphasizes welded, bolted, nailed and cast connections and joints. Loading conditions are key to many studies and have included quasi-static, fatigue, impact, blast and seismic conditions.

HSS under Impulsive Loading: The blast resistance of buildings and many infrastructure components has become an important design consideration. Embassies and other government buildings, petrochemical facilities and many other civilian structures are considering blast protection as a design feature. In fact, both the United States (ASCE, 2011) and Canada (CSA, 2012) have developed national blast design standards for civilian buildings. A design guide tailored to blast design of steel structures has recently been published by AISC (2013).

The direction from which blast loading is imposed is generally unknown, and this makes round or square HSS an ideal design element because such sections have no weak axis in bending. Further, wide flange shapes—if relatively thin—may be susceptible to flange folding and web distortion under high blast pressures. Researchers at the recently created Centre for Resilience of Critical Infrastructure at the University of Toronto (www.crci.utoronto.ca) examined the behavior of cold-formed HSS through full-scale air blast tests. The tests were conducted in a remote desert location with various types of shaped charges and explosives. Two sizes of HSS columns with several wall thicknesses were tested as simply supported beams (without axial load).

Further, vertical members were tested in duplicate (unfilled and concrete-filled) pairs; they were clad with steel decking to provide a uniformly distributed lateral blast load to one side. Figure 1 shows one of the wall assemblies after the test, viewed from the rear of the wall and inside the containment structure. The HSS has been significantly plastically deformed.

In conjunction with the blast testing of HSS members, the performance of cold-formed HSS material is being studied experimentally under various high strain rates using a Split-Hopkinson pressure bar, as shown in Figure 2. The test specimens are taken from several locations around the HSS, including the corners, and are tested in compression as well as tension. The high strain rate properties and dynamic strength enhancement will be implemented into numerical models for use in simulation of HSS members under blast or impact loading.

The Charpy V-Notch (CVN) impact toughness of typical North American cold-formed HSS has typically been low (Kosteski, Packer and Puthli, 2005). Further, the CVN specimen to be used in product manufacturing standards is specified to be taken in the longitudinal direction from the flat face of a square or rectangular HSS. This gives the most optimistic toughness reading for the cross-section and has led to the cautionary note in ASTM A500 (2013) that the product "…may not be suitable for those applications such as dynamically loaded elements in welded structures." The recent release of an improved HSS product, the new ASTM A1085 with a CVN requirement of 25 ft-lb at 40 °F, is a considerable improvement. The measurement of CVN for various product types is continuing within the study of HSS under dynamic loading conditions. Complete toughness-temperature transition curves are generated experimentally for multiple locations and orientations around the HSS cross-sections.

Fig. 1. HSS structural wall assembly after testing (photograph courtesy of Professor J. A. Packer).

Welding of HSS: The design of welds to and between HSS members has been a topic of research at the University of Toronto since the 1980s. Two approaches to the design of such welds have been proposed:

1. Design the welds to achieve the yield strength of the connected branch member walls, which presents an upper bound on weld size as it satisfies any loading conditions.

2. Design the welds to be "fit for purpose" and resist the applied loads.

The latter approach, due to the flexibility of HSS connections, requires the use of effective weld lengths or effective weld section properties, which are now prescribed for square and rectangular HSS members in Section K4 of the 2010 AISC *Specification*. Some weld effective properties in the *Specification* are supported by research, while others, developed previously from informed knowledge, are now being investigated.

One recent project undertaken by the University of Toronto research team for AISC has dealt with examining the branch weld effective section modulus, for HSS-to-HSS T-connections under branch in-plane bending. A series of laboratory experiments, with varying influential connection parameters and weld-critical joints, were performed in a quasi-static manner until failure by weld fracture. All of the test welds were deposited by welding robots at the Lincoln Electric Automation Division in Cleveland, Ohio. Stepped as well as matched box connections were tested, where branch width equals the chord width, and so were fillet and partial-joint-penetration (PJP) groove welds. The PJP welds were deposited along rounded corners of the chord.

Equation K4-6 in the 2010 AISC *Specification* was ultimately shown to be conservative, and a more accurate version has now been developed (McFadden and Packer, 2013). It was also concluded that the fillet weld directional strength enhancement factor should not be used for strength calculations of welded joints to square and rectangular HSS. At this time, a second phase to this AISC research project is being undertaken in which weld-critical joints in overlapped HSS

K-connections are being tested, within a large-scale truss. The validity of further aspects of Table K4.1 in the AISC *Specification* will be analyzed.

Figure 3a shows a tested connection with a typical weld fracture, and Figure 3b shows the setup for the welded connections.

Elliptical Hollow Section Connections: For the last several years, research work examining the strength and performance of elliptical hollow sections (EHS) has been conducted at the University of Toronto. Although produced in Europe to Euronorm standard EN 10210 (CEN, 2006), architects worldwide like the geometry and general appearance of these shapes. As a result, a number of projects have used EHS in North America. Much work has been done on the section classification of the EHS (e.g., for compression and other members), but connections continue to be difficult. An international team with members from the University of Toronto, the National University of Singapore and Delft University of Technology in the Netherlands was established to address welded EHS-to-EHS connections. T-connections and X-connections have now been tested and analyzed, with chord and branch members oriented in multiple directions. It has been shown that the design of the EHS connections

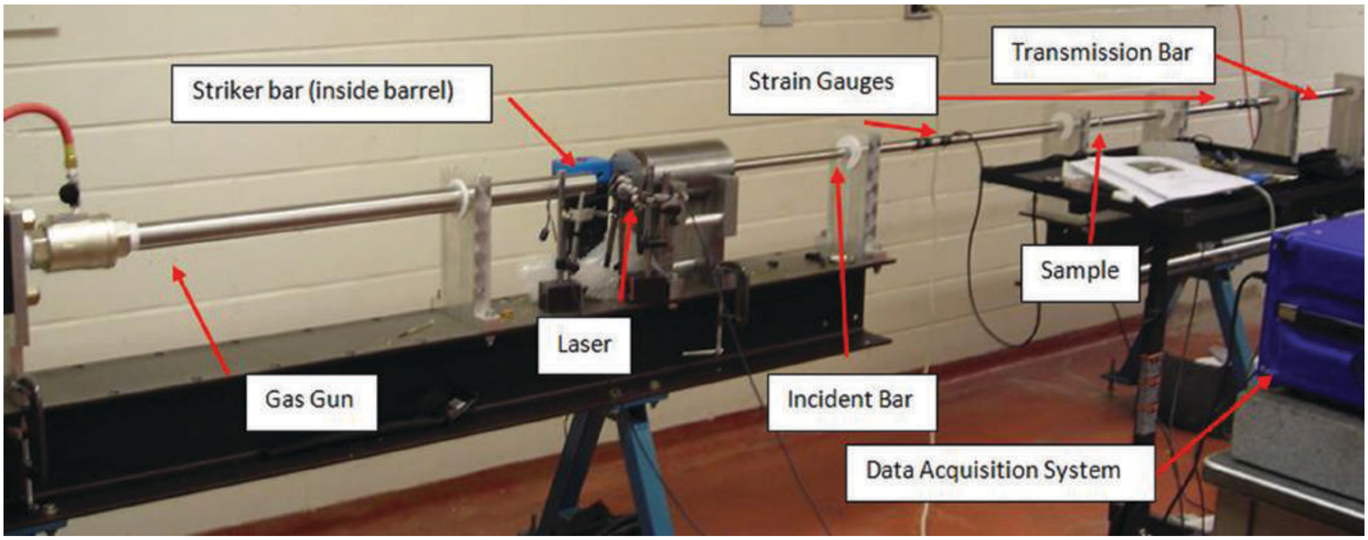

Fig. 2. Split-Hopkinson pressure bar apparatus at University of Toronto (photograph courtesy of Professor J. A. Packer).

(a) *(b)*

Fig. 3. Testing of welded connections: (a) typical weld fracture; (b) test setup (photographs courtesy of Professor J. A. Packer).

can be related to their circular and rectangular HSS counterparts (Packer et al., 2012; Haque and Packer, 2012; Shen et al., 2013a, 2013b). The complexity of the design of these connections has been effectively mitigated.

Figure 4a shows the appearance of a tested connection, Figure 4b illustrates the finite element model and its response at the same load level as the physical connection.

Cast Steel Connectors: Since 2004, much research work at the University of Toronto has addressed cast steel connectors for seismic applications. Steel castings have already been re-introduced in structural applications in Europe and China, but North America has been slow to capitalize on their advantages: the high material quality now achievable in steel castings, the ability to provide 3D freedom with connection arrangements, the ability to pre-engineer connectors to address specific connection performance requirements, and improved aesthetics (Herion et al., 2010). An innovative casting for application to the ends of a circular HSS brace member for a braced steel frame under inelastic seismic loading was engineered to provide a connection design solution (de Oliveira, Packer and Christopoulos, 2008). This high strength connector (HSC) was designed to remain elastic during seismic energy dissipation at mid-length of the brace and in the gusset plates. Subsequent research led to a new energy-dissipating device, in which the steel casting itself was designed to perform inelastically as a cast steel–yielding fuse. This yielding brace system (YBS) dissipates energy through the stable, single-curvature flexural yielding of specially designed “fingers” and provides an almost perfectly symmetric hysteretic response (Gray, Christopoulos and Packer, 2013). At the material level, the properties and fracture resistance of modern structural steel castings have also been checked (Iwashita, Packer and de Oliveira, 2012).

Figure 5a shows the use of high strength connectors in a braced frame in California; Figure 5b shows a full-scale seismic loading protocol test assembly for a yielding brace connector with a wide-flange diagonal brace.

Selected Projects of Professor Constantin Christopoulos

Professor Christopoulos is the director of the Structural Testing Laboratories at the University of Toronto and holds the Canada Research Chair in Seismic Resilience of Infrastructure. His current research focuses on the development of new high-performance, seismic-resistant systems that enhance the response of buildings subjected to extreme dynamic loads.

Self-Centering Energy Dissipative Braces for the Protection of Structures against Extreme Loading: Since 2003, Professor Christopoulos has collaborated with Professor Tremblay of École Polytechnique of Montréal on the development of the self-centering energy dissipative (SCED) bracing system. The system exhibits a flag-shaped response when subjected to extreme loading conditions. It is not only capable of accommodating large deformations, but also eliminates residual deformations and is practically undamaged even after a major earthquake. The concept has now been extended to incorporate the telescoping SCED (T-SCED) system (Erochko, Christopoulos and Tremblay, 2012). Full-scale experimental validations of the T-SCED system have shown that it is capable of accommodating up to 3.9% drift without any damage and with full recentering capabilities.

Development of Self-Centering Steel Moment-Resisting Frames: Professor Christopoulos has furthered the

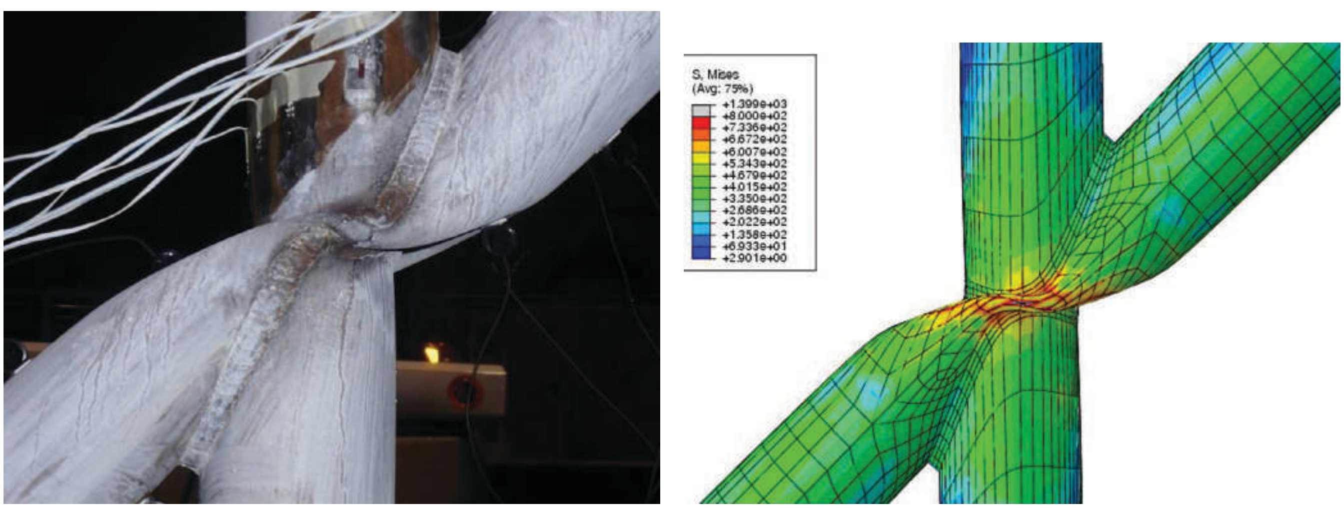

(a) (b)

Fig. 4. Elliptical hollow section connection: (a) testing; (b) modeling (figures courtesy of Professor J. A. Packer).

development of post-tensioned "damageless" steel moment frames. The work has led to the development of friction-damped self-centering steel frames, as illustrated in Figure 6. The work has also led to a new design approach for detailing the beams to enable them to develop inelastic mechanisms for very large drift demands.

Eccentrically Braced Steel Frames with Replaceable Yielding Links: Professors Christopoulos and Tremblay developed this concept for seismic design of steel buildings. The work resulted in the development of a new method for constructing eccentrically braced frames with replaceable yielding links. This allows for more efficient construction and the ability to inspect and replace the yielding elements following an earthquake. Figure 7 shows one of the tested connections.

Base Rocking Steel Frames with Higher Mode Control Mechanisms: Professors Christopoulos and Tremblay have also led work on the development of steel rocking braced frames. Using higher mode limiting mechanisms it has been demonstrated that the seismic response of structures with base flexural mechanisms can be significantly enhanced by either using multiple flexural mechanisms over the height of the structure or by incorporating a self-centering shear mechanism in the first story to control the higher mode response.

(a)

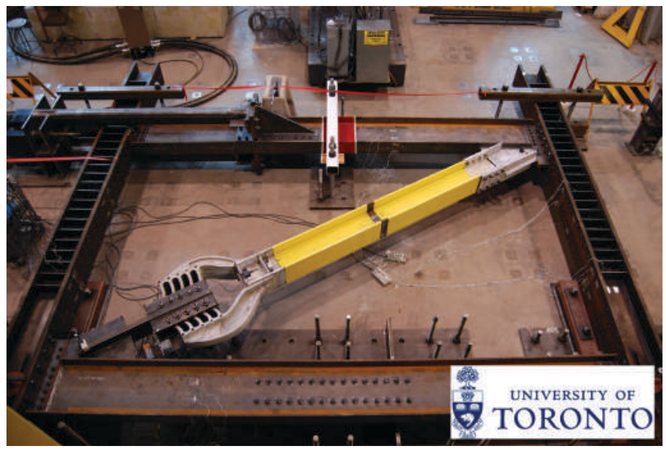

(b)

Fig. 5. (a) Use of high-strength cast connectors in a braced frame; (b) testing of a frame subassembly with a yielding brace connector (photographs courtesy of Professor J. A. Packer).

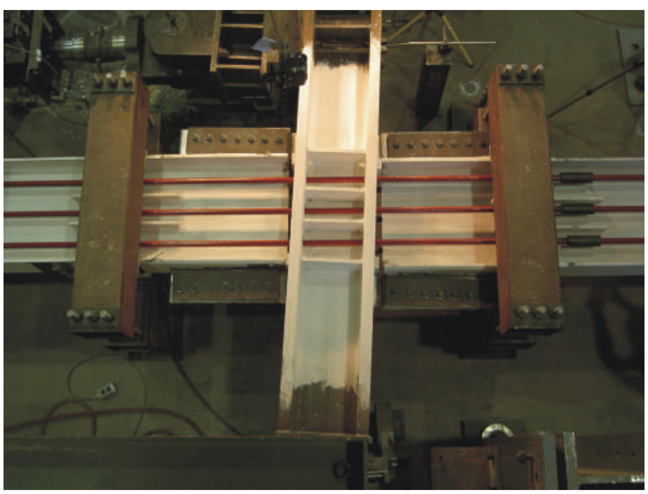

Fig. 6. Undamaged post-tensioned moment-resisting frame at 4% drift (photograph courtesy of Professor C. Christopoulos).

Fig. 7. Replaceable eccentrically braced link at 0.11 rad of rotation (photograph courtesy of Professor C. Christopoulos).

Selected Projects of Professor Oh-Sung Kwon

Hybrid (Analytical-Experimental) Simulation Method: Professor Kwon's research group focuses on simulation methods for a structural system subjected to dynamic load and seismic fragility assessment. A simulation framework has been developed, where the physical specimens can be integrated with a numerical model (Kwon, Elnashai and Spencer, 2008). The framework also allows geographically distributed simulation to exploit unique equipment at various institutions. In comparison with pure numerical simulations, the hybrid method can predict the response of a structural system more accurately when the system level response is influenced by the behavior of the physically represented components. It is especially beneficial when a reliable numerical model does not exist for a new structural component.

The hybrid simulation method was recently applied to evaluate the seismic fragility of a six-story steel structure with telescoping self-centering energy dissipating (T-SCED) braces (Erochko et al., 2012). The T-SCED brace exhibits a stable flag-shape hysteresis loop, which allows self-centering capability and seismic energy dissipation. In the hybrid simulation, one of the braces in the six-story building was experimentally represented at the University of Toronto's Structural Testing Facility, and the rest of the structure was analytically modeled. Because the T-SCED brace does not experience damage, it was possible to run more than 40 simulations to evaluate the seismic fragility of the structure statistically. The results showed that the six-story structure with T-SCED braces meets the performance limits specified in ASCE 41 and confirmed that the structure does not develop permanent deformation after earthquakes (Kammula et al., 2012).

SOME CURRENT RESEARCH WORK AT ÉCOLE POLYTECHNIQUE OF MONTRÉAL

The Department of Civil Engineering at École Polytechnique of Montréal (EPM) was established in 1873 and has since played a key role in the training of structural engineers in eastern Canada. Research in structural engineering was initiated in the late 1950s, with the construction of a major structural testing facility in 1958. The laboratory houses a 1,200-ft^2 strong floor and was subsequently equipped with a large reaction steel frame and various load control actuators and large capacity testing machines. In the early 1990s, it was decided to focus a significant part of the structural engineering research to seismic engineering, and a shake table facility was installed in 1995. This was the first implementation in North America of an earthquake simulator with a digital three-variable controller system (Filiatrault et al., 1996). In the aftermath of the 1994 Northridge earthquake, the facility was used for dynamic testing of reduced beam section beam-to-column connections (Tremblay, Tchebotarev and Filiatrault, 1997).

In 2003, the laboratory underwent a major expansion that was completed in 2006. The facility now offers 6,800 ft^2 of net strong floor testing area with a clear height up to 40 ft and a 33-ft tall L-shaped reaction wall with two 40-ft long wings. Loading equipment includes two new tension/compression frames, one with a 560-kip capacity and a larger one with a 2700-kip capacity, together with 10-ft wide and 26-ft high test space, 18 high performance actuators with capacities ranging from 22 kips to 450 kips, five digital control systems, and real-time hybrid testing capabilities. The shake table was moved; it can now accommodate 36-ft-tall specimens, and the actuator force capacity was increased to 100 kips. A new multi-axis loading system is currently being installed; it will be capable of imposing any combination of forces and deformations with 6 degrees of freedom to large structural components. Figure 8 shows a partial view of the facility. The system has eight actuators, four of which are horizontally mounted against the reaction wall (Tremblay et al., 2009; Tremblay, 2012).

The unique combination of large test beds and advanced testing equipment has permitted the completion of major testing programs on full- and reduced-scale structural components and systems. The facility plays a key role in the Canadian structural engineering research community. For instance, between 2006 and 2012, a total of 66 major projects involving graduate students have been completed. Half of the projects involved two or more researchers; a total of 15 researchers from seven other universities participated in the experimental programs. Some current and future projects are described in the next section, including tests on ductile fuses and collapse response following brace connection fracture, including buckling restrained braces.

Selected Projects of Professor Robert Tremblay

Ductile Fuses for HSS and I-Shaped Braces: In the past 20 years, a number of test programs have been performed at EPM to enhance the understanding of the inelastic cyclic response of bracing members and braced frames. Braces exhibit pronounced unsymmetrical response due to the difference between their tensile and compressive resistances and the degradation of the compressive strength under cyclic loading. These responses are illustrated in Figure 9a. For SCBF and OCBF, the braces are sized to resist the required compressive strength C_u, and their expected tensile strength may significantly exceed the required tensile strength ($T_{exp} > T_u$). Because compression and tension braces are used in pairs at every level, this overstrength offers beneficial effects on the response of braced frames because it compensates for the degrading resistance of the compression braces. In multistory frames, it also contributes to distributing the inelastic demand over the building height. However, brace connections, beams and columns must be designed for loads associated to the expected resistance, T_{exp}, which may have a significant effect on the cost of the structure.

That force demand can be minimized by introducing a ductile brace fuse created by locally reducing the brace cross-section area, as shown in Figure 9b. The fuse length, L_F, must be sufficient to accommodate the anticipated plastic deformations. Such fuses can be sized to yield both in tension and compression, such that brace buckling can also be avoided. However, achieving a stable inelastic straining in compression requires careful detailing to prevent local buckling and to avoid premature failure due to low-cycle fatigue. This is likely to add significant complexity. A simpler approach focuses on designing the fuses to be stronger than the braces in compression. The fuse yielding then only occurs in the form of successive unidirectional (tension) inelastic excursions. This allows for taking full advantage of the ductility of the steel without having to consider local inelastic buckling and low-cycle fatigue. This concept has been applied to the HSS braces shown in Figure 10 and the I-shaped braces in Figure 11. Full-scale tests have been performed for both designs (Kassis and Tremblay, 2008; Egloff and Tremblay, 2012).

For HSS braces, the brace member is cut near the end connection, and four angles are welded to connect the two HSS portions. The legs of the angles are trimmed to develop the required compressive strength. The fuse is enclosed in a built-up box to prevent angle buckling away from the HSS. Full-scale testing has been completed recently in a multi-purpose test frame that simulates the boundary conditions of a braced frame story (Figure 10b). A typical test result is shown in Figure 10c: the brace tensile strength is reduced, as intended, while preserving the compressive resistance and the axial deformation capacity. The fuse design for I-shaped braces was initially proposed by the Canam Group, whereby portions of the brace cross-section at the flange to web intersection are removed (Vincent, 2008). The tensile axial

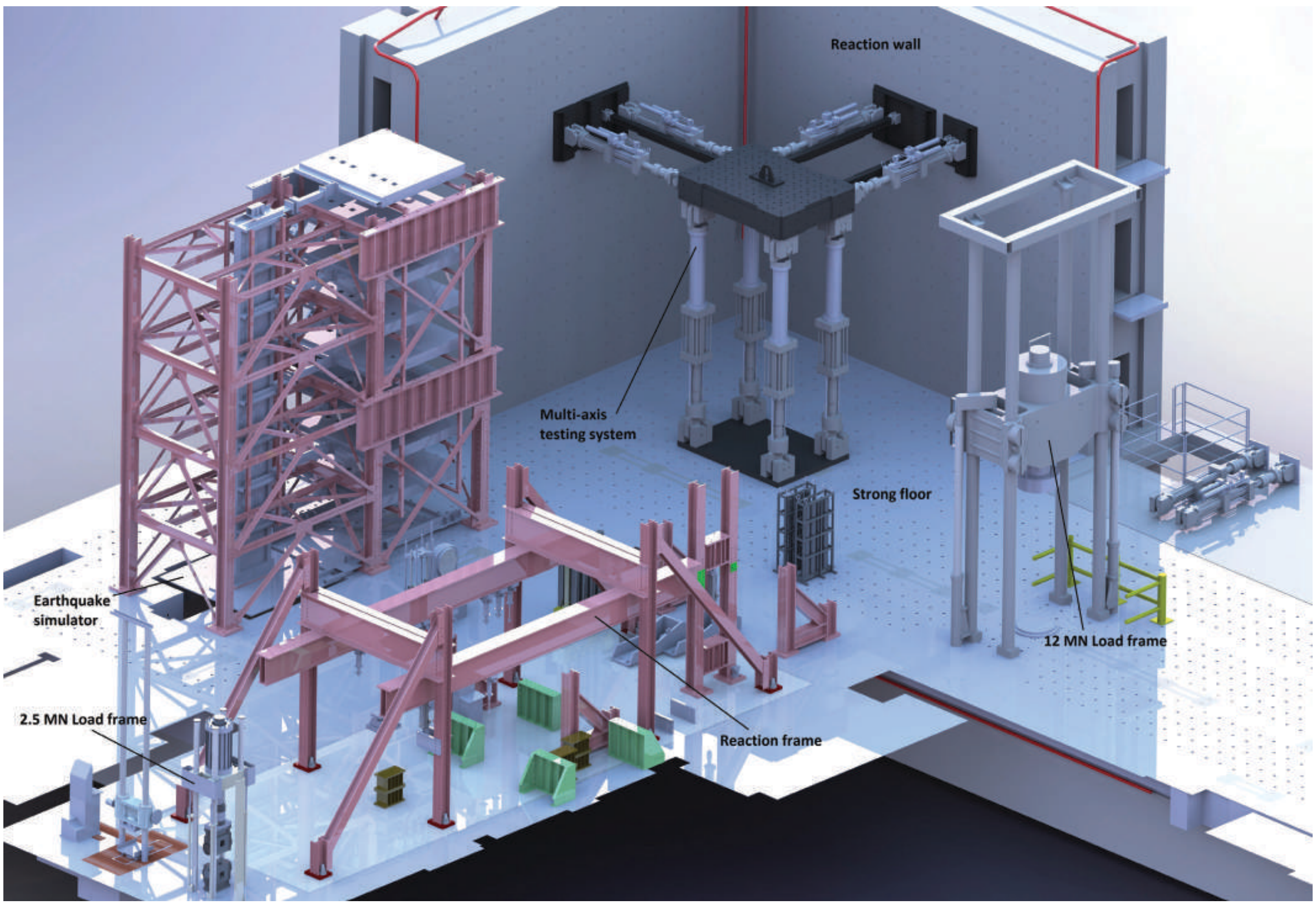

Fig. 8. Three-dimensional view of the EPM structural engineering laboratory (illustration courtesy of Professor Robert Tremblay).

strength can be reduced with a minimum impact on the brace buckling strength, as shown in Figure 10a. Confinement created by cold-formed C-shapes and flange cover plates must be provided to maintain the integrity of the cross-section upon brace buckling. Design equations were first proposed for the detailing of the fuse and confinement system, based only on detailed finite element analyses (Egloff and Tremblay, 2012). Full-scale testing was then performed to confirm the validity of the design expressions for various fuse geometries.

Both fuse systems can be constructed by steel fabricators. They are particularly suitable for long, slender braces, where the difference between tension and compression brace resistance is large, which is often the case in tall, single-story buildings. Reducing the brace overstrength for these structures has no or limited detrimental consequences on the building overall response. Ongoing research includes numerical simulations to verify the impact on multistory structures.

Seismic Response of X-Braced Frames: Results from past numerical studies and experimental programs have suggested that a K-factor of 0.5 is appropriate when determining the in-plane and out-of-plane buckling strengths of bracing members in an X-bracing system. In most tests, the braces were directly connected to each other at intersection points. This does not correspond to the case where bolted splice connections are used, as is commonly done in practice. This is illustrated in Figure 12a. In this situation, the flexibility of the overlapping plates may reduce the brace compressive resistance. The situation may be even more critical if single shear splices are used because an eccentricity is introduced that induces bending moments.

A project was started to resolve these questions and to develop design criteria for seismic and nonseismic applications. Fourteen specimens with HSS braces and single- and double-shear splice connections were tested. The brace size, the thickness of the connecting plates and the type of joint (single or double shear) were varied. Specimens with back-to-back double-angle braces were also tested. Testing was conducted using the same test frame as for the brace fuses (Gélinas, Tremblay and Daravan, 2012, 2013).

The HSS specimens were designed and detailed to force brace buckling out-of-plane of the frame. Examples of buckling modes that were generally observed for the continuous and discontinuous braces are shown in Figures 12b and 12c. In most cases, the discontinuous brace in tension could develop sufficient out-of-plane stiffness at the brace intersecting point to force buckling of the continuous brace at mid-length. Conversely, buckling of the discontinuous brace segments occurred in the form of a three-hinge mechanism, forming in the connecting plates at the brace intersecting point and the corner gusset plate (only a mid-connection plate is shown in Figure 12b). The buckling load associated with this mode was less than the brace compressive strength determined with K = 0.5. In some specimens, the cyclic rotation demand on the connecting plates led to premature failure of the plates in the tension cycle, which would not be adequate for ductile seismic performance. Analytical and numerical models have been developed to reproduce the measured brace capacities and simplified equations are being formulated to design connections that can develop the brace axial strength and prevent the buckling modes that were observed (Tremblay, Daravan and Gélinas, 2013).

Slotted Gusset Plate Connections for Slotted HSS Brace Connections: Slotted end connections as shown in Figure 13 are commonly used for HSS braces. The HSS members are slotted at their ends in the fabrication shop. At the construction site, they are inserted into the gusset plates to which

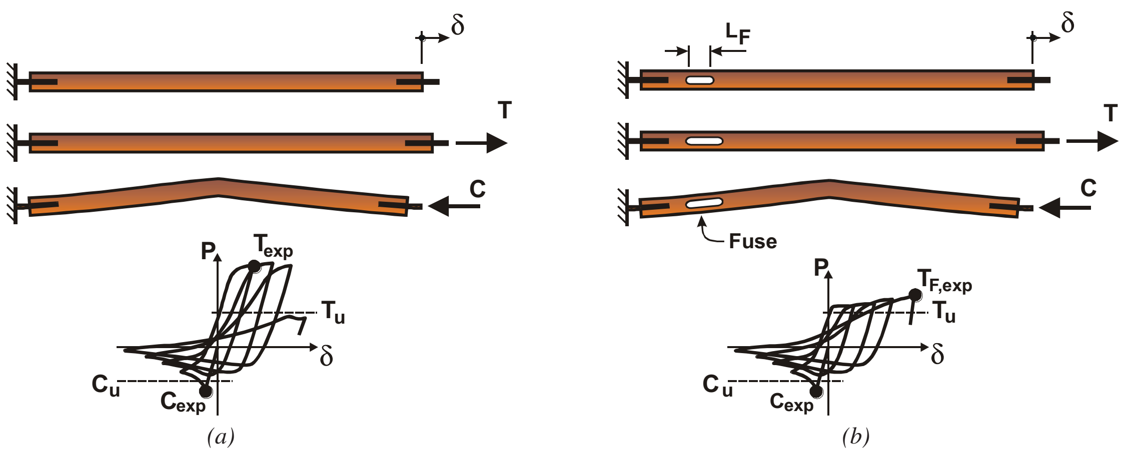

Fig. 9. Hysteretic brace responses: (a) without brace fuses; (b) with brace fuses (illustrations courtesy of Professor Robert Tremblay).

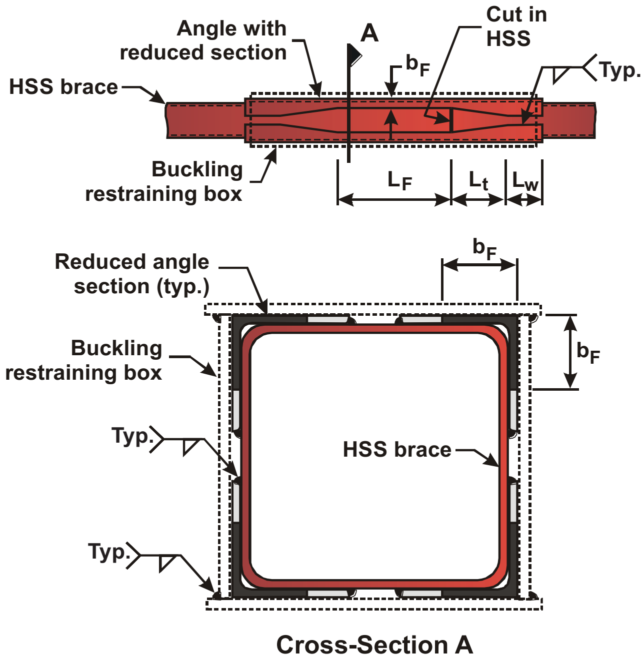

(a)

(b)

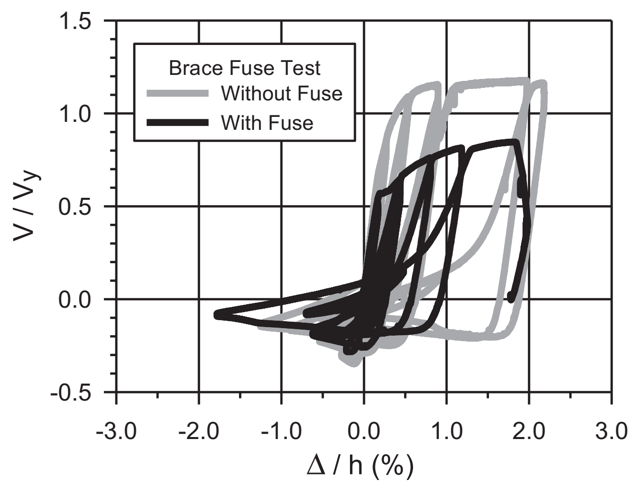

(c)

Fig. 10. Ductile tension fuses for HSS braces: (a) fabrication details; (b) full-scale testing in a re-usable test vertical frame; (c) typical hysteretic responses with and without fuses (illustrations courtesy of Professor Robert Tremblay).

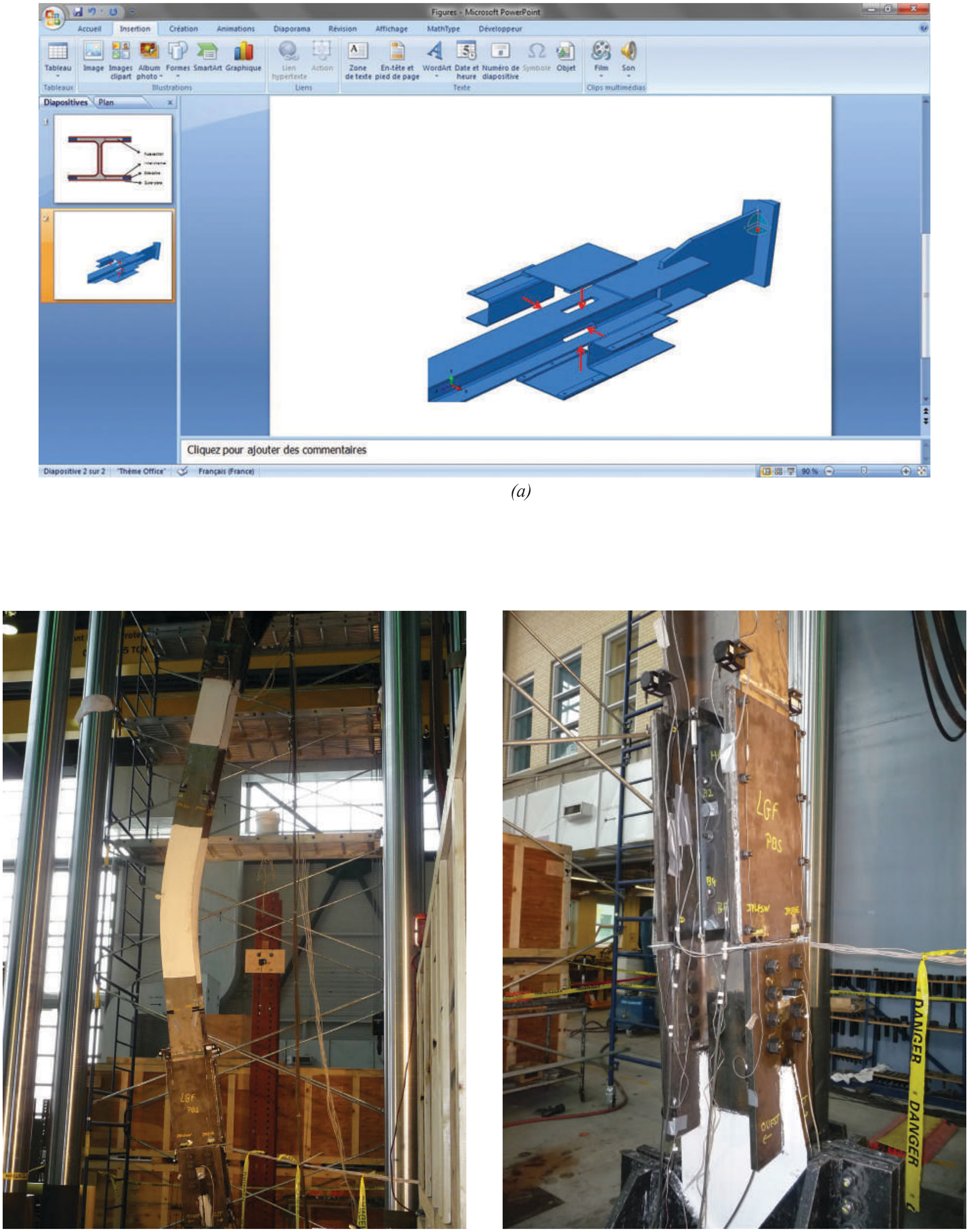

(a)

(b)

(c)

Fig. 11. Ductile tension fuse for I-shaped brace: (a) detail; (b) buckled brace with fuse in test; (c) bolted end connection with fuse (illustrations courtesy of Professor Robert Tremblay).

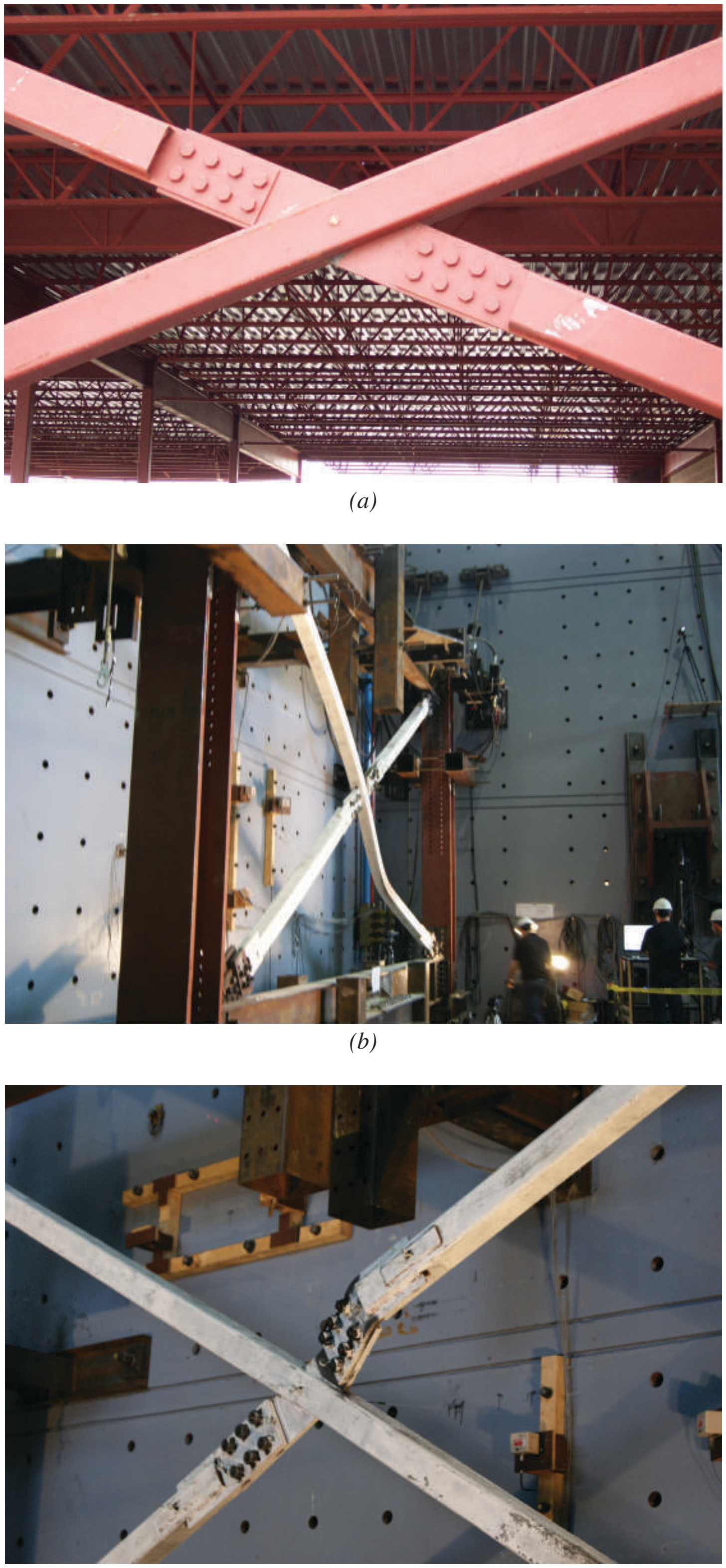

(a)

(b)

(c)

Fig. 12. Single splice mid-connection with through-plates in the continuous brace: (a) actual connection; (b) buckling of the continuous brace; (c) detail of the buckled shape at mid-connection with a three-hinge buckling mode of the discontinuous brace (photographs courtesy of Professor Robert Tremblay).

they are welded using two pairs of fillet welds. When used in special concentrically braced frames, these connections must be capable of developing the full tensile yield strength of the braces. However, test results from other projects have shown that a fracture may occur in the HSS on the net section at the ends of the slots before the brace yields. This will especially occur when shear lag causes a stress concentration at the weld ends. The problem can be solved by adding net section reinforcement. Other studies have shown that the target performance can still be achieved with unreinforced slotted HSS connections, provided that the net section resistance exceeds the brace yield capacity. This can be satisfied when shear lag effects are minimized by using long welds compared to the HSS cross-section dimensions.

ACKNOWLEDGMENTS

Professors Jeffrey Packer, Robert Tremblay, Constantin Christopoulos and Oh-Sung Kwon have provided significant assistance in the development of this paper. Their efforts are sincerely appreciated.

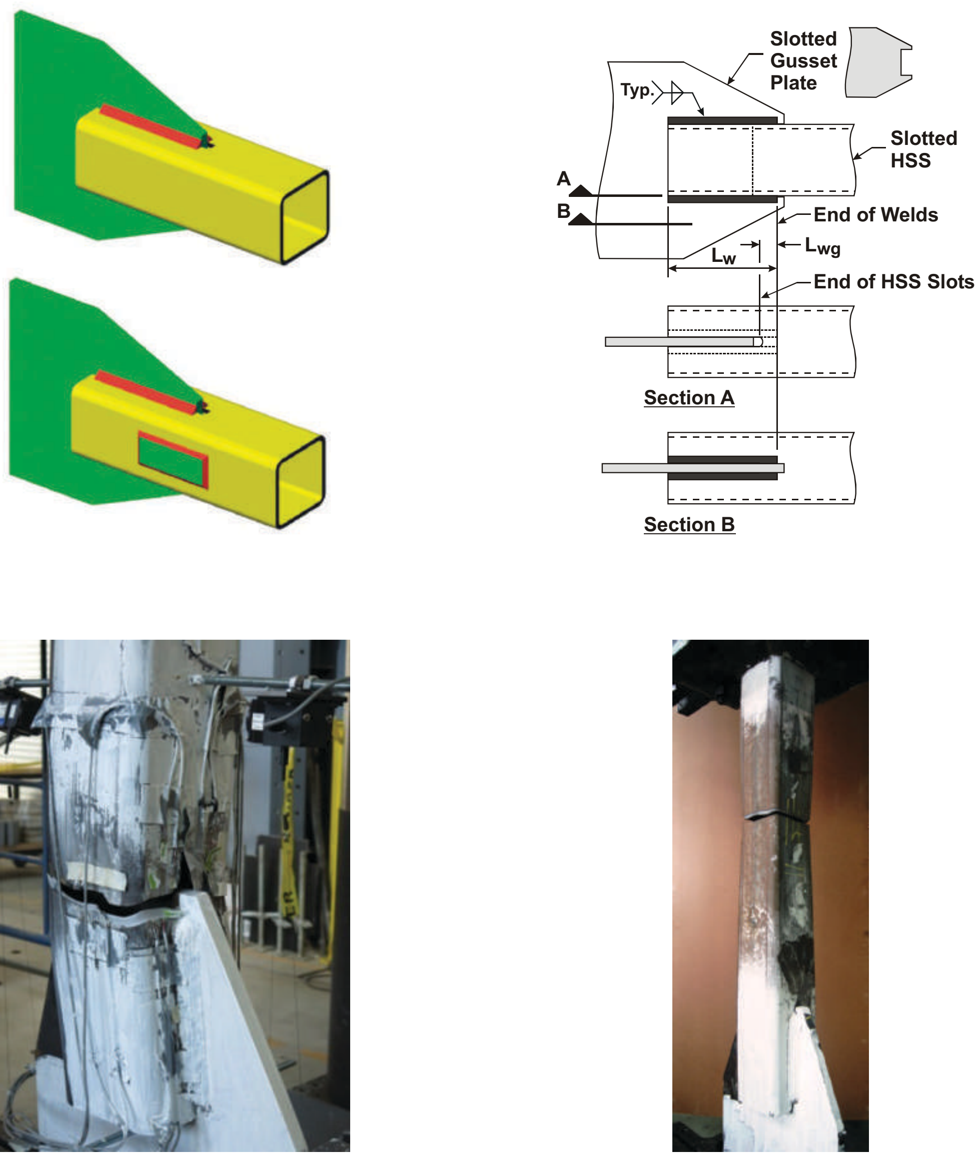

Fig. 13. Various slotted connections and failure modes for HSS bracing members (illustrations courtesy of Professor Robert Tremblay).

REFERENCES

AISC (2010), *Specification for Structural Steel Buildings*, ANSI/AISC 360-10, American Institute of Steel Construction, Chicago, IL.

AISC (2013), *Blast Resistant Steel Design, Steel Design Guide No. 26*, American Institute of Steel Construction, Chicago, IL.

ASCE (2011), *Blast Protection of Buildings*, ASCE/SEI 59-11, American Society of Civil Engineers, Reston, VA.

ASTM (2013), *Standard Specification for Cold-Formed Welded Carbon Steel Hollow Structural Sections (HSS)*, Standard No. A1085, American Society for Testing and Materials, West Conshohocken, PA.

CEN (2006), *Hot Finished Structural Hollow Sections of Non-Alloy and Fine Grain Steels—Part 1: Technical Delivery Conditions; Part 2: Tolerances, Dimensions and Sectional Properties*, EN 10210, European Committee for Standardization, Brussels, Belgium.

CSA (2012), *Design and Assessment of Buildings Subjected to Blast Loads*, Standard S850-12, Canadian Standards Association, Mississauga, ON.

de Oliveira, J.C., Packer, J.A. and Christopoulos, C. (2008), "Cast Steel Connectors for Circular Hollow Section Braces under Inelastic Cyclic Loading," *ASCE Journal of Structural Engineering*, Vol. 134, pp. 374–383.

Egloff, O. and Tremblay, R. (2012), "Finite Element Analysis of Ductile Fuses for W-Shape Steel Bracing Members," *Proceedings, 15th World Conference on Earthquake Engineering*, Lisbon, Portugal, Paper No. 5190.

Erochko, J., Christopoulos, C. and Tremblay, R. (2012), "Design and Testing of an Enhanced-Elongation Telescoping Self-Centering Energy Dissipative (T-SCED) Brace," *Proceedings, 15th World Conference on Earthquake Engineering*, Lisbon, Portugal.

Filiatrault, A., Tremblay, R., Thoen, B. and Rood, J. (1996), "A Second Generation Earthquake Simulation System in Canada: Description and Performance," *Proceedings, 11th World Conference on Earthquake Engineering*, Acapulco, Mexico, Paper No. 1204.

Gélinas, A., Tremblay, R. and Davaran, A. (2012), "Seismic Behavior of Steel HSS X-Bracing of the Conventional Construction Category," *Proceedings, ASCE Structures Congress*, Chicago, IL, pp. 1649–1660.

Gélinas, A., Tremblay, R. and Davaran, A. (2013), "Buckling Response of Bolted Mid-Connections in Steel X-Bracing," *Proceedings, CSCE 2013 Annual Conference*, Montréal, QC, Paper No. GEN-104.

Gray, M.G., Christopoulos, C. and Packer, J.A. (2013), "Cast Steel Yielding Brace System (YBS) for Concentrically Braced Frames: Concept Development and Experimental Validations," *ASCE Journal of Structural Engineering*, Vol. 139, in press.

Haque, T. and Packer, J.A. (2012), "Elliptical Hollow Section T and X Connections," *Canadian Journal of Civil Engineering*, Vol. 39, pp. 925–936.

Herion, S., de Oliveira, J.C., Packer, J.A., Christopoulos, C. and Gray, M.G. (2010), "Castings in Tubular Structures—The State of the Art," *ICE Structures and Buildings Journal*, Vol. 163, No. SB6, pp. 403–415.

Iwashita, T., Packer, J.A. and de Oliveira, J.C. (2012), "Defect Tolerance for Cast Steel Connections in Braced Frames," *ASCE Journal of Structural Engineering*, Vol. 138, pp. 1455–1464.

Kammula, V., Erochko, J., Kwon, O.-S. and Christopoulos, C. (2012), "Performance Assessment of the Self-Centering Energy Dissipative (SCED) Bracing System Using Hybrid Simulation," *Proceedings, 15th World Conference on Earthquake Engineering*, Lisbon, Portugal.

Kassis, D. and Tremblay, R. (2008), "Brace Fuse System for Cost-Effective Design of Low-Rise Steel Buildings," *Proceedings, CSCE 2008 Annual Conference*, Quebec, QC, Paper No. 248.

Kosteski, N., Packer, J.A. and Puthli, R.S. (2005), "Notch Toughness of Internationally Produced Hollow Structural Sections," *ASCE Journal of Structural Engineering*, Vol. 131, pp. 279–286.

Kwon, O.-S., Elnashai, A.S. and Spencer, B.F. (2008), "A Framework for Distributed Analytical and Hybrid Simulation," *Structural Engineering and Mechanics*, Vol. 30, No. 3, pp. 331–350.

Martinez-Saucedo, G., Packer, J.A. and Christopoulos, C. (2008), "Gusset Plate Connections to Circular Hollow Section Braces under Inelastic Cyclic Loading," *ASCE Journal of Structural Engineering*, Vol. 134, pp. 1252–1258.

McFadden, M.R. and Packer, J.A. (2013), *Effective Weld Properties for RHS-to-RHS Moment T-Connections*, Report to AISC, University of Toronto, Toronto, ON.

Packer, J.A., Choo, Y.S., Shen, W., Wardenier, J., van der Vegte, G.J. and Mustard, T. (2012), "Axially Loaded T and X Joints of Elliptical Hollow Sections," *CIDECT Final Report No. 5BW-2/12*, University of Toronto and National University of Singapore.

Shen, W., Choo, Y.S., Wardenier, J., Packer, J.A. and van der Vegte, G.J. (2013a), "Static Strength of Axially Loaded Elliptical Hollow Section X Joints with Braces Welded to the Wide Sides of the Chord. Part I: Numerical Investigations Based on Experimental Tests," *ASCE Journal of Structural Engineering*, Vol. 139, in press.

Shen, W., Choo, Y.S., Wardenier, J., Packer, J.A. and van der Vegte, G.J. (2013b), "Static Strength of Axially Loaded Elliptical Hollow Section X Joints with Braces Welded to the Wide Sides of the Chord. Part II: Parametric Study and Strength Equations," *ASCE Journal of Structural Engineering*, Vol. 139, in press.

Tremblay, R., Davaran, A. and Gélinas, A. (2013), "Stability of X-Bracing Systems with Traditional Bolted Connections," *Proceedings, 2013 ASCE Structures Congress*, Pittsburgh, PA, pp. 2662–2674.

Tremblay, R. (2012), "Seismic Testing of Steel Frame Structures," *Proceedings, International Workshop on Advances in Seismic Experiments and Computations*, Nagoya, Japan.

Tremblay, R., Léger, P., Rogers, C., Bouaanani, N., Massicotte, B., Khaled, A. and Lamarche, C.-P. (2009), "Experimental Testing of Large Scale Structural Models and Components Using Innovative Shake Table, Dynamic, Real-Time Hybrid Simulation and Multi-Directional Loading Techniques," *Proceedings, 3rd International Conference on Advances in Experimental Structural Engineering*, San Francisco, CA, Paper No. 26.

Tremblay, R., Tchebotarev, N. and Filiatrault, A. (1997), "Seismic Performance of RBS Connections for Steel Moment Resisting Frames: Influence of Loading Rate and Floor Slab," *Proceedings, 2nd International Conference on the Behaviour of Steel Structures in Seismic Areas*, Kyoto, Japan, pp. 664–671.

Vincent, R.B. (2008), "Minimizing the Strength of Bracing Connections," *Proceedings, 6th International Workshop on Connections in Steel Structures*, Chicago, IL, pp. 117–141.

GUIDE FOR AUTHORS

SCOPE: The ENGINEERING JOURNAL is dedicated to the improvement and advancement of steel construction. Its pages are open to all who wish to report on new developments or techniques in steel design, research, the design and/or construction of new projects, steel fabrication methods, or new products of significance to the uses of steel in construction. Only original papers should be submitted.

GENERAL: Papers intended for publication may be submitted by mail to the Editor, Keith Grubb, ENGINEERING JOURNAL, AMERICAN INSTITUTE OF STEEL CONSTRUCTION, One East Wacker Drive, Suite 700, Chicago, IL, 60601, or by email to grubb@aisc.org.

The articles published in the *Engineering Journal* undergo peer review before publication for (1) originality of contribution; (2) technical value to the steel construction community; (3) proper credit to others working in the same area; (4) prior publication of the material; and (5) justification of the conclusion based on the report.

All papers within the scope outlined above will be reviewed by engineers selected from among AISC, industry, design firms, and universities. The standard review process includes outside review by an average of three reviewers, who are experts in their respective technical area, and volunteers in the program. Papers not accepted will not be returned to the author. Published papers become the property of the American Institute of Steel Construction and are protected by appropriate copyrights. No proofs will be sent to authors. Each author receives three copies of the issue in which his contribution appears.

MANUSCRIPT PREPARATION: Manuscripts must be provided in Microsoft Word format. Include a PDF with your submittal. View our complete author guidelines at **www.aisc.org/ej**.

UNITED STATES POSTAL SERVICE®

Statement of Ownership, Management, and Circulation
(All Periodicals Publications Except Requester Publications)

1. Publication Title	2. Publication Number	3. Filing Date
Engineering Journal	0 0 1 3 - 8 0 2 9	9/13/2013
4. Issue Frequency	5. Number of Issues Published Annually	6. Annual Subscription Price
Quarterly	4	$40.00

7. Complete Mailing Address of Known Office of Publication *(Not printer) (Street, city, county, state, and ZIP+4®)*
One E. Wacker Drive, Suite 700, Chicago, IL 60601
Contact Person: Areti Carter
Telephone *(Include area code)*: 312.670.5427

8. Complete Mailing Address of Headquarters or General Business Office of Publisher *(Not printer)*
One E. Wacker Drive, Suite 700, Chicago, IL 60601

9. Full Names and Complete Mailing Addresses of Publisher, Editor, and Managing Editor *(Do not leave blank)*
Publisher *(Name and complete mailing address)*
American Institute of Steel Construction, One E. Wacker Drive, Suite 700, Chicago, IL 60601
Editor *(Name and complete mailing address)*
Keith Grubb, One E. Wacker Drive, Suite 700, Chicago, IL 60601
Managing Editor *(Name and complete mailing address)*
Areti Carter, One E. Wacker Drive, Suite 700, Chicago, IL 60601

10. Owner *(Do not leave blank. If the publication is owned by a corporation, give the name and address of the corporation immediately followed by the names and addresses of all stockholders owning or holding 1 percent or more of the total amount of stock. If not owned by a corporation, give the names and addresses of the individual owners. If owned by a partnership or other unincorporated firm, give its name and address as well as those of each individual owner. If the publication is published by a nonprofit organization, give its name and address.)*

Full Name	Complete Mailing Address
American Institute of Steel Construction	One E. Wacker Drive, Suite 700, Chicago, IL 60601

11. Known Bondholders, Mortgagees, and Other Security Holders Owning or Holding 1 Percent or More of Total Amount of Bonds, Mortgages, or Other Securities. If none, check box → ☒ None

Full Name	Complete Mailing Address

12. Tax Status *(For completion by nonprofit organizations authorized to mail at nonprofit rates) (Check one)*
The purpose, function, and nonprofit status of this organization and the exempt status for federal income tax purposes:
☒ Has Not Changed During Preceding 12 Months
☐ Has Changed During Preceding 12 Months *(Publisher must submit explanation of change with this statement)*

PS Form **3526,** September 2007 *(Page 1 of 3 (Instructions Page 3))* PSN 7530-01-000-9931 **PRIVACY NOTICE**: See our privacy policy on *www.usps.com*

13. Publication Title: Engineering Journal
14. Issue Date for Circulation Data Below: Third Quarter 2013

15. **Extent and Nature of Circulation**			**Average No. Copies Each Issue During Preceding 12 Months**	**No. Copies of Single Issue Published Nearest to Filing Date**
a. Total Number of Copies *(Net press run)*			1,235	1,236
b. Paid Circulation *(By Mail and Outside the Mail)*	(1)	Mailed Outside-County Paid Subscriptions Stated on PS Form 3541(Include paid distribution above nominal rate, advertiser's proof copies, and exchange copies)	654	634
	(2)	Mailed In-County Paid Subscriptions Stated on PS Form 3541 *(Include paid distribution above nominal rate, advertiser's proof copies, and exchange copies)*	0	0
	(3)	Paid Distribution Outside the Mails Including Sales Through Dealers and Carriers, Street Vendors, Counter Sales, and Other Paid Distribution Outside USPS®	0	0
	(4)	Paid Distribution by Other Classes of Mail Through the USPS (e.g. First-Class Mail®)	0	0
c. Total Paid Distribution *(Sum of 15b (1), (2), (3), and (4))*			654	634
d. Free or Nominal Rate Distribution *(By Mail and Outside the Mail)*	(1)	Free or Nominal Rate Outside-County Copies included on PS Form 3541	0	0
	(2)	Free or Nominal Rate In-County Copies Included on PS Form 3541	0	0
	(3)	Free or Nominal Rate Copies Mailed at Other Classes Through the USPS (e.g. First-Class Mail)	0	0
	(4)	Free or Nominal Rate Distribution Outside the Mail *(Carriers or other means)*	50	50
e. Total Free or Nominal Rate Distribution *(Sum of 15d (1), (2), (3) and (4))*			50	50
f. Total Distribution *(Sum of 15c and 15e)*			704	684
g. Copies not Distributed *(See Instructions to Publishers #4 (page #3))*			531	552
h. Total *(Sum of 15f and g)*			1,235	1,236
i. Percent Paid *(15c divided by 15f times 100)*			92%	92%

16. Publication of Statement of Ownership
☒ If the publication is a general publication, publication of this statement is required. Will be printed in the Fourth Quarter 2013 issue of this publication.
☐ Publication not required.

17. Signature and Title of Editor, Publisher, Business Manager, or Owner: Areti Carter
Date: 9/13/2013

I certify that all information furnished on this form is true and complete. I understand that anyone who furnishes false or misleading information on this form or who omits material or information requested on the form may be subject to criminal sanctions (including fines and imprisonment) and/or civil sanctions (including civil penalties).

PS Form **3526,** September 2007 *(Page 2 of 3)*

There's always a solution in steel.

ENGINEERING JOURNAL
American Institute of Steel Construction
One East Wacker Drive, Suite 700
Chicago, IL 60601

312.670.2400 www.aisc.org